Investigations on mercury sensitivity and molecular determinants of selectivity in two plant aquaporins

Vom Fachbereich Biologie der Technischen Hochschule Darmstadt
zur
Erlangung des akademischen Grades
eines Doctor rerum naturalium
genehmigte
Dissertation von

Muhammad Ayaz
BSc (Hons), MPhil (Botanik)
aus
Multan (Pakistan)

Berichterstatter: Prof. Dr. Ralf Kaldenhoff
Mitberichterstatter: Prof. Dr. Gerhard Thiel

Tag der Einreichung: 05.08.2011
Tag der mündlichen Prüfung: 18.10.2011

Darmstadt 2011

D 17

To the
memories of
my late father

Acknowledgements

I am thankful to my advisor Prof Dr Ralf Kaldenhoff for providing me an opportunity to win the higher ideal of life, his patience, cooperation and continued supervision throughout the research project.

I am grateful to Prof Dr Gerhard Thiel for his willingness to serve as co-supervisor. His productive comments and insights are highly appreciated.

I extend my gratitude towards Prof Dr Adam Bertl (then a senior colleague in the lab) for his unequivocal support and encouragement to get through the difficult times especially during my early days in Darmstadt. I was indeed benefitted from his uncanny ability to turn one's predicament into the moments of delight.

I am thankful to all my lab-mates for providing a pleasant and a friendly work atmosphere. I would like to particularly acknowledge the support rendered by Beate Otto, Dr Matthias Fischer, Dr Norbert Uehlein-Rössner and Nadine Priem. My gratitude is extended to Prof Dr Harald Kolmar and Dr Andreas Christmann for sharing their skills and their support in producing monoclonal antibody.

I will be forever indebted to my parents, sister and brother who enriched my life with love and friendship. I wish to thank my parents for their grooming, their moral support and their affection. The pursuit of a PhD won't have been possible without the financial support of my mother.

Muhammad Ayaz

Structure of the Thesis

This thesis is split into following chapters:

Ch. 1
This chapter introduces aquaporins, their structure and the mechanism of water permeation. Further, it also gives a brief account of various ammonia transporters as well as mechanism of ammonia transport in bacterial AmtB. It also gives detailed review of literature on molecular determinants of selectivity in AQPs.

Ch. 2
This chapter includes description of the results as well as their graphical presentation. Also, the results have been discussed in this chapter. The chapter 2 has been split into 3 sub-chapters.

The sub-chapter 1 involves studies on identification of Hg sensitive site in TaTIP2;2. The effects of some other metals on the pore function have also been investigated. Further, the contrasting mercury sensitivity between ammonia and water permeabilities in TaTIP2;2 has been discussed in detail.

The sub-chapters 2 and 3 involve studies on molecular determinants of selectivity in AQPs, the former sub-chapter deals with the amino acids substitutions outside the selectivity regions whereas the latter one deals with the substitutions inside the said regions. A couple of residues were distinguishable in the sequence alignment comparing water conducting and ammonia conducting AQPs. In sub-chapter 2, these residues were substituted at the corresponding positions between TaTIP2;2 and NtPIP2;1. The outcome of the functional studies as well as the homology models helped discuss the results.

The sub-chapter 3 deals with the corresponding mutations inside the selectivity regions. A remarkable part of this sub-chapter involves studies on chimeric proteins in which a number of structural domains were swapped between TaTIP2;2 and NtPIP2;1.

Ch. 3
This chapter includes material used and the procedures and protocols adopted for manipulating DNA, proteins, bacteria and yeast. The stopped-flow spectroscopy has been introduced in this chapter along with an account of the way permeability coefficients were determined in the present study.

Ch. 4
This chapter concludes the entire research work, briefly highlights significance of the results and gives future recommendations.

Ch. 5 and 6
These chapters include Bibliography and Appendices, respectively.

Table of Contents

1 INTRODUCTION

1.1 Introduction to Aquaporins

Aquaporins are water conducting channels found in animals, plants and microbes. All the aquaporins are water conducting and many of them have been characterized as facilitators of gases like carbon dioxide, ammonia and the larger solutes like glycerol and urea. The physiological roles of aquaporins are continued to be investigated in prokaryotes as well as in eukaryotes and the scientists are much more convinced of their significance as they were at the time of their discovery in 1992 (Preston *et al*., 1992) that was rewarded by the Nobel Prize to Peter Agre.

Aquaporins belong to the family of major intrinsic proteins (MIPs). Based on the phylogeny, the higher plant AQPs can be classified into the following subgroups: (i) The largest of the four subgroups are PIPs (plasma membrane intrinsic proteins), with 13 isoforms in *Arabidopsis*, (ii) Tonoplast intrinsic proteins (TIPs), (iii) Nodulin 26-like intrinsic proteins (NIPs) which are mainly found in nitrogen-fixing root nodules of legumes, (iv) small basic intrinsic proteins (SIPs) which are localized at the endoplasmic reticulum (Ishikawa *et al*., 2005). Johanson *et al*. (2001) provided the nomenclature for the current divisions within each of the AQP subgroup mentioned above.

The experimental evidences on specific subcellular localizations are rapidly accumulating, challenging the common AQP classification and demanding its revision (Wudick *et al*., 2009). Based on function, AQPs were categorized into water-specific aquaporins (AQP1, 2, 4, 5, 6, 8) and aquaglyceroporins (AQP 3, 7, 9, 10) (Jahn *et al*., 2004). Another family has been informally propounded which is called the super family of AQPs (or superaquaporins). This family is comprised of those AQPs which possess deviations in the NPA motifs, suh as AQP11 and AQP12.

Most of the TIP and PIP isoforms are water specific channels, however, some of those may be permeable to other solutes including ammonia, urea and gylcerol (Biela *et al*., 1999, Uehlein *et al*., 2003, Loque *et al*., 2005, Liu *et al*., 2003). TIPs also contribute towards controling transcellular water transport in roots. The increased vacuolar aquaporin activity may accelerate both cell expansion and cell division by increasing water permeability through the vacuolar membrane (Okubo-Kurihara *et al*., 2009). Most of the AQPs are localized at the plasma membrane, however, intracellular AQPs also commonly exist (see review of Nozaki *et al*., 2008). TIP1 (formerly called γ-TIP) of *Arabidopsis* was the first intracellular plant AQP to be found as water permeable (Maurel *et al*., 1993) and later found to be also ammonia permeable (Loque *et al*., 2005).

Although the PIP, TIP, NIP and SIP subfamilies are conserved in plants, homology comparisons demonstrate that plant aquaporins have divergent sequence and function. The divergence is found even among the close relatives within a subgroup

for instance members of the TIP sub-family (discussed later in this chapter) and AtPIP2;x (Alexandersson *et al*., 2005, Sutka *et al*., 2011).

The expression of each aquaporin gene member is regulated differentially. Some are expressed in a constitutive manner and others are expressed in response to external stimuli, such as water stress (Park *et al*., 2010). Most PIP transcripts were found to be down-regulated under the influence of water stress (Alexandersson *et al*., 2005).

1.2 Metal binding in proteins

Almost one-third of the known proteins bind metal ions which serve a variety of roles including regulatory, catalytic and structural (Cousins, 1995). Copper is required by living organisms for cellular processes including signalling of transcription, protein trafficking, oxidative phosphorylation, oxygen transport, electron transfer and respiration (Yruela *et al*., 2005, Singleton *et al*., 2008). However, it is highly toxic if its level exceeds the required limits. Nickel and cobalt are essential components of many metalloenzymes (Mulrooney and Hausinger, 2003). Nature has also evolved metal-binding sites which possess no function at all (Banaszak, 2000).

A metal can form a definite or varying complex species with any particular binding site in a protein depending on pH, metal to ligand ratios and metals concentration with variations in the way it would coordinate (La Mendola *et al*., 2008). The metals like copper and nickel have high affinity for amine groups (Kim *et al*., 2006). Cu in Plastocyanin is coordinated by one Cys, two His and one weakly bound methionine as in most blue-copper proteins (Ullmann, 2001). Nickel has a high affinity for N of the imidazole ring (Ermler *et al*., 1998), although it can also bind to negatively charged amino acids (Bar-Or *et al*., 2001, Jensen *et al*., 2005). A number of Ni-binding enzymes including Urease in eukaryotes (Dixon *et al*., 1975), cis-trans isomerase in *E. coli* (Wülfing *et al*., 1994) and Y3HAO in *Saccharomyces* yeast (Li *et al*., 2006) have been discovered. Ni also regulates the activity of the water channel AQP3 (Zelenina *et al*., 2003).

Among all the known functional groups, thiol is the most reactive group. Thiol is the preferential site for binding of toxic metals and hence toxicologically important (Shaw *et al*., 2004). Mercury has the highest affinity for thiol group and least for phosphate. This characteristic of Hg has been of particular concern in aquaporins (Zelenina *et al*., 2003). Apart from thiol, imidazole group after losing its proton at a pH of 6-7 also becomes a very good ligand for mercury (Yukutake *et al*., 2008).

Sulfur exists in a reduced form (-SH) in cysteine and in an oxidized form (-S-S) as the dual molecule cystine. The Hg-S bond distance is 2.4Å (Marking *et al*., 1998) whereas a disulfide bond is 2.05 Å in length (Hazes and Dijkstra, 1988). The primary sulfur-containing amino acids are cysteine and methionine. Cysteine has unique biological functions, such as being a chelating site for metal ions, or as the active site

of disulfide-reshuffling enzymes (Freedman *et al*., 1994). The voltage-gated ion channel HCN (Hyperpolarization-activated cation) is blocked by Cd and Mg through coordination with Cys. Probably, multiple Cys residues coordinate with a particular metal ion, however, the involvement of single but different Cys residues is also not ruled out (Rothberg *et al*., 2002, Vemana *et al*., 2008). The redox switch in Hsp33 (heat shock protein) is composed of 4 highly conserved cysteines arranged in a C-X-C and C-X-Y-C motif, forming a coordination site for zinc in reduced Hsp33 (Jakob *et al*., 1999).

1.2.1 Mercury sensitivity in AQPs

Excessive water uptake through AQPs can be life-threatening and the discovery of potent and specific inhibitors of AQPs would open new avenues for manipulating the channel proteins for agricultural and pharmacological applications. Despite their enormous importance, specific AQP inhibitors are still lacking and discovering reversible inhibitors is highly desirable.

The effect of Hg too may be non-specific by targeting various other membrane proteins and it may also hinder cellular metabolism. Hg has a higher affinity for the thiol group and this property of Hg was exploited in the present study for prediction of the pore structure as well as to resolve the contrasting mercury sensitivity between ammonia and water permeabilities as reported by Bertl and Kaldenhoff (2007).

AQP1 was the first aquaporin reported to be blocked by $HgCl_2$ owing to a Cys residue located at position 189 (Preston *et al*., 1993). Its side-chain extends into the pore from the extracellular side of the constriction site indicating that inhibition by $HgCl_2$ is a result of physical blocking of the aqueous pathway (Murata *et al*., 2000). The mercury-sensitive Cys residue is located 3 residues N-terminal to the second NPA motif. It is now established in case of mammalian AQPs that the presence of a Cys at either a corresponding position to the above-mentioned residue or in the region close to the second NPA motif confers Hg sensitivity (Preston *et al*., 1993, Raina *et al*., 1995,Verkman *et al*., 1995). The AQP7 is insensitive to Hg because of the absence of a Cys at the required position (Ishibashi *et al*., 1997). In the present study, the above-mentioned position together with nearby residues located inside the pore will be referred to as the "consensus region of metal sensitivity".

However, there are some exceptional cases including AQP2 (Bai *et al*., 1996) and AQP4 (Jung *et al*., 1994a) which could not gain Hg sensitivity even by introducing a Cys at the consensus region. AQP3 is also an interesting case which is sensitive to Hg owing to a residue (Cys11) located in N-terminus (Kuwahara *et al*., 1997). It seems that the molecular mechanisms behind the mercury effects vary in some AQPs (Yukutake *et al*., 2008). Hg sensitivity has been demonstrated in AQPs, otherwise insensitive to Hg, by introducing a Cys residue usually in the afore-mentioned consensus region (Kuwahara *et al*., 1997). AQP4 was reported to be Hg

insensitive when expressed in oocytes (Hasegawa *et al*., 1994), but Hg sensitive in the case of liposomes (Yukutake *et al*., 2008). It was reasoned that in case of liposomes, AQP4 is oriented in a bidirectional manner as against its unidirectional orientation in oocytes. In the former situation, 50% of the reconstituted AQP4 loop D may be exposed to the outside of the proteoliposome. As both the NPA motifs are placed in an antiparallel manner inside the pore, introduction of a Cys residue in loop B (close to the first NPA motif) may take the same charge as Cys189 of AQP1 (Jung *et al*., 1994b, Shi and Verkman, 1996, Kuang *et al*., 2001).

An important case is that of AQP6, which is rather activated after treatment of the cells with mercury and the rise in permeability coefficient was almost two-fold compared to the control (Yasui *et al*., 1999). Similarly, water permeability in AQP1 (from *Anguilla* sp.) was also increased by copper (MacIver *et al*., 2009).

The reversal of inhibition of the permeability can be achieved in AQPs by using a reducing agent like 2-mercaptoethanol. However, in most cases, the recovery was partial (Yang *et al*., 2006, Zilli *et al*., 2009, Jung *et al*., 1994b) and the lack of complete recovery has been proposed to be the result of several factors (see "Results and Discussion"). With respect to the presence of a separate pore possibly conducting gases, detailed studies on mercury inhibition of ammonia permeability are still awaited. Inhibition of water permeability was either absent (Bertl and Kaldenhoff, 2007) or 10 times less than the inhibition of P_{NH_3} (Niemietz and Tyerman, 2000). These reports support the view of separate pathways for water and gas, i.e. the presence of a putative fifth pore in the aquaporin tetrameric topology.

Apart from Hg, mammalian AQPs (AQP1, 2 and 4) are also inhibited by TEA which is a K^+ ion channel blocker (Müller *et al.,* 2008). It was expected that TEA would inhibit other AQP sub-families, which possess a Tyr at the position homologous to Tyr186 in AQP1. However, introducing a Tyr at the homologous position in otherwise insensitive AQPs didn't show any sensitivity, indicating that Tyr alone doesn't suffice (Brooks *et al*., 2000, Detmers *et al*., 2006). Gold and silver have also been reported to inhibit the water specific AQP1 (Niemietz and Tyerman, 2002).

There are two hypotheses prevailing, concerning the inhibitory mechanism of mercury in AQPs: (i) AQPs are inhibited merely because of a steric mechanism inflicted by the presence of mercury atoms in the pore (Fig 1.1) and (ii) Mercury inflicts a conformational change in the AQP because of its interaction with Cys located in the ar/R region (in case of AQP1).

Savage and Stroud (2007), on the basis of structural and functional analyses of the AqpZ mutant, proposed that mercury sterically inhibits AQPs. Based on the Hg-sensitive site Cys189 of AQP1, they constructed the T183C mutant of AqpZ. They superimposed the apo- and Hg-bound structures and found no conformational rearrangement. In a contrasting study, Hg inhibited the water permeability in AQP1 by inducing conformational changes and subsequently collapsing the ar/R region.

However, they did not rule out a simultaneous steric hindrance and/or presence of different mechanisms in different isoforms of AQPs (Hirano *et al*., 2010).

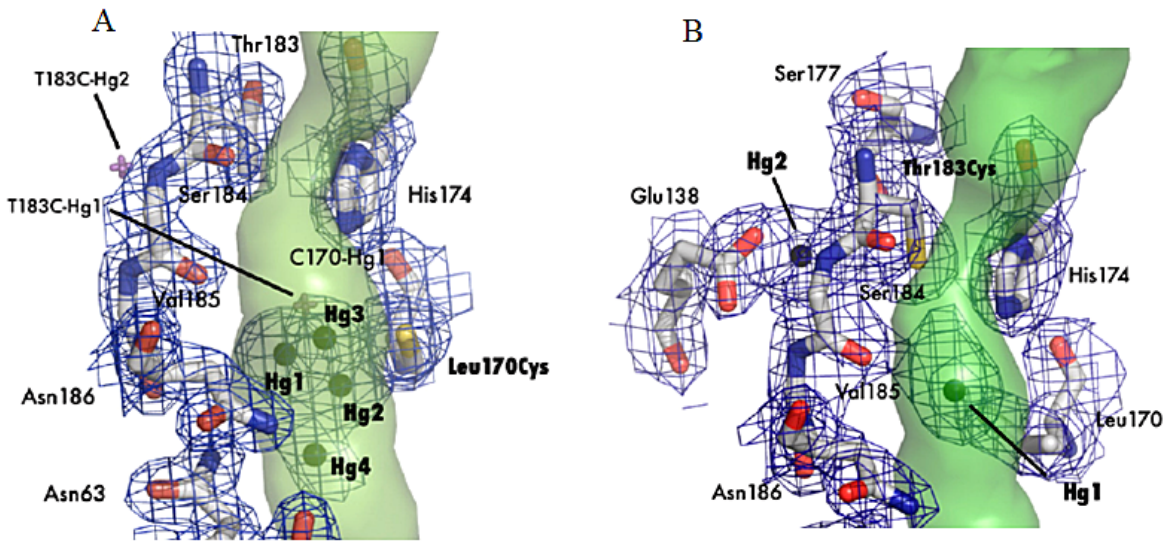

Fig 1.1: Structure of the blocked channel showing steric inhibition by Hg. Amino acids involved with water binding in AQPs are shown as sticks and with 2Fo–Fc electron density mapped contoured at 1.2σ drawn in blue. Mercury atoms are shown as spheres. ***(A)*** Superpositions of Hg atoms from the T183C structure are shown as magenta crosses. This orientation shows that all 3 Hg atoms sterically block the pore. ***(B)*** This orientation shows that T183C-Hg1 sterically blocks the pore (green surface) (Adopted from Savage and Stroud, 2007).

1.3 Structural characteristics of aquaporins

Aquaporins exist as a homotetrameric arrangement, where each subunit is an independent water pore. An aquaporin subunit has six membrane spanning domains linked by three extra- and two intracellular loops and both N- and C-terminals are localized in the cytosol (Fujiyoshi *et al*., 2002). AQP1 tetramers are held together by extensive interactions between the monomers (Murata *et al*., 2000, Sui *et al*., 2001). Transmembrane helices 1 and 2 from one monomer form a left-handed coiled-coil interaction with helices 4 and 5 of a neighboring monomer. Helices from neighboring monomers also interact outside the membrane: helix 1 interacts with helix 5 of the adjacent monomer at the extracellular surface and helix 2 interacts with helix 4 of the adjacent monomer at the cytoplasmic surface (Murata *et al*., 2000, Sui *et al*., 2001).

1.3.1 Structure of the AQP pore

The AQP pore acts as a two-stage filter. The first and major barrier is the narrowest constriction in the pore known as "ar/R" (aromatic/Arginine) region, which is located towards the extracellular side. The second stage filter in the pore is the NPA (Asn-Pro-Ala) region located at the center of the pore (de Groot and Grubmüller, 2001). The distance between both the selectivity regions is approximately ~10 Å whereas the entire pore length is ~25 Å (Newby *et al*., 2008).

The two highly conserved NPA motifs are located in loops B and E, which meet in an antiparallel manner and form part of the central pore constriction. Loop B connecting TM helices 2 and 3 folds back to place the first NPA motif at the middle of the membrane. Likewise, the loop E connecting TM helices 5 and 6 folds back to place the second NPA motif opposite to the first one. Both NPA regions are held together by van der Waals interaction between the two Pro residues and also between Pro and Ala residues (belonging to different motifs). Each monomeric channel is composed of two half-membrane spanning repeats, and about half of each repeat is α-helical. The N-termini of the helical repeats meet at the NPA motifs, located near the channel center (Fu *et al*., 2000, Nollert *et al*., 2001, de Groot *et al*., 2003).

The ar/R region (commonly known as selectivity filter; SF) is constituted by 4 amino acids, one constituent is completely conserved Arg (except TIP1 and SIP1) giving the constriction its name. SF of the best known human AQP1 comprises of Phe, His, Cys and Arg. The ar/R region of PIPs, particularly in the case of *Arabidopsis,* contains Phe, His, Thr apart from the Arg. The respective positions will be hereafter referred to as H2, H5, LE1 and LE2. However, TIPs sub-family shows a lot of diversity as compared to PIPs (Wallace and Robert, 2004) (also see Table 1.1). TIPs have 5 different kinds of selectivity filters. The position H2 is always occupied by His in case of TIP1, 2, 3, 4(s). The position H5 is occupied by a smaller hydrophobic residue (Ile, Val, Ala etc) (Bansal and Sankararamakrishnan, 2007). The positions LE1 and LE2 in aquaporins could be important candidates for determining metal sensitive site and the selectivity mechanism, respectively. The former position corresponds to the Hg-sensitive site Cys189 in AQP1 and the latter position has a conserved Arg with interesting exceptions in some TIP isoforms (details will follow in this chapter).

Table 1.1: Aromatic/Arginine signatures that are identical or similar in *Arabidopsis*, rice and maize.

MIP Members	H2	H5	LE1	LE2
PIP family				
All OsPIPs, ZmPIPs and AtPIPs	F	H	T	R
TIP family				
OsTIP1;1/1;2 ZmTIP1;1/1;2 AtTIP1;1/1;2/1;3	H	I	A	V
OsTIP2;1/2;2/2;3/3;1/3;2/4;3 ZmTIP2;2/2;3/3;1/4;4 AtTIP2;1/2;2/2;3/3;1/3;2/4;1	H	I/M/V	G/A/S	R
AtTIP5;1	N	V	G	C
NIP family				
OsNIP1;1/1;2/1;3/1;4/1;5 ZmNIP1;1 AtNIP1;1/1;2/2;1/4;1/4;2	W	V	A	R
OsNIP3;1/3;3 ZmNIP3;1 AtNIP5;1/6;1/7;1	A	I/V	A/G	R

Adopted from: Bansal and Sankararamakrishnan (2007)

1.3.2 Mechanism of water permeation

The mechanism of water permeation in human AQP1 is described in brief to illustrate the general behavior of the AQP pore. The pore can accommodate only one water molecule at any place in the pore and the molecules are conducted in a single file. At the extracellular side, the hAQP1 pore is wider and the water molecule entering the pore would interact with the A and C loops through Lys36 and Ser123, respectively (de Groot and Grubmüller, 2001). The first major site of interaction with the water molecules is ar/R, which is located close to the extracellular pore mouth and forms the narrowest constriction in the pore (Fig 1.2a). The SF region has a diameter of almost 2.8 Å, which is similar to the size of a water molecule. Water conduction through the SF is facilitated by the presence of hydrophilic moieties however, the rest of the channel is lined by mostly hydrophobic residues exposing the main chain carbonyl oxygens, which serve as hydrogen bonds acceptor for the small-sized solutes (Lee *et al*., 2005, Sui *et al*., 2001, Murata *et al*., 2000). The role of SF in imposing the selectivity barrier in AQPs is discussed elsewhere in this chapter. At this site, a water molecule is rotated at 180^0 under the influence of electrostatic forces imposed by the short helices HB and HE (de Groot and Grubmüller, 2001). The next site for a major interaction of a water molecule is the NPA region.

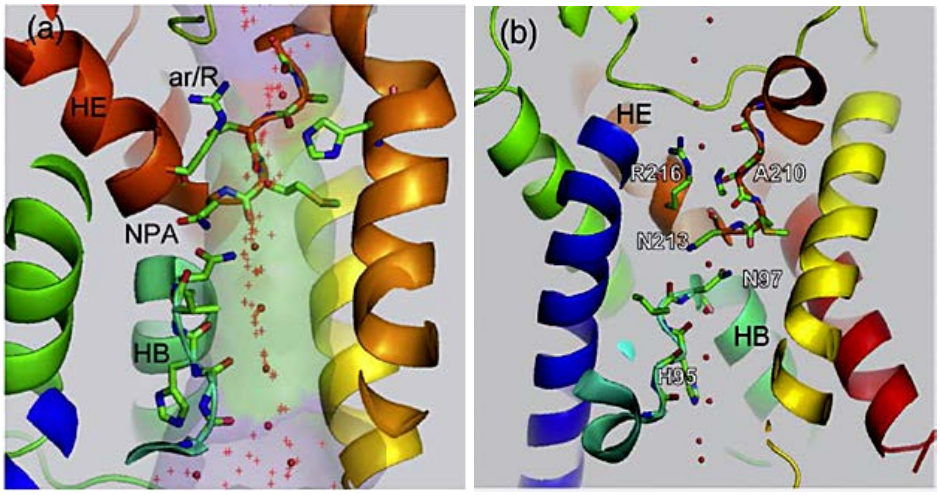

Fig 1.2: Pore view of the AQP4 channel. ***(a)*** A side view showing pore diameter presented as a transparent surface. The positions of water molecules seen in other AQP structures available to date are shown as red crosses. The narrowest ar/R region is shaded as red ***(b)*** Residues interacting with water molecules (red spheres) in the pore are shown as ball-and-stick models. Adopted from Tani *et al*. (2009).

The Asn residues belonging to both NPA motifs are juxtaposed (Fig 1.2b) and serve in the hydrogen bonding with water molecules (de Groot *et al*., 2001). Two different modes of coordination between water and the two Asn residues of both NPA motifs have been demonstrated. In bacterial AqpZ and *E. coli* aquaglyceroporin GlpF, a single water molecule inside the pore which is positioned between the NPA motifs, receives hydrogen bonds from both the Asn residues of the motifs (Savage *et al*., 2003, Tajkhorshid *et al*., 2002). On the contrary, in AQP4, water is not positioned between the motifs. Also a given water molecule would interact with Asn of only one NPA motif (Ho *et al*., 2009).

Water molecules keep on moving down the pore interacting with carbonyl groups of the pore-lining residues (Cys189, Gly190 and Ile191 in case of AQP1) (de Groot and Grubmüller, 2001).

The pore widens again toward the intracellular side (Fig 1.2b). After leaving the selectivity regions, water molecules interact just weakly with the narrow constriction formed by Gly72, Ala73 and His74 located in loop B (de Groot and Grubmüller, 2001, de Groot *et al*., 2003). After interaction with the backbone carbonyl groups of this constriction, water is ready to exit from the pore. Water molecules are escorted out of the pore by a mechanism comprising of His76 and Val155. Interestingly, His76 often kept the pore blocked and was proposed to control the water flow (Sui *et al*., 2001, Smolin *et al*., 2008). AQP0 also has a similar phenyl barrier, both at the extracellular (owing to Tyr23) and the cytoplasmic side (owing to Tyr149); both residues are capable of occluding the pore, though by different mechanisms (Jensen *et al*., 2008).

An important feature of the AQPs pore is preventing the proton conductance. Two mechanisms for exclusion of protons from the pore have been demonstrated: (i) interruption of the hydrogen-bond network for which the short pore helices HB and HE are crucially important (Tani *et al*., 2009, de Groot and Grubmüller, 2005) (ii) the presence of a strong energy barrier inside the pore. The major barrier, while comparing both the selectivity regions, originates from the ar/R region (Li *et al*., 2011, Wu *et al*., 2009). One of the amino acids constituting the ar/R region is a highly conserved Arg. The positive electrostatic potential prevailing in this narrow constriction when shifted towards neutral or even negative would result into leakage of protons through the pore (Beitz *et al*., 2006, Oliva *et al*., 2010, Chen *et al*., 2007). Apart from the Arg, His and the positive dipoles of the short helices HB and HE also impose a strong energy barrier to prevent the conduction of protons (de Groot *et al*., 2003, see review of Agre *et al*., 2002).

1.3.3 Gas permeation through the tetrameric pore

AQPs are not only water conducting channels, but have also been demonstrated to facilitate solutes including gases like CO_2 (Prasad *et al*., 1998, Uehlein *et al*., 2003) and NH_3 (Jahn *et al*., 2004, Loque *et al*., 2005). It is however, still a matter of debate if the gases permeate through the water pore or through the central pore of the tetramer.

The MD simulations revealed full permeation events through the central pore during which both CO_2 and O_2 were observed inside the central pore (Yu *et al*., 2006, Wang *et al*., 2007). The water pore was less permeable to gases than the central pore because of the higher energy cost required to replace the interacting water with the protein. Although the conditions are favorable to more hydrophobic O_2, the water pore may conduct CO_2 more efficiently.

Two hydrophobic residues in AQP4 (Leu66 and Leu191) form the outermost gates that restrict the water to enter the central pore (Wang and Tajhorshid, 2010). A similar gating mechanism was also observed in AQP1 (Yu *et al*., 2006).

1.4 Ammonia transport through membrane proteins

Ammonia is an important nutrient which is taken by living organisms from their surroundings as a source of nitrogen for amino acid synthesis. Higher levels of ammonia are toxic and are to be lowered down at the expense of significant energy. It is present in all compartments of the cell, although its concentration varies depending on a number of factors including ammonia concentration in the neighbouring compartment, changes in electrical potential and pH (Perez-Garcia, 2011, Wright *et al*., 1995, Miller *et al*., 2001).

Plants have evolved separate, high affinity transport systems for NH_4^+ and K^+ which may be classified into 2 categories: (i) The low-affinity transport system (LATS) appears to be constitutively expressed and discriminates less well between K^+ and NH_4^+. (ii) The high-affinity transport system (HATS) is regulated by the nitrogen status of plants; the depletion of nitrogen will lead to an increase in the activity of HATS (Howitt and Udvardi, 2000).

Ammonia exists as two molecular forms NH_3 and NH_4^+ in aqueous solutions. At physiological pH, >98% of total ammonia is present as NH_4^+ (Woeber *et al*., 1963). The permeability of NH_4^+ is 175 times lower than that of NH_3. However, the concentration of NH_4^+ available is higher by a factor of 110 because at a neutral pH and a total concentration of 100 mM, only 0.90 mM will be in the form of NH_3 (Abdoun *et al*., 2005). The manipulation of both factors suggests that for every single millimole passing through the membrane, more than 60% of the total ammonia will be conducted as NH_3. The Henderson-Hasselbalch equation can be used for determining the ratio between both forms of ammonia at any particular pH. In the present study, the term "ammonia" will be used to refer to both the ammonia species, i.e. NH_3 and NH_4^+.

The membrane ammonia transporters comprise a family in which ammonium transporter in plants (Amt) (Ninnemann *et al*., 1994), methylamonium permease (MEP) in yeast (Marini *et al*., 1994) and the homologues of AMTs in animals that is Rhesus (Rh) (Marini *et al*., 2000, Liu *et al*., 2000) are collectively termed as Amt/MEP/Rh.

Although, aquaporins have been widely characterized for their water function, many of these are expected to be ammonia conducting. The molar volume of ammonia (24.9 cm^3/mol) is not much higher than that of water (18 cm^3/mol). Also, the AQPs are already known to conduct another gas CO_2 (Prasad *et al*., 1998, Uehlein *et al*., 2003).

Ammonia-permeable aquaporins are found among those which exclude solutes larger than water (Zeuthen *et al*., 2006). AQP1 was the first aquaporin reported to be ammonia permeable (Nakhoul *et al*., 2001). Since then several AQPs have been characterized for their ammonia function which include mammalian AQP8 (Holm *et al*., 2005, Yang *et al*., 2006) and plant TIP2;1 (Jahn *et al*., 2004) among the aquaporins, and mammalian AQP3, 9 among the aquaglyceroporins (Holm *et al*., 2005).

A. Which ammonia species is transported?

Whether ammonia is transported through the channels in electroneutral (NH_3) or electrogenic (NH_4^+) form is not yet fully understood. In fact, several modes of ammonia transport have been suggested which support electroneutral NH_3 transport,

NH_4^+/H^+ antiport, NH_3/H^+ symport, or NH_4^+ transport (see review by Søgaard *et al*., 2009).

The plant Amt proteins studied to date transport charged species i.e. NH_4^+ (Ludewig *et al*., 2002, 2003, Mayer *et al*., 2006). In a similar report, Sohlenkamp *et al*. (2002) changed the pH in the external medium between 5.5 and 8.0 and observed no effect on Km of the ammonium, implying that it is NH_4^+ and not NH_3 which is being transported through AMT1;1. The crystal structures of bacterial AmtB suggested that the species bound may be NH_4^+ but the one transported is probably NH_3 (Zheng *et al*., 2004, Khademi *et al*., 2004). The fate of dissociated H^+ was however not determined.

Sequence alignments of the members from MEP and Rh transporters reveal that the pore lining residues are highly conserved, indicating that the entire family conducts uncharged NH_3 (Winkler, 2006). AQPs probably prefer ammonia to permeate as electroneutral species as observed in case of AQP8 (Saparov *et al*., 2007).

B. Mechanism of ammonia transport:

Crystal structures (Gruswitz *et al*., 2010, Khademi *et al*., 2004, Zheng *et al*., 2004) and MD simulations (Akgun and Khademi, 2011, Yang *et al*., 2007, Lamoureux *et al*., 2010, Nygaard *et al*., 2006) data have demonstrated the mechanism of ammonia transport in bacterial AmtB (Fig 1.3) and the human RhCG. The channel lies between the outer (periplasmic) and the inner (cytoplasmic) vestibules. Ammonia transport involves a periplasmic vestibule, where it is recruited as well as deprotonated because of the reason that the channel would allow only the electroneutral form NH_3. The channel must lower the pK_a of ammonia to ensure that it retains its neutral form throughout the pore length.

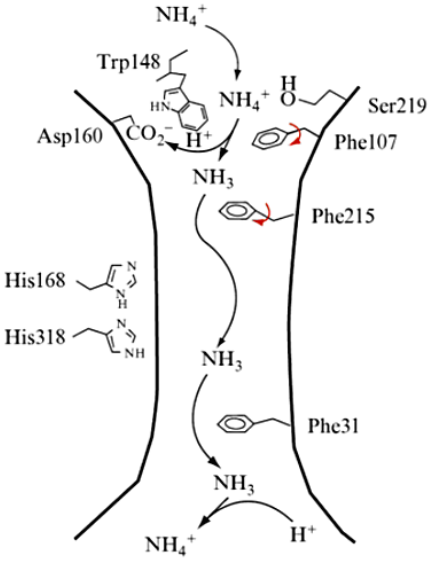

Fig 1.3: Illustration of the NH_4^+/NH_3 transport mechanism through the *E. coli* ammonia transporter AmtB (Adopted from Khademi *et al*., 2004).

This periplasmic vestibule is rich in aromatic rings and can bind NH_4^+ through cation-π interactions. It is comprised of Phe103, Phe107, Trp148, Phe215 and Ser219. The channel pathway is controlled by the aromatic rings of two highly conserved residues, Phe107 and Phe215, which are located between the periplasmic vestibule and the lumen. The Phe gate is commonly present in AmtB and the human Rhesus channel. The channel lumen is 20Å in length and is too hydrophobic to transport water (Khademi and Stroud, 2006). Some reports however demonstrated the presence of water molecules inside the pore lumen (Nygaard *et al*., 2006, Lamoureux *et al*., 2007). Ammonia is reprotonated at the cytoplasmic site again to form NH_4^+ and is ready to exit.

1.4.1 Molecular determinants of selectivity in AQPs

Both size and hydrophobicity in the ar/R region determine ammonia selectivity. Although the larger solutes like glycerol and urea are restricted sterically, even smaller solutes like H_2O, CO_2 and O_2 may be restricted by higher hydrophobicity in AQP pore (Hub and de Groot, 2008, Wu *et al*., 2009, Savage *et al*., 2010). The amino acid composition and their arrangement also don't suffice for selective permeability. An interesting example is Glpf (an aquaglyceroporin) which has a lower water conductance than the water specific pores. The SF of Glpf and the PfAQP (aquaporin of protozoa) are identical but the water permeability of the former AQP is lower (Hub and de Groot, 2008).

The ammonia permeability in AQP8 and TIP2;1 requires that a histidine directly flanks the conserved Arg at the LE1 position of the SF (Zeuthen *et al*., 2006). If an AQP1 mutant is generated in which the His at position 180 is substituted by Ala, the water specific AQP1 becomes ammonia permeable (Beitz *et al*., 2006).

Litman *et al*. (2009) compared the variations in the selectivity regions of the predominantly water conducting pores against the ammonia conducting ones (see a logoplot in Appendix I.1). At position H5, water specific AQPs (AQP1, 2, 4, 5, 6) have a His residue, aquaporins permeable to water, glycerol, and ammonia (AQP3, 7, 9, 10) have mostly got a smaller residue, Gly, ammonia- and water permeable AQP8 has an Ile. In case of the ammonia permeable TaTIP2.1, replacing Ile by a His and the Gly at LE1 position by Cys (mimicking the SF composition of AQP1) abolished the ammonia transport function whereas the P_f remained unaffected (Jahn *et al*., 2004). Focusing the same positions, water specific AQP1 was converted into a ammonia channel (Beitz *et al*., 2006).

The determinants of selectivity in AQPs are extended beyond the SF region (Liu *et al*., 2005a, Savage *et al*., 2010). The AtPIP2 mutants mimicking the ar/R region of AtTIP1, 2 and 4 did not (or minimally) conduct urea, although native TIP1, TIP2 and TIP4 homologs are known to transport this solute. This implied that TIP-like SF

doesn't suffice to induce NH_3 permeability in PIP2. TIP1 channels have a unique ar/R filter, in which the highly conserved Arg is replaced by Val (Table 1.1), this variation however is not critical for ammonia/urea transport (Dynowski *et al*., 2008).

1.5 Aims of the present study

The present study was aimed at achieving the following objectives:

1. Investigating the already reported contrasting effect of mercury to inhibit water/ammonia permeability in TaTIP2;2 with particular reference to the putative tetrameric pore. Also, it was aimed to determine the mercury-sensitive site by sequentially substituting the native Cys residues.

2. Determination of molecular signatures taking part in ammonia/water selectivity in TaTIP2;2 (ammonia/water channel) and NtPIP2;1 (water specific channel):
(i) Functional studies on corresponding point mutations outside the selectivity regions; mutations were suggested by the sequence comparison.
(ii) Studies on mutations of corresponding residues in the selectivity regions. The functional studies were also extended to involve the exchange of certain loops and TM helices.

2 RESULTS & DISCUSSION

2.1 Studies on metal sensitivity in wheat TIP2;2

The TaTIP2;2 investigated in the present study is known to be permeable to both water and ammonia. In an earlier report, the ammonia transport was significantly inhibited by $HgCl_2$ however; the water transport was proved to be insensitive (Bertl and Kaldenhoff, 2007). This difference of sensitivities led me to postulate that water and ammonia transport follows different pathways in TaTIP2;2. The present study was conducted to determine which of the native Cys residue (if at all) is involved in coordination with mercury and subsequent decrease in ammonia permeability. Apart from mercury, other heavy metals like copper and nickel were also employed in this study to determine their effect on water and ammonia transport function of wheat TIP.

2.1.1 Comparison of ammonia permeability in various yeast strains

The present study involved investigation of ammonia and water transport function in a number of variants of the wheat TIP2;2. Incidentally, this aquaporin was contained by the SY1 strain of *Saccharomyces cervisiae*, which is not perfect for the studies on ammonia transport function as it contains endogenous ammonia/ammonium transporters. Some preliminary experiments, however, revealed that SY1 and a yeast strain (31019b) which has all three putative ammonium transporters MEP1, MEP2, and MEP3 deleted were both nonfunctional for ammonia transport. Despite these results, the strain 31019b was chosen for the entire studies.

Owing to the above-mentioned outcome, it was decided to investigate various yeast strains for their ammonia transport function under our experimental conditions. Altogether, three strains, i.e. SY1 (Nakamoto *et al*., 1991), BJ5458 (Suga and Maeshima, 2004) and 31019b (Marini et al.,1997) were investigated. All three strains showed a rather low background ammonia permeability; a quite surprising outcome in case of SY1 and BJ5458 strains, which contain the afore-mentioned ammonia transporters. Raw kinetics are presented in Fig 2.1.1. Currently, the only available explanation is that the Mep transporters possess a high affinity for ammonia and are saturated at very low ammonia concentrations (in the μM range) (Loque and Wiren, 2004). In the present study, ammonia concentration used in the outer solution was 25mM which is several orders of magnitude higher. The initial phase of ammonia conductance is fastest but is very brief hence it remains (at least) partially undetected by the photomultiplier. However, this outcome was not further investigated as it was beyond the scope of the present study.

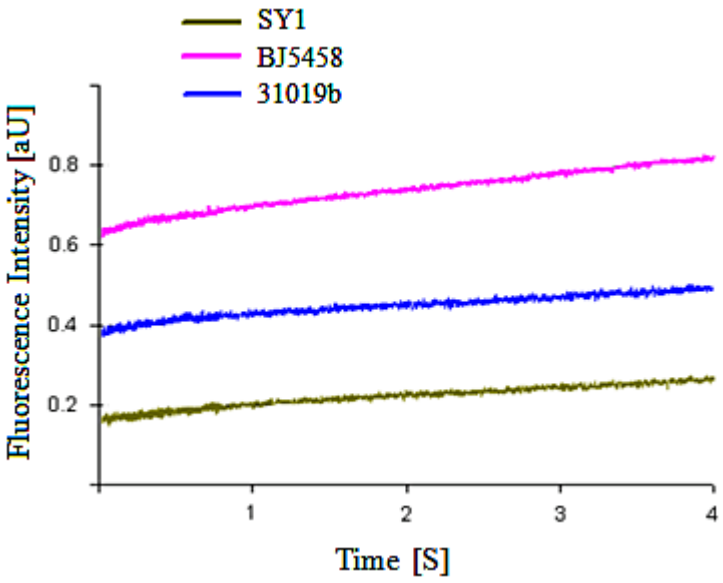

Fig 2.1.1: Ammonia permeability in various strains of *Saccharomyces* is presented as raw kinetics (without normalizing). The time courses represent changes in fluorescence intensity due to change in pH after subjecting the yeast cells to an outer solution containing 25mM NH_4Cl. Each time course is the average of 20-40 kinetics obtained from 3 individual experiments. The total number of traces acquired for each of the constructs was at least 50. Note: (i) the strain 31019b is devoid of any endogenous ammonia transporters (see the text for details on given strains), (ii) the time courses of ammonia permeability in non-transfected yeast as well as the yeast cells containing an empty vector were similar.

2.1.2 Functional studies in Cys mutants

There are three native Cys residues in TaTIP2;2 at positions 63, 123 and 237. Cys63 is located in transmembrane helix 2, Cys123 in TM 3 and Cys237 in the C-terminus (Fig 2.1.2). Cys123 has been presumed to be of particular significance being a possible "analog" to the well-characterized mercury-sensitive Cys residues located in loop E of a number of orthodox AQPs (for instance Cys189 in AQP1) (Preston *et al*., 1993). In contrast, Cys237 was considered to be least significant as there is no report available to-date concerning the involvement of any C-terminal residue in heavy metals sensitivity of AQPs.

Therefore the latter Cys was omitted and the other two native Cys residues were mutated to alanine resulting in the C63A and C123A mutants. Further, a double mutant (C63A/C123A) was also generated substituting both the native Cys residues. To analyse the function of these mutants in comparison to the wild type wheat TIP, the constructs were transferred into the heterologous yeast expression system. Water permeability coefficients (P_f) of yeast protoplasts were determined after hypoosmotic shock prior to or after $HgCl_2$ pre-treatment. The time courses of wild type and various mutants of TaTIP2;2 are presented in Fig 2.1.2 The data revealed that P_f values for wild type TaTIP2;2 and the mutant C63A were not significantly different.

However, the rest of the mutants including C123A and the double mutant C63/123A exhibited significantly higher coefficients of osmotic permeability (Fig 2.1.4A). See Appendix 1A for detailed P_f values comparison. The increased P_f due to substitution of Cys123 implies a structural and/or functional role of Cys at this position.

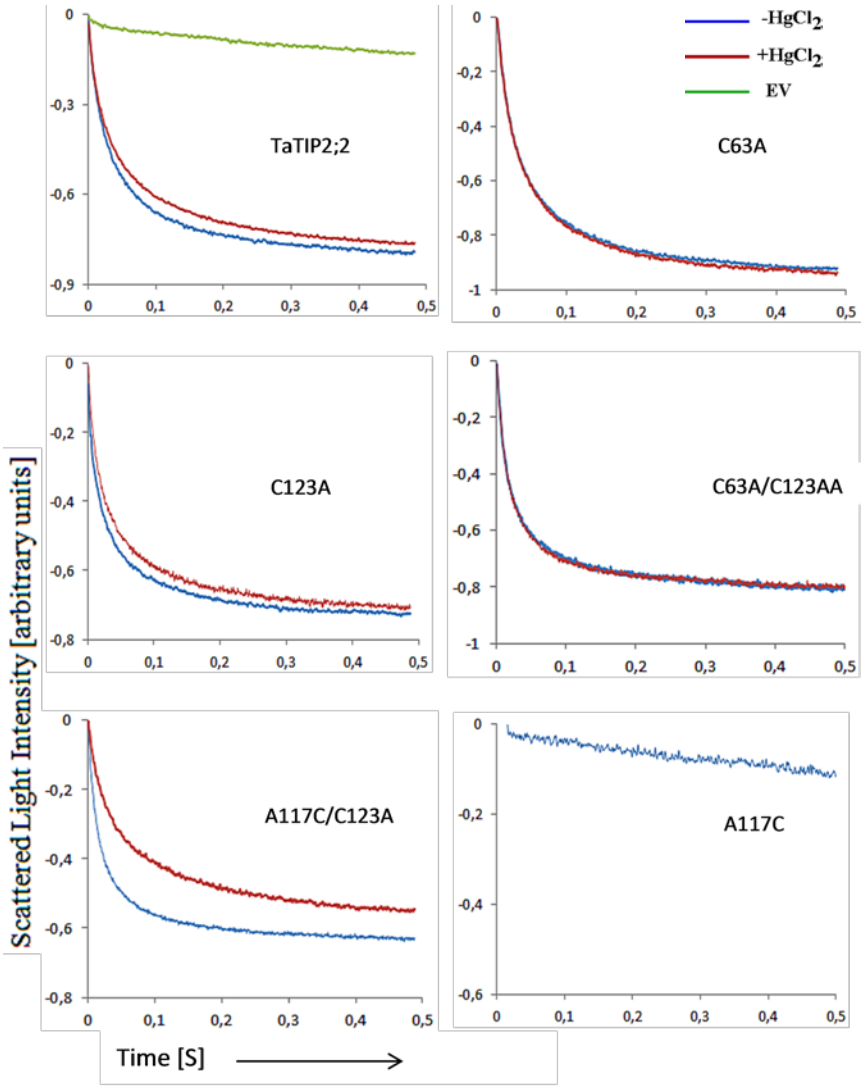

Fig 2.1.2: Water permeability and its inhibition by mercury in protoplasts of *Saccharomyces cerevisiae* yeast cells. The figure contains time courses of changes in scattered light intensity in TaTIP2;2 and its mutants after subjecting the yeast cells to a hypoosmotic shock of 300 mosmol with and without preincubation with 1mM $HgCl_2$. All the time courses are presented after normalization, however the panel for A117C mutant shows a raw time course (without normalizing) due to the reason that normalization elevates the initial brief but faster component by several orders of magnitude. Each time course the is the average of 20-40 traces obtained from 3 individual experiments. The total number of traces acquired for each of the constructs was at least 50. Note different scales along the y-axis. Also note that the followings are described in detail under separate captions in this chapter: (i) the investigation on Hg-sensitivity in TIP is described in detail under the caption 2.1.3, (ii) the Ala-to-Cys mutants (single and double) involve introduction of a Hg-sensitive site into TIP and are described in detail under caption 2.1.3.1.

The afore-mentioned Cys-to-Ala mutants were also subjected to stopped-flow spectroscopy to study ammonia permeation. The time courses of wild type TIP and its various mutants are presented in Fig 2.1.3. All the single and double mutants (except C63A) were faster in P_{NH_3} (Fig 2.1.4B) compared to the wild type TIP. The rise of P_{NH_3} in case of the single mutant Cys123 as well as both the double mutants (C63/123A, A117C/C123A) was approx. 30% of the P_{NH_3} value of wild type TIP. The mutant C63A was just slightly slower than the wild type (See Appendix 1B for detailed comparison of P_{NH_3} values). It is important to note that simultaneous replacement of native cysteines (the case of double mutant C63/123A) increased both water and ammonia permeabilities.

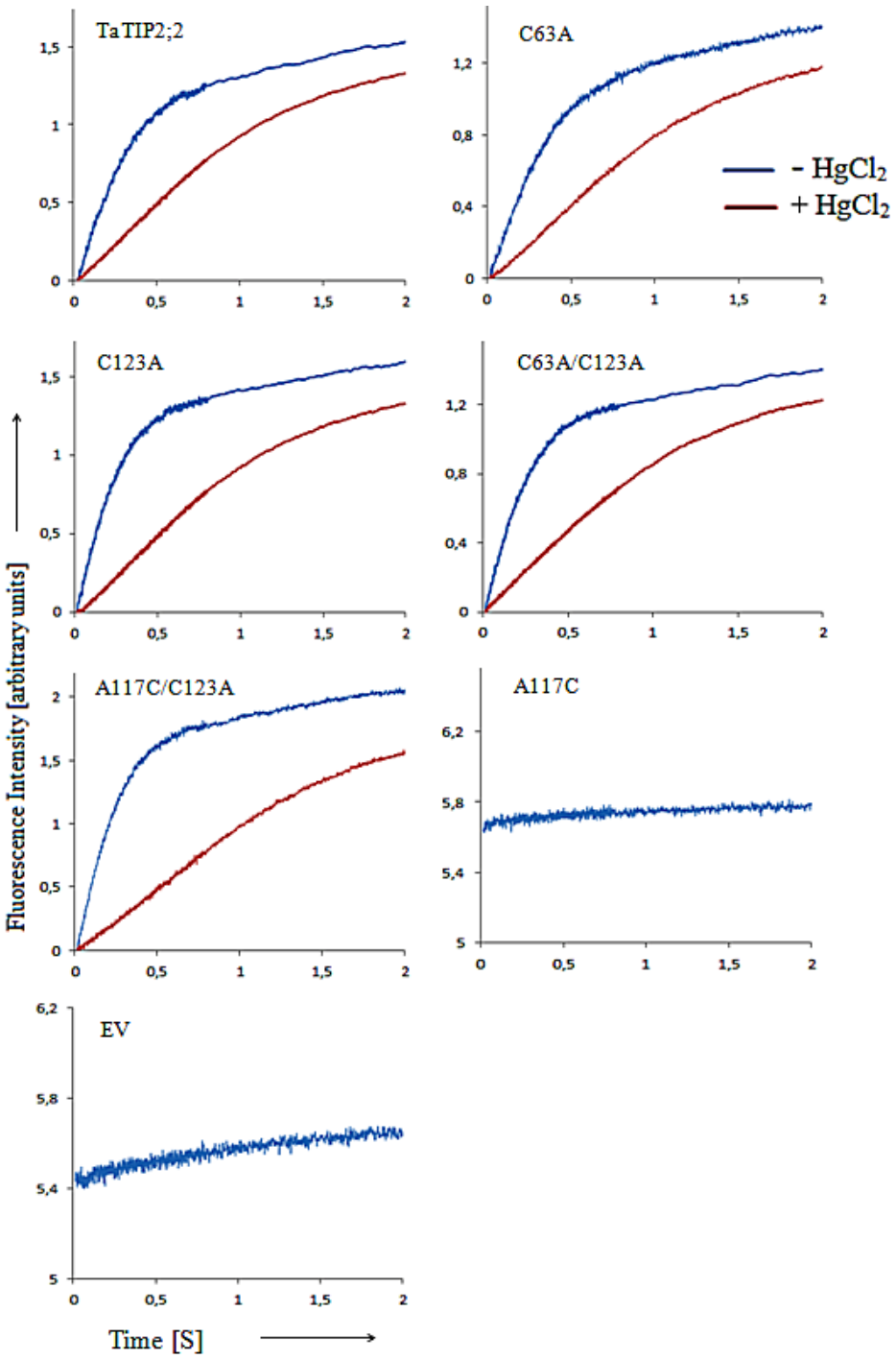

Fig 2.1.3: Ammonia permeability and its inhibition by mercury in *Saccharomyces cerevisiae*-yeast cells. The figure contains time courses of changes in fluorescence intensity in TaTIP2;2 and its mutants after subjecting the yeast cells to an outer solution containing 25mM NH_4Cl with and without preincubation with 1mM $HgCl_2$. All the time courses are presented after normalization, however the panel for A117C mutant shows a raw time course (without normalizing) due to the reason mentioned in the previous figure. Each trace is the average of 20-40 kinetics obtained from 3 individual experiments. The total number of traces acquired for each of the construct was at least 50. Note different scales along the y-axis. Also note that the followings are described in detail under separate captions in this chapter: (i) the investigations on Hg-sensitivity in TIP are described in detail under the caption 2.1.3, (ii) the Ala-to-Cys mutants (single and double) involve introduction of a Hg-sensitive site into TIP and are described in detail under the caption 2.1.3.1.

Cys63 is located in the transmembrane helix 2 which takes part in pore formation (Kjellbom *et al.*, 1999, Murata *et al.*, 2000). The TM2 in combination with TM5 adopts the mechanism of "fitting of ridges into grooves" and the two AQP1 helical bundles are locked together near the 4-fold axis of the tetramer (Murata *et al.*, 2000). A residue (Asn60) located in the middle of TM2 was reported to be involved in anion permeability of AQP6 (Liu *et al.*, 2005a). The ar/R region is widely believed to impart solute selectivity to the AQPs and is constituted by a tetrad of amino acids, one of which always belongs to TM2 (further details are given in Section 2.3 of results and discussion) (Gupta and Sankararamakrishnan, 2009).

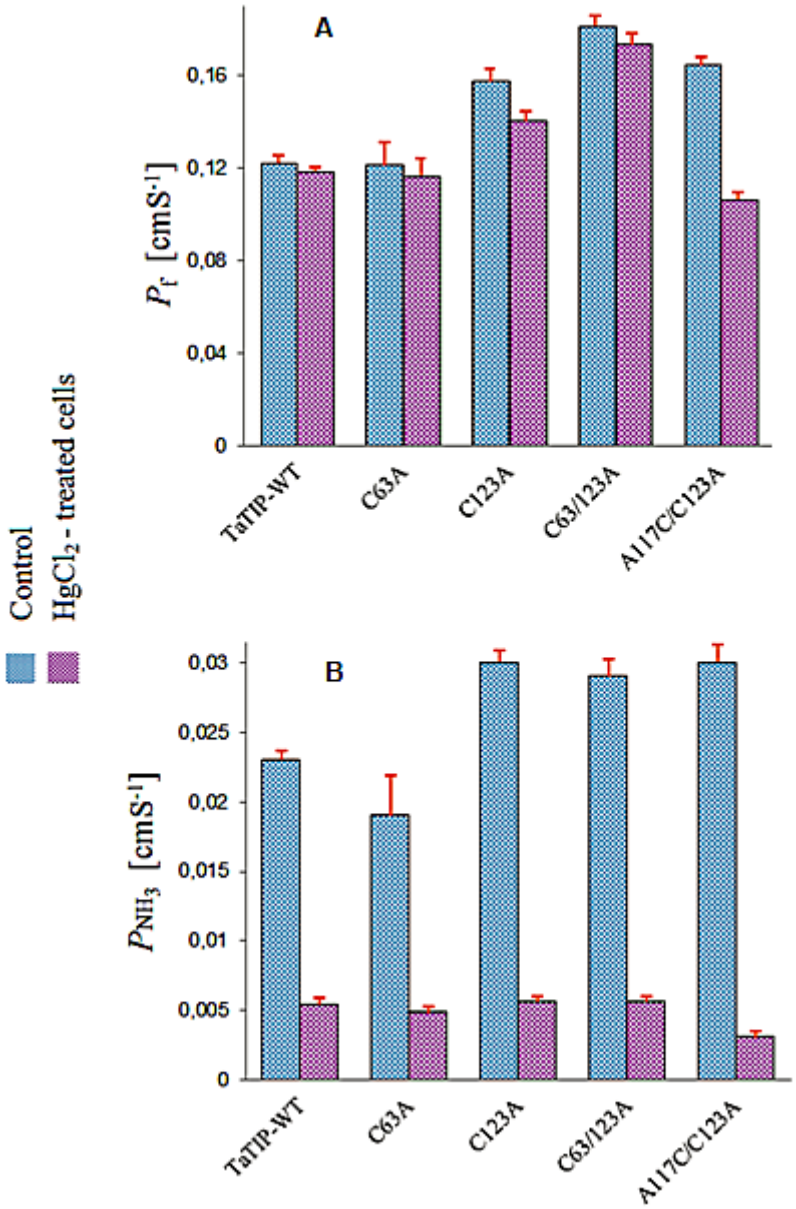

Fig 2.1.4: Coefficients of water ***(A)*** and ammonia ***(B)*** permeabilities determined in various mutants of TaTIP2;2 are presented in the bar chart. *Saccharomyces* protoplasts (in case of water permeability) or whole cells (in case of ammonia permeability) were treated with 1mM $HgCl_2$ for 5 min to determine the inhibitory effect. The data presented are the averages of 20-40 kinetics acquired from 3 individual experiments. The total number of

traces acquired for each of the construct was at least 50. Error bars indicate standard error of the mean. Note that the followings are described in detail under separate captions in this chapter: (i) the investigation on Hg-sensitivity in TIP is described in detail under the caption 2.1.3, (ii) the double mutant A117C/C123A involves introduction of a Hg-sensitive site into TIP and is described in detail under the caption 2.1.3.1.

The substitution of cysteines at positions 63 and 123 in combination increased water as well as ammonia permeabilities, which implies their role in solute permeability. The single mutant Cys63Ala, however, had P_f and P_{NH_3} values similar to the wild type. (Fig 2.1.4B, Appendix 1A, 1B). As no resolved structural data is available for the TIP sub-family of AQPs, a homology model of TaTIP2;2 was drawn to locate the positions of Cys residues using the "SWISS-MODEL" online tool. The tool performed a database-search for the availability of crystal structure of the closest homolog of the TaTIP2;2, which was hAQP4 (Tani *et al.*, 2009). This tool used crystal structure of AQP4 as template to provide the coordinates which were used to draw a model (Fig 2.1.5) which indicated that all the cysteines including Cys123 were located away from the pore and as such they seemed to have no role in influencing the pore dynamics and are unable to coordinate with the metals.

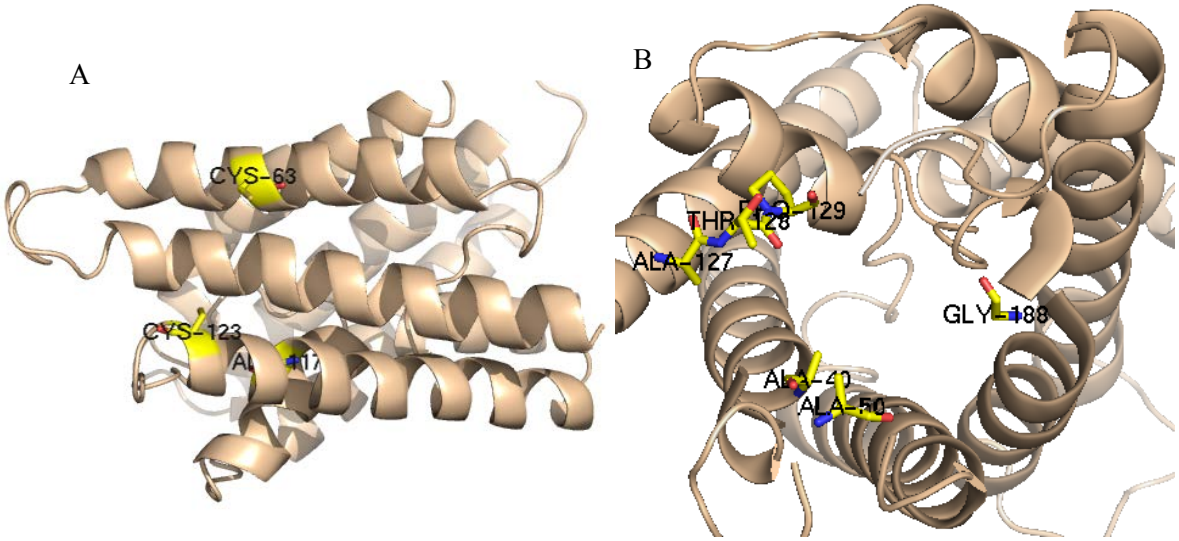

Figure 2.1.5: Homology models of TaTIP2;2 ***(A)*** A side view to show the location of native Cys63 and Cys123 residues in ribbon representation. Also shown is Ala117 which is homologous to Hg-sensitive Cys in γ-TIP. ***(B)*** The residues constituting the extracellular vestibule of the pore in TaTIP2;2-WT. Ala40, Ala50, Gly188, Ala127, Thr 128, Pro129 have been highlighted. The coordinates provided by the online tool "SWISS-MODEL" were used to draw the model in the software PYMOL. SWISS-MODEL used the hAQP4 crystal structure (PDB entry # 3GD8) as template.

2.1.3 Mercury sensitivity in TaTIP2;2

A typical feature of most of the AQPs characterized so far is their sensitivity against mercury. TaTIP2;2 is reported to be one of the several AQPs that are insensitive against mercury (Bertl and Kaldenhoff, 2007). In the present study, the single (Cys63 and Cys123) as well as the double (C63/123A and A117C/C123A) mutants were investigated for their sensitivity against mercury. The yeast protoplasts (in case of P_f determinations) and the whole cells loaded with fluorescein (in case of P_{NH_3} determinations) were subjected to mercury treatment prior to stopped-flow measurements. Surprisingly, in all the mutants, P_f remained unchanged (Fig 2.1.2, 2.1.4A) whereas P_{NH_3} was reduced by the mercury treatment (Fig 2.1.3, 2.1.4B). The optimal concentration required for the inhibition of ammonia transport was 1mM giving almost 80% inhibition after 5 minutes of pre-incubation with mercury. The pattern of inhibition in wild type as well as in all the mutants was comparable which implied that none of the cysteines had any role in inhibition and a common mechanism is responsible for the decrease in P_{NH_3}. The detailed comparison of P_{NH_3} values is given in Appendix 1B.

It was decided to thoroughly investigate the contrasting effect of mercury on P_f and P_{NH_3}. The yeast cells or protoplasts were preincubated with different concentrations of $HgCl_2$ to study the inhibition pattern against the concentration gradient of mercury and to determine the minimum possible concentration required for maximum inhibition of ammonia transport function. This experiment was performed only with the wild type TIP (no mutants were studied) and $HgCl_2$ concentration ranged from 1 µM to 5 mM. The normalized kinetics are presented in Fig 2.1.6. Regarding water permeability, none of the mercury concentrations had any effect on the mutants involving substitutions of native cysteines. However, the double mutant A117C/C123A exhibited a remarkable decrease in P_f (data are shown only for 1mM concentration in the present study). A detailed description of the results as well as a detailed account on the significance of Cys at position 117 will follow under the caption 2.1.3.1. A slight decrease in P_f observed in the case of mutant C123A is probably due to experimental artifacts as the double mutant C63/123A didn't show any inhibition.

In the case of ammonia permeability, increasing mercury concentration beyond 10 µM resulted in an increase in inhibitory effect on P_{NH_3}. The lowest concentration i.e. 1 µM had a rather slightly activating effect, whereas the highest concentration i.e. 5mM completely inhibited P_{NH_3} (Fig 2.1.6). The mercury inhibition took place in a concentration dependent manner and the rise of P_{NH_3} at 1µM Hg can be attributed to the changes in pore characteristics as such a low concentration is not expected to cause any toxic effect to the membrane (Loitto *et al.*, 2002). The modulatory effects,

irrespective of increase or decrease in P_{NH_3}, caused by very low concentrations of Hg indicate that a 1000 times higher concentration, i.e. 1mM may bring about some toxic effects.

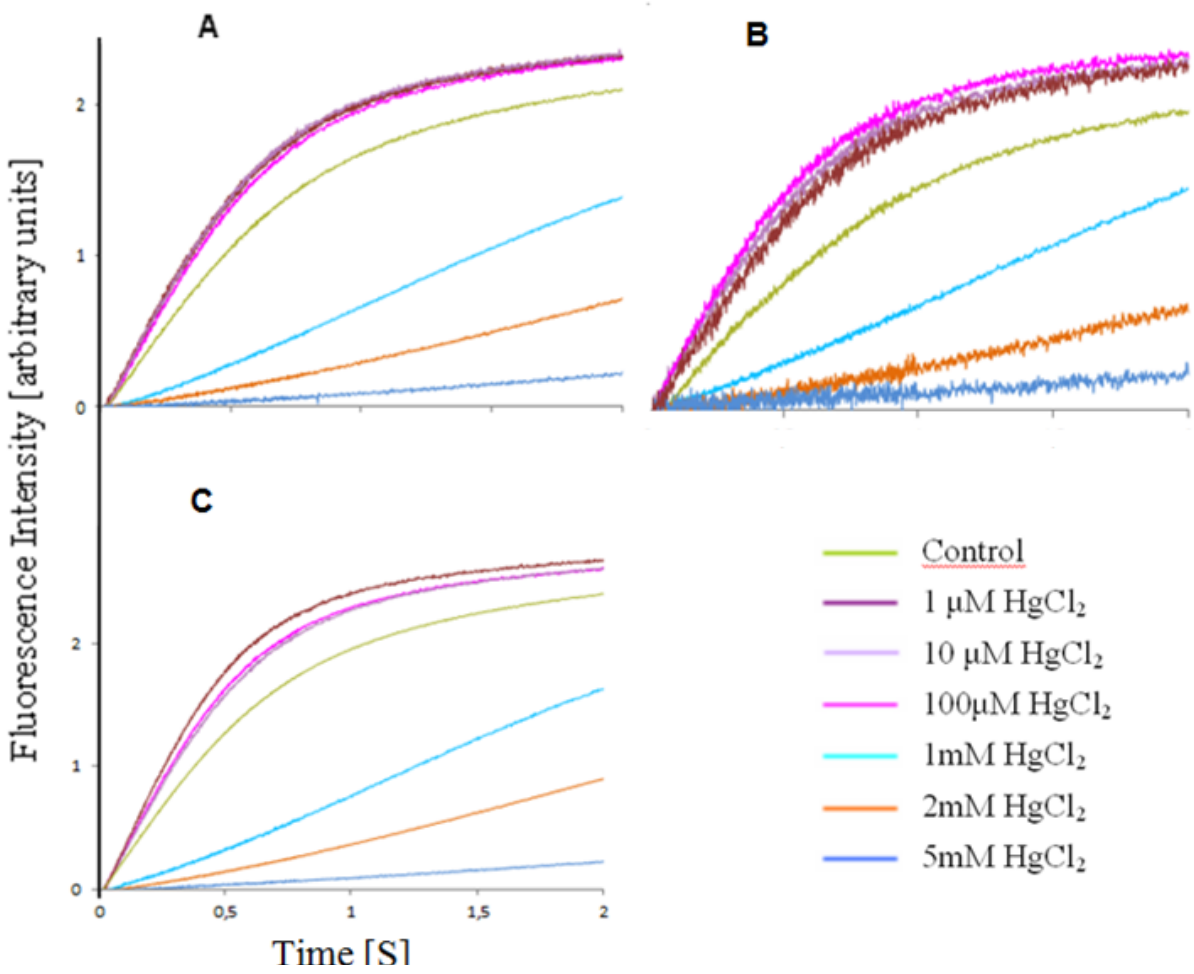

Fig 2.1.6: Ammonia permeability in *Saccharomyces cerevisiae* cells loaded with Fluorescein in ***(A)*** TaTIP2;2-wt ***(B)*** C63A and ***(C)*** C123A. The time courses represent changes in fluorescence intensity due to a rise in cytoplasmic pH after subjecting the yeast cells to an outer solution containing 25mM NH_4Cl. Each panel contains a set of kinetics obtained before (control) and after treatment with varying concentrations of $HgCl_2$. Only the rapid initial alkalinization phase is shown. Each trace is the average of 20-40 kinetics obtained from at least 3 individual experiments. The total number of traces acquired for each of the mercury concentrations (or the constructs) was at least 50. Note: Refer to Figure 2.1.3 for comparing the given kinetics with that obtained in the case of empty vector.

The homology model (Fig 2.1.5) suggests a distant location of all the native cysteines from the monomeric pore. The lack of sensitivity in the water pore may also be owing to any possible hindrance that prevents the access of Hg to the thiol

group of one of the Cys residues. The results, however, verify the lack of coordination site for metals (mercury in particular) in native TaTIP2;2 and also suggest, as expected, the structural similarity between the γ-TIP (TIP2;1) and the δ-TIP (TIP2;2). The sequences of the two TIPs show an identity of 60.7 % (sequence alignment is not shown).

The contrasting effect of $HgCl_2$ treatment on water and ammonia permeabilities can be explained on the basis of following evidences:

(i) As the previous reports suggested, a central pore exists and ammonia is following this tetrameric pore instead of the water (monomeric) pore (Yool and Weinstein, 2002, Yu *et al.*, 2006, Bertl and Kaldenhoff, 2007). A supportive evidence was also provided by Niemietz and Tyerman (2000), who reported that both P_f and P_{NH_3} were reduced by Hg however, the inhibition of ammonia transport was 10x higher.

(ii) Although molecular sizes of water and ammonia are similar (close to 3Å), there is a possibility that mercury changed the pore characteristics due to conformational changes in the protein. The altered pore may have imposed some selective hindrance on permeating solutes. The structural and functional studies in the T183C mutant (corresponding to Cys189 of AQP1) of bacterial AqpZ suggested that inhibition by mercury was merely because of steric hindrance in the pore as no conformational change in the protein was observed (Savage and Stroud, 2007). According to a contrasting report, mercury caused structural conformation resulting in the collapse of the ar/R region. The broken ar/R region in turn hindered the solute permeation. However, the presence of a steric mechanism could not be completely ruled out (Hirano *et al.*, 2010). It is speculated that different mechanisms of metal inhibition are prevailing in different AQP isoforms.

The phenomenon of decreased P_{NH_3} in the present study is based on parsimonious assumptions as the data can merely authenticate that inhibition is the result of the presence of mercury in the incubation buffer. In fact, the present study doesn't provide any concrete evidence to support coordination of mercury with Cys in TIP. Although a triple mutant with all the native cysteines knocked out (including Cys237 located in the C-terminal) is missing in the present study yet the fact that the native as well as the introduced Cys residues are equally accessible to Hg seems extremely unlikely.

2.1.3.1 Attempt to introduce a Hg-sensitive site in TaTIP2;2

As the TIP was lacking mercury sensitive Cys, it was decided to introduce a Cys from an already-known Hg-sensitive AQP at the homologous position in TIP. Fortunately, a close isoforms of TaTIP2;2 that is Arabidopsis TIP2;1 (commonly known as γ-TIP according to old nomenclature) has already been functionally characterized and reported to be sensitive to Hg, owing to a Cys located at position 118 (Daniels *et al.*, 1996). The corresponding position in TIP as suggested by the sequence alignment (Fig 2.1.7) was Ala117 located in transmembrane helix 3. The mutant Ala117Cys was nonfunctional for both water (Fig 2.1.2) and ammonia (Fig 2.1.3). The protein expression couldn't be determined due to the lack of appropriate antibody. It was attempted to produce monoclonal antibody against the TIP but it didn't show any affinity against the protein (data not presented). However, there was a convincing evidence available to believe that the protein in this mutant was expressed. In a double mutant where Ala117 was mutated to Cys and the nearby native Cys (position 123) was mutated to Ala, both water and ammonia transport functions could be observed (Figs 2.1.2, 2.1.3). The double mutant A117C/C123A exhibited significantly higher osmotic as well as ammonia permeability coefficients (Fig I.4). See Appendices 1A and 1B for a detailed comparison of P_f and P_{NH_3} values, respectively.

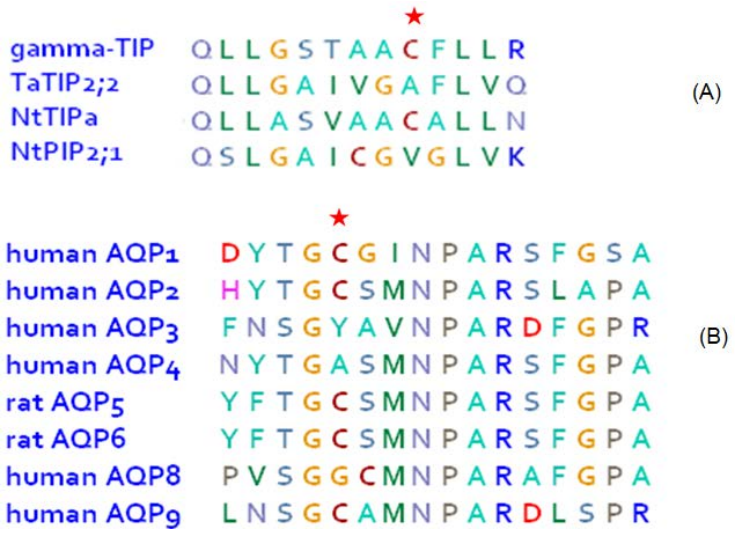

Fig 2.1.7: Partial sequence alignments to locate the Hg-sensitive residues in AQPs (indicated by asterisk). ***(A)*** A part of TM3 domain is aligned, which shows Hg-sensitive residue in gamma-TIP and its homologues in some functionally characterized plant AQPs. Note the homologous Alanine of TaTIP2;2 which has been substituted with Cys in the present experiment. ***(B)*** Alignment of a portion of the loop E sequences showing the well-characterized position of AQPs containing Hg-sensitive residues in various orthodox AQPs (belonging to mammals). Note this position is located N-terminal to the second NPA motif and has been referred to as "consensus region of metal sensitivity" in the present study.

The loss of function in case of the A117C mutant may possibly be attributed to the disulfide bonding between the two cysteine residues at positions 117 and 123. It is generally believed that the disulfide bridges enhance the conformational stability of a protein. However, some studies indicate that they are not always required for structural stability (Siddiqui *et al.*, 2005). Also, disulfide groups entropically destabilize the folded state by reducing the hydrophobic effect (Doig and Williams, 1991). The homology model (Fig 2.1.8), suggests that the distance between these positions is greater than required for any such interaction (Bondi, 1964). Both positions are located 6.9Å apart from each other which is beyond the Van der Waals distance. In view of the model, disulfide-bridge formation between Cys117 and Cys123 seems unrealistic but it can't be verified based on the available experimental data.

It should have been attempted to breakdown the covalent bond by using a reducing agent such as DTT or β-mercaptoethanol. If there had been any function, it would have proved not only the expression of protein but also the absence of disulfide bonding between the concerned cysteines. It may also be possible that water permeability remained undetected. The water permeation phase which is quicker than that of gases might have elapsed before the photomultiplier begins to detect the signal. In case of ammonia conductance, however, it doesn't hold true because of the low affinity of AQPs for ammonia (Loque *et al.*, 2005, Holm *et al.*, 2005).

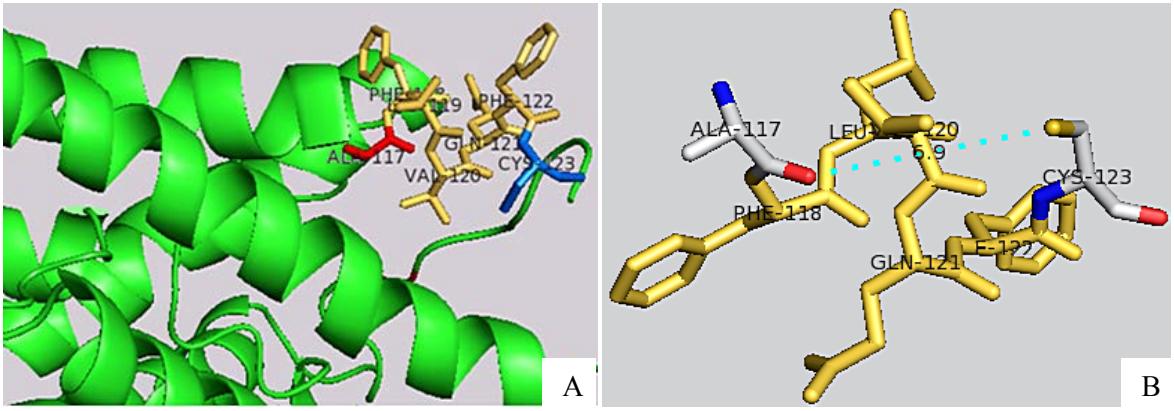

Fig 2.1.8: Homology models highlighting the positions 117 and 123 in TaTIP2;2. ***(A)*** A side view showing the environment around the two positions as a ribbon and stick representation. ***(B)*** Distance between the two positions in a figure showing Cα backbones and the side chains of various amino acids. The coordinates provided by the online tool "SWISS-MODEL" were used to draw the model in the software PYMOL. SWISS-MODEL used hAQP4 crystal structure (PDB entry # 3GD8) as template.

A. Metal sensitivity requires a Cys residue and this has to be at a particular position

It has been maintained for years that the metal sensitivity of an AQP is owing to the presence of functional groups available for metal coordination in the region located almost 3 residues N-terminal to the second NPA motif (in the loop E). Hg-sensitive residues are usually located in this region for instance, among orthodox aquaporins, Cys189 in AQP1 (Preston *et al.*, 1993), Cys181 in AQP2 (Bai *et al.*, 1996), Cys182 in AQP5 (Raina *et al.*, 1995), AQP8 because of Cys208 (Liu *et al.*, 2005b) and Cys213 in AQP9 (Ishibashi *et al.*, 1998). The importance of this region is further signified as the Cys residue at this position mostly also constitutes the ar/R region. AQP7 doesn't contain a Cys residue in this region and was reported to be Hg insensitive (Ishibashi *et al.*, 1997). Plasmodium aquaglyceroporin PfAQP (Hansen *et al.*, 2002) contains six cysteines but is still insensitive as none of them is located in the "consensus region". Introduction of Cys at this position imparts mercury sensitivity to the AQPs, which are otherwise insensitive. The mutant T223C was Hg-sensitive in the otherwise insensitive wild type *Arabidopsis* PIP2 (Daniels *et al.*, 1994). Recently, it was reported that AtPIP2;1 is inhibited by divalent cations with higher efficiency achieved with Ca^{2+}, Cd^{2+} and Mn^{2+} (Verdoucq *et al*. 2008). Although less is known about the potential region carrying metal sensitive residues in plant AQPs, NtAQP1 (Biela *et al.*, 1999), γ-TIP (Daniels *et al.*, 1996) and δ-TIP (Bertl and Kaldenhoff, 2007) were found to be mercury-insensitive.

Our study provides evidence supporting the presence of a "consensus region of metal sensitivity" in plants similar to that of mammalian AQPs. This region, at least in case of TIPs, is not located N-terminal to the second NPA motif, rather it is located in TM3. Whether a Hg coordination site can be introduced in this region throughout the plant AQPs should be investigated in future studies, no data is available even in well-characterized PIPs.

There are however some exceptions to the location of Hg-coordinating Cys residues. For instance, AQP3 is lacking any Cys in loop E and the sensitivity is because of Cys11 located in the N-terminus. It contains a Tyr residue at the position homologous to Cys189 of AQP1. The Cys substituted at this position increased Hg sensitivity. However, both P_f and P_{gly} were inhibited in a non-reversible manner (Kuwahara *et al.*, 1997). Also in the bacterial aquaporin AQPcic, the sensitivity is because of Cys82 located in loop B (Lagree *et al.*, 1998).

An interesting case is that of AQP4 which has been reported to be insensitive to Hg in oocytes (Yukutake *et al.*, 2004), but sensitive in liposomes (Yukutake *et al.*, 2008). The differences of sensitivity were because of varying orientations of loop D between oocytes and liposomes. The Hg sensitive site Cys178 was unusually located

in loop D. This site is normally inaccessible on the intracellular side however, it was reasoned that the membrane proteins in proteoliposomes are randomly oriented thereby 50% or more of the proteins are in access of mercury. The residue at the equivalent position in AQP1 is Thr157.

Although in rare cases, a Cys residue introduced at the position close to the "first" NPA motif might take the same charge as a Cys at the above-mentioned consensus region. Jung *et al*. (1994b) constructed a double mutant C189S/A73C of AQP1 the sensitivity of which was lower compared to the one exhibited by Cys 189 as the position 73 was located deep in the pore.

Surprisingly, AQP6 is rather activated by Hg (Yasui *et al*., 1999) although it contains a Cys (position 190) homologous to the Hg-coordinating Cys189 of AQP1. It was found that Cys in this "consensus region" is one of the sites of mercury activation besides another Cys located in transmembrane helix 4, which might regulate the dynamic conformational changes in the channel (Hazama *et al*., 2002). It is speculated that the mechanism of mercury binding is different in AQP6 as compared to other AQPs as mercury is not occluding in this case. Both conformational changes because of disintegration of the ar/R region (Hirano *et al.*, 2010) as well as steric hindrance in the pore (Savage and Stroud, 2007) are the mechanisms reported so far that bring about mercury inhibition in different aquaporins.

2.1.3.2 Reversal of mercury inhibition by β-mercaptoethanol

The reducing agents when added to the cell suspension break the covalent interaction between thiol groups and mercury. In the present experiment, recovery of decreased P_{NH_3} was only 40% by 10 mM β-mercaptoethanol (Fig 2.1.9). The lack of full recovery of ammonia permeability could be due to (i) the presence of more than one AQP isoforms (one sensitive to ME and the other not) or (ii) it could be caused by the toxic effects of $HgCl_2$ and/or ME (Zilli *et al*., 2009).

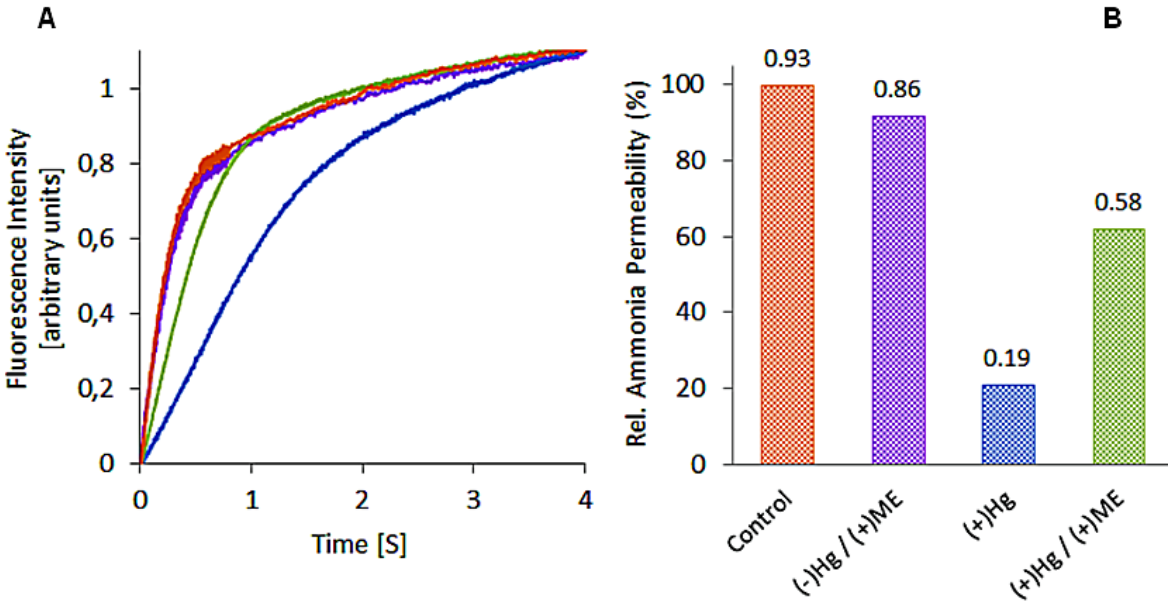

Fig 2.1.9: Reversal of mercury inhibition by 2-mercaptoethanol in TaTIP2;2-wt. *Saccharomyces* cells were pretreated with 1 mM $HgCl_2$ for 5 min or were pretreated with 1 mM $HgCl_2$ followed by incubation with 10 mM 2-mercaptoethanol for an additional 10 min and ammonia permeability was determined. ***(A)*** The time courses represent changes in fluorescence intensity due to rise in pH after subjecting the cells to an outer solution containing 25mM NH_4Cl. Each time course is the average of 20-40 kinetics obtained from 3 individual experiments. The total number of traces acquired for each of the treatment was at least 50. ***(B)*** Coefficients of ammonia permeability for various treatments were calculated to present the reversal effect of 2-mercaptoethanol in terms of percentage of the control. The data labels on each bar represent P_{NH_3} value (x 10^{-2}). Control represents the untreated cells.

The reversal of solute permeability was more than 50% in most of the AQPs for instance an AQP of *Trypanosoma cruzi* (Montalvetti *et al*., 2004) and AQP3 (Watanabe *et al*., 2005). In the former case, P_f was inhibited by both Hg and Ag to a similar extent. But in some cases it was just marginal (Yang *et al*., 2006, Zilli *et al*., 2009). γ-TIP was found to be marginally reversed by mercaptoethanol (Reizer *et al*., 1993). The reversal was only marginal (less than 20%) in the plasmodium AQP mutant W124C located at the pore mouth (Beitz *et al*., 2004). The reversal by β-mercaptoethanol was partial in case of AQP10 (Ishibashi *et al*., 2002) and AQPcic (Le Cahérec *et al*., 1996). There was no reversal at all in the case of sea bream AQP (Santos *et al*., 2004).

ME recovered water transport only in sea bream AQP1a and not in sea bream aquaglyceroporin, suggesting different physiological roles of these AQPs (Zilli *et al*., 2009). The lack of reversal by a reducing agent such as DTT or β-mercaptoethanol doesn't necessarily reflect the absence of interaction between sulfhydryl group and the cysteine. Podsiadlo *et al*. (2004), while studying inhibitors of proprotein convertase, proposed that irreversibility of Zn inhibition is caused by a

combination of poor lability of the Zn to aromatic nitrogen bond and to blocking of the pathway for ligand exchange on metal after binding to the protein.

2.1.4 Estimation of cytosolic pH

This experiment was aimed at estimating the rise in pH of *Saccharomyces* cells as a result of ammonia influx in the functional studies. For this reason, a calibration curve was drawn by exploiting the pH-dependent changes in fluorescence intensities of an appropriate dye namely Fluorescein. The ratios of the fluorescence intensities acquired at 490nm and 430nm excitation were calculated. The ratios were plotted against the corresponding pH to get the calibration curve as shown in Fig 2.1.10.

The cytosolic pH values obtained using the given method are merely apparent (and not absolute) values. The yeast cells were loaded with Fluorescein and changes in fluorescence intensities were determined both before and after mixing with the outer solution containing NH_4Cl. Using the calibration curve, pH values corresponding to the given fluorescence intensities were estimated and are given below:

Apparent cytosolic pH before mixing with outer solution	6.73
Apparent cytosolic pH after mixing with outer solution	7.15
Apparent rise in pH	0.38

The ratios of fluorescence intensities acquired at two distinct excitation wavelengths are plotted in a calibration curve as ratiometric measurements eliminate potential artifacts. The artifacts may arise due to the loss of intracellular fluorescent agent, changes of cell thickness during an experiment, changes in detector sensitivity etc. (http://www.teflabs.com/ion-indicators)

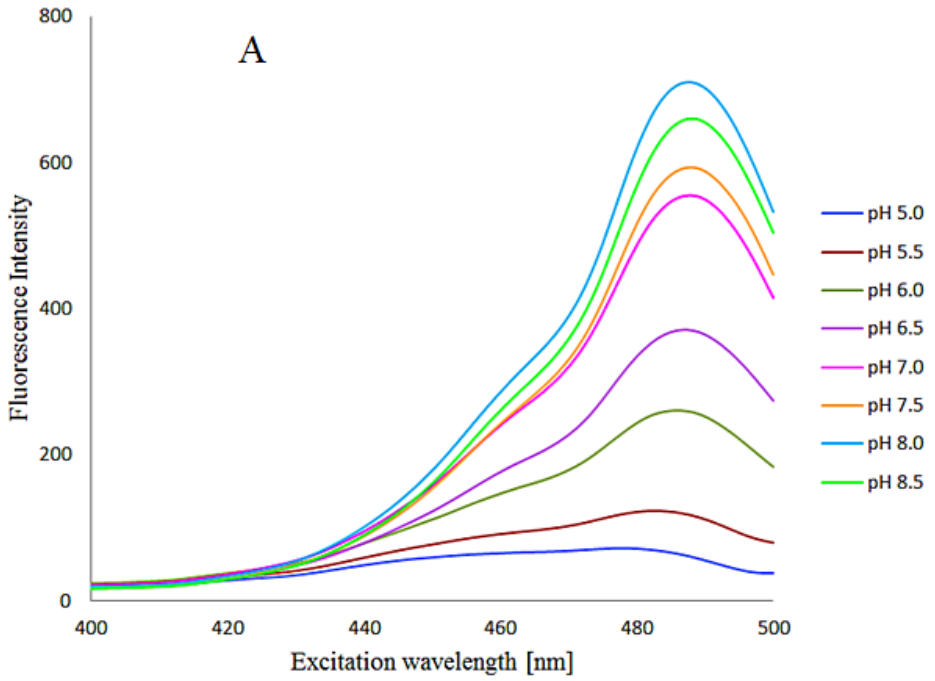

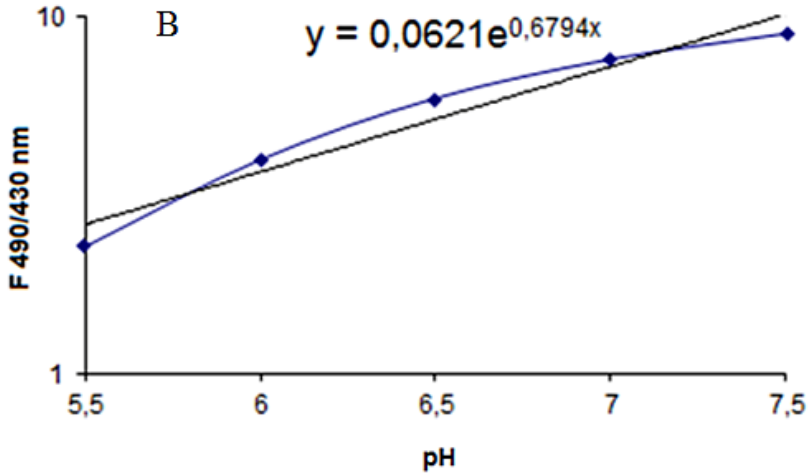

Fig 2.1.10: Fluorescence excitation spectra of *Saccharomyces* cells loaded with Fluorescein in various pH-adjusted buffers were determined with a spectrofluorimeter. ***(A)*** The fluorescence intensities were acquired at excitation wavelengths between 400 and 500 nm, and the emission was collected at 520nm. ***(B)*** *In vitro* calibration curve presented as a logarithmic plot of the ratio of fluorescence emission at 520nm with excitations of 430nm and 490nm, versus pH of the buffer. Values are the means from triplicate determinations.

2.1.5 Effects of Cu^{2+} and Ni^{2+} preincubation on TIP function

In order to further investigate the contrasting inhibition response between water and ammonia permeabilities in TIP, other heavy metals like Cu^{2+} and Ni^{2+} were also employed. In this experiment, however, only the wild type TIP was pre-treated with the metals. Ni^{2+} didn't exert any inhibitory effect on P_f (Fig 2.1.11) or P_{NH_3} (data not shown) whereas Cu^{2+} exhibited the similar outcome as in the case of mercury. P_f was not inhibited by Cu^{2+}, but P_{NH_3} followed a concentration-dependent inhibitory pattern similar to the one observed under mercury treatments (Fig 2.1.12). The native TIP contains no Cys at the required location, hence it didn't exhibit any inhibition of P_f**.** It would have been interesting to test mercury, copper and nickel also on the double mutant containing a Hg-sensitive Cys that is A117C/C123A. As such, this experiment couldn't contribute to elucidate the mechanism of inhibition in TIP but it verified the following phenomena: (i) The decrease in P_{NH_3} was intrinsic to the influence of Hg^{2+} or Cu^{2+}. (ii) Whatsoever the underlying mechanism could be, it would be the same in case of both Cu^{2+} and Hg^{2+}.

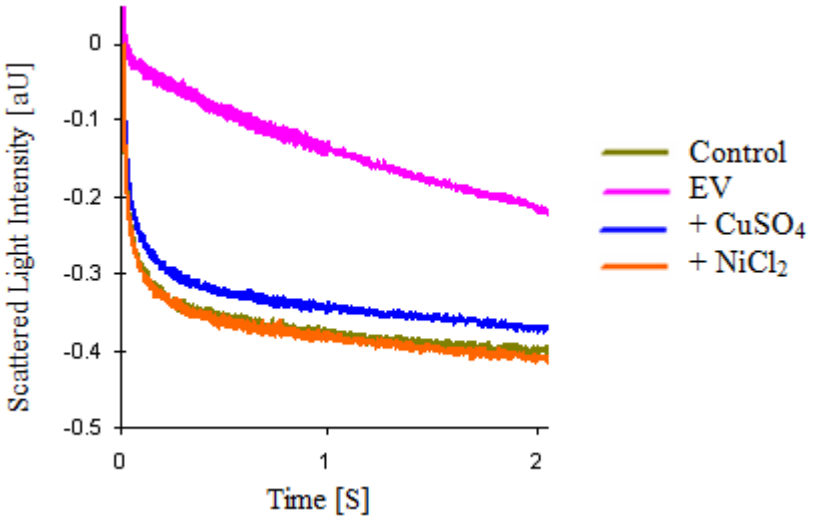

Fig 2.1.11: Inhibition of osmotic permeability due to copper and nickel in protoplasts of *Saccharomyces cerevisiae* yeast cells. The figure contains time courses of changes in scattered light intensity in TaTIP2;2-wt after subjecting the yeast cells to a hypoosmotic shock of 300 mosmol. For studying the effect of metal inhibition, yeast cells were incubated with 1mM of $CuSO_4$ or $NiCl_2$. Each time course is the average of 20-40 kinetics obtained from 3 individual experiments. The total number of traces acquired for each of the given metals was at least 50. Control stands for untreated TaTIP2;2-wt cells, whereas EV stands for empty vector.

No particular study was carried out to assess the accessibility of metals. However, the fact that the inhibition by $HgCl_2$ was partially reversible in wild type TIP indicates that the native cysteines were accessible to mercury. However, no data concerning the reversibility of Cys mutants is available hence the present study can't distinguish various Cys residues with regard to their accessibility. Distant location of all the native cysteines from the "consensus region of sensitivity" as well as the homology model (Fig 2.1.5) further ambiguate the issue of accessibility of heavy metals.

The chances of damage to the membrane because of mercury (and not any non-specific effect) can't be completely ruled out in this study. The reason being that the phenomenon of mercury inhibition was though reversible by β-mercaptoethanol, it occurred to a smaller extent compared to what has been reported in previous studies. The literature reports preincubation of AQPs with even as high as 3mM concentration of $HgCl_2$ (Mitani *et al*., 2008) and its full recovery (Rivers *et al*., 1997) indicating that toxic concentrations of Hg vary among various proteins.

All the metals employed in the present study carry a net positive charge however, molar volume of Ni is less than Hg and Cu. Copper is able to act on aquaporins extracellularly (Zelenina *et al*., 2004), whereas mercury has to penetrate through the membranes to inhibit. Copper and nickel exhibited contrasting inhibition response

despite similarity in their molar volumes (7.11 and 6.59 cm^3/mol, respectively). Likewise, mercury which is bigger in size (14.8 cm^3/mol) than the other two metals gave similar inhibition pattern as did the copper. Therefore it can be concluded that size and charge of the metals are not the only crucial factors determining their accessibility to the ligands and the subsequent coordination (Pelis *et al*., 2007).

Binding of the transition metals doesn't always follow a set of general principles, therefore the mechanism involved in a particular protein should be investigated as an individual case. The soft metals (e.g., copper, cadmium, mercury) preferentially bind to ligands containing sulfur as the sulfhydryl group. The hard metals (e.g., calcium, sodium, iron, magnesium) prefer to bind to ligands containing oxygen over sulfate and phosphate functional groups (Sandrin and Hoffman, 2007). Cu^{2+} is capable of binding with the imidazole of His and the thiol of Cys (Banci *et al*., 2009, Duncan *et al*., 2006). Ni^{2+} can also effectively bind to the sulfhydryl group of Cys (Desrochers *et al*., 2007, Kozlowski *et al*., 1987).

Mercury has a higher affinity to cysteine than copper and nickel (Bremner and Beattie, 1990). The sulfhydryl group of cysteine may also coordinate with other metals like Zn (Schumacher *et al*., 1998), copper and iron (Yukutake *et al*., 2009). The heavy metal ions were found to inhibit the activity of urease in the following order $Hg^{2+} > Cu^{2+} > Cd^{2+}$ (Tsai and Doong, 2005).

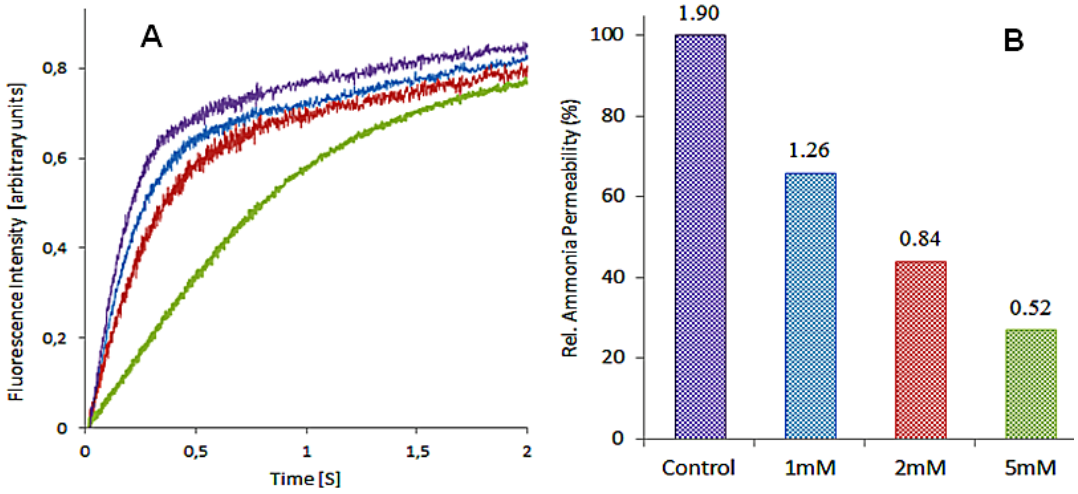

Fig 2.1.12: Inhibitory effect of copper on ammonia permeability in TaTIP2;2-wt. *Saccharomyces* cells were treated with 1 mM $CuSO_4$ for 5 min before ammonia permeability was determined. ***(A)*** The time courses represent changes in fluorescence intensity due to rise in pH after subjecting the cells to an outer solution containing 25mM NH_4Cl. Each time course is the average of 20-40 kinetics obtained from 3 individual experiments. The total number of traces acquired for each of the concentration employed in this experiment was at least 50. ***(B)*** Coefficients of ammonia permeability for various treatments were calculated to present the inhibitory effect of various concentrations of copper in terms of percentage of the control**.** Control represents the cells not preincubated with copper. The data labels on each bar represent P_{NH_3} value (x 10^{-2}).

Copper is a trace element essential to life. Its role in enzyme catalysis and gene expression is well established. Binding of copper to the Cys-binding domains in the N-terminal is required for protein-protein cooperativity in a P-type ATPase (Banci *et al*., 2007). The copper-transporting ATPases coordinate with copper through a mechanism involving two Cys resides found in the MXCXXC motif (Ralle *et al*., 2004). Another P-type ATPase also contains a MTCAAC binding motif which plays a role in the resistance of the cell to copper by affecting the export of the metal across the cell membrane (Singleton *et al*., 2008).

Copper and nickel may become an important tool in pharmacological interventions because of their quick and reversible effects on biological molecules. Zelenina *et al*. (2003) reported similarity in the mechanism of inhibition by Cu and Ni as the same residues were involved in P_f and P_{gly} inhibition in response to both metals. Three amino acid residues in the second and the third extracellular loops, Trp128, Ser152, and His241, were shown to be involved in the copper-mediated AQP3 inhibition. P_{gly} (but not P_f) in AQP4 was inhibited by copper. Ni inhibited AQP3 but not AQP4 and AQP5. In AQP0, copper had no effect but nickel was found to increase the P_f (Nemeth-Cahalan *et al*., 2007).

Silver and gold also inhibited the osmotic permeability in AQPs of mammals and plants origin; the former was more effective than Hg, but not reversible by reducing agents (Niemietz and Tyerman, 2002). The mechanism of inhibition was however not described. The widely-studied AQP1 is also inhibited, apart from mercury, by TEA. This inhibition is associated with Tyr186 residue located in loop E, which doesn't directly coordinate with TEA, rather it gives structural flexibility essential for the inhibitory effect (Detmers *et al*., 2006). In oocytes expressing AQP3, water and urea permeabilities were partially inhibited by 0.1 mM phloretin and 0.3 mM $HgCl_2$ (15–20%), whereas glycerol permeability was unchanged (Tsukaguchi *et al*., 1998).

2.1.6 General Discussion

Cys and Ala both are nonopolar and hydrophobic amino acids. The Cysteine to Alanine mutation does not dramatically alter the side-chain polarity, length, or volume therefore minor changes in terms of solute permeabilities in the Cys-to-Ala single mutants could easily be comprehended.

Two modes of how proteins are affected by metal ions have been described to date: the metal ions either bind to free thiol and other functional groups of certain native proteins or replace zinc and other essential metal ions in metal-dependent proteins (reviewed by Sharma *et al*., 2008). Metal ions are particularly inclined to bind with the functional groups of amino acid side chains for instance, the carboxylate groups

of Asp and Glu, and the ring nitrogen of His. However, the metals may also bind to the side chains for instance, ring nitrogen of Trp, thiol group of Cys, hydroxyl groups of Ser, Thr, Tyr etc (Glusker *et al*., 1999).

Inorganic mercury and other heavy metals used in this study share some common features which have been mostly investigated while studying metalloproteins. Hg, Cu and Ni are all membrane-permeant metals. The ability of only mercury and copper and not of Nickel to inhibit P_{NH_3} can't be explained with the given results. Differences in the mechanism of various heavy metal inhibitors have already been reported. The preferential site for Ni^{2+} binding in AQP3 was a Histidine (Zelenina *et al*., 2003). In hAQP1 and a plant NIP, the metals Cu, Ni and Cd had no effect but silver and gold inhibited the water permeability. Further, silver and mercury were proposed to have different mechanism as inhibition by the former was not reversed by the application of mercaptoethanol (Niemietz and Tyerman, 2002).

Most metal ions react with electron-pair donors to form coordination compounds or complexes. Copper (II) has a coordination number of four. Copper when complexed with ammonia results in a cationic complex, $Cu(NH_3)_4^{2+}$. Likewise, mercury can also form complexes with ammonia through the following chemical reactions:

Aqueous ammonia, through the following oxidation-reduction reaction with mercury(I), would yield a fine dust of black metallic mercury and white amido salt:

$Hg_2Cl_2(aq) + 2NH_3(aq) <==> 2NH_4^+(aq) + Cl^-(aq) + HgNH_2Cl(white\ solid) + Hg(black\ liquid)$
mercury(I) ------ *Equation Ia*

or
Aqueous ammonia would yield a mixture of metallic mercury and a white basic amido salt

$2Hg_2^{2+}(aq) + 4NH_3(aq) + NO_3^-(aq) + H_2O(l) ==> 2Hg(l) + Hg_2ONH_2NO_3(s) + 3NH_4^+(aq)$
mercury(I) ----- *Equation Ib*

These salts are not soluble in excess aqueous ammonia, but do dissolve in acids.
$HgNH_2Cl(s) + 2H^+(aq) + Cl^-(aq) <==> HgCl_2(aq) + NH_4^+(aq)$
mercury(II) ----- *Equation Ic*

Because of the above-mentioned mercury-ammonia complex formation, the amount of ammonia available at the pore entrance would decrease. It may have reflected in terms of a decrease in ammonia permeability. Despite complexing of mercury with ammonia, the decrease in P_{NH_3} after Hg treatment may still be attributed to the

Cys–Hg coordination. A remarkable clue in this direction was that the inhibition by $HgCl_2$ was reversible, though merely to an extent of 40%. As the protoplasts were treated with a concentration as high as 1mM, it might have inflicted a non-specific effect on TIP. It must be noted that cell viability decreases with time and the value obtained is definitely under-estimated. As discussed earlier in this section, the recovery after mercury inhibition was never reported to be 100%; in some cases it was rather marginal. The issue was, however, not further investigated. Stoichiometric studies for the above-mentioned reaction (at varying concentrations of ammonia and mercury) as well as resolving the structure of TIP would help in understanding the fate of mercury and ammonia.

AQP3 inhibition by copper is principally different from inhibition by mercury, which is also a divalent heavy metal. Mercury binds covalently to the proteins therefore the effect of mercury is reversed only by using a reducing agent, such as ß-mercaptoethanol. In contrast, copper forms coordination bonds with proteins and the effect of copper is reversed by simple washout of the metal ions (reviewed by Zelenina *et al*., 2004). Even in case of mercury agents, the molecular mechanism of inhibition may vary among the AQPs as proposed in AQP1 and AQP4 (Yukutake *et al*., 2009).

The similar pattern of inhibition by Hg and Cu in the present study highly disfavors the concept of an independent central pore for gas permeation. Mercury inhibition of ammonia permeability has already been reported in NOD26 (Niemietz and Tyerman, 2000) and TaTIP2;2 (Bertl and Kaldenhoff, 2007). As P_{NH_3} but not P_f was affected by mercury, two independent pathways were proposed for water and ammonia conductance. Some evidences suggest that gases may pass exclusively through the tetrameric pore of AQPs (Yool and Weinstein 2002, Yu *et al*., 2006). The phenomenon of coordination of mercury with ammonia needs immediate attention so that the said discrepancy between contrasting inhibition of water and ammonia could be solved. Such an ambiguity was further enhanced by the fact that all the three Cys-to-Ala mutants exhibited similar inhibition pattern. All the native cysteines in TIP2;2 are not expected to be projecting into the pore. Also the presence of all cysteines at equally-accessible position seems extremely unlikely (see homology model of TaTIP2;2 in Fig 2.1.5).

2.1.7 Conclusions

The present study aimed at determining the Hg-sensitive site in TaTIP2;2. In the mutational analysis, a series of single and double mutants were generated replacing the native Cys residues in a sequential manner. Besides mercury, copper and nickel

were also employed to get a deeper insight of the inhibitory mechanism in TIP. Unfortunately, because of contradictory results, the present study is too restricted to shed light on the location of Cys residues and even on the accessibility of heavy metals to these residues.

The following inferences could be drawn based on the results obtained:

(i) None of the native Cys residues played any remarkable role in the pore structure or function of the TIP. However, keeping in view the osmotic permeability of the double mutant A117C/C123A (which is higher than the wild type TIP), it is tantalizing to propose that the substituted Cys projects into the pore and is capable of modulating the solute permeability. This phenomenon implies similarity in the structure of γ and the δ-TIP.

(ii) Present results support the existing postulate that usually both Cys and its position are necessary to impart mercury sensitivity to an AQP. At least in TIPs, if not true for the entire plant AQPs, there may exist a "consensus region of metal sensitivity" in TM3, which is analogous to the one present in mammalian AQPs. However, Hg sensitivity can't be considered as a phenomenon based on a certain uniform mechanism across the family of AQPs and ideally it requires thorough investigation involving the reconciliation of functional data, Cys scanning analysis (focusing the region near to NPA motifs), structural data about apo- and Hg-bound forms of the protein etc.

(iii) The present results do not provide any concrete evidence either supporting or against the existing view of presence of a separate gas pore in AQPs. The selective monomeric and tetrameric pore inhibitors may be helpful in this regard for future studies. In case the central pore exists in AQPs at all, it is blocked by cadmium, but not by TEA (Yu *et al*., 2006), whereas the water pore is blocked by TEA and not by cadmium (Jung *et al*., 1994a).

(iv) The discrepancy of similar inhibition by mercury and copper (as against nickel) couldn't be solved and the involvement of some other metal-coordinating residues/sites may be given due attention in future studies.

2.2 Molecular determinants of selectivity in AQPs: *Investigations outside the selectivity regions*

This section involves a comprehensive mutational analysis to study the molecular determinants of ammonia selectivity. As discussed in chapter 1, the determinants of ammonia selectivity are extended beyond the selectivity filter and the NPA region in aquaporins. The experiments presented in this section involved the identification of the unique residues (apart from the constituents of the above-mentioned constrictions) and studying their role in the ammonia transport function of the protein by adopting site directed mutagenesis approaches. The aims of this study are summarized as follows:

(i) identifying the molecular signatures taking part in the selective recruitment of ammonia in the pore, (ii) an attempt to convert an ammonia impermeable AQP into an ammonia permeable AQP (and vice versa) by focusing on these molecular signatures and (iii) to have some insight into the mechanisms of substrate specificity and ammonia conductance in AQPs.

2.2.1 Identification of molecular signatures potentially relevant for selectivity

Sequences of some of the aquaporins, the ammonia permeability of which has already been characterized, were aligned (Fig 2.2.1). The aquaporins included in the alignment belong to plants (TIPs, PIPs and NIP) and mammals (AQP1, 2, 3 and 8). According to the alignment, some of the residues appeared to be unique between the ammonia-conducting and non-conducting plant AQPs. The identified amino acid signatures were also observed in some of the mammalian AQPs. One candidate each from ammonia facilitating and non-facilitating plant AQPs that is (respectively) TaTIP2;2 and NtPIP2;1 were selected for the present experiment. The prospective residues were: Ile97, Leu168 and Gly224 in case of TaTIP2;2, whereas in case of NtPIP2;1, the corresponding residues were Val117, Val197 and Ala256. The respective positions will be hereafter referred to as position I, II and III.

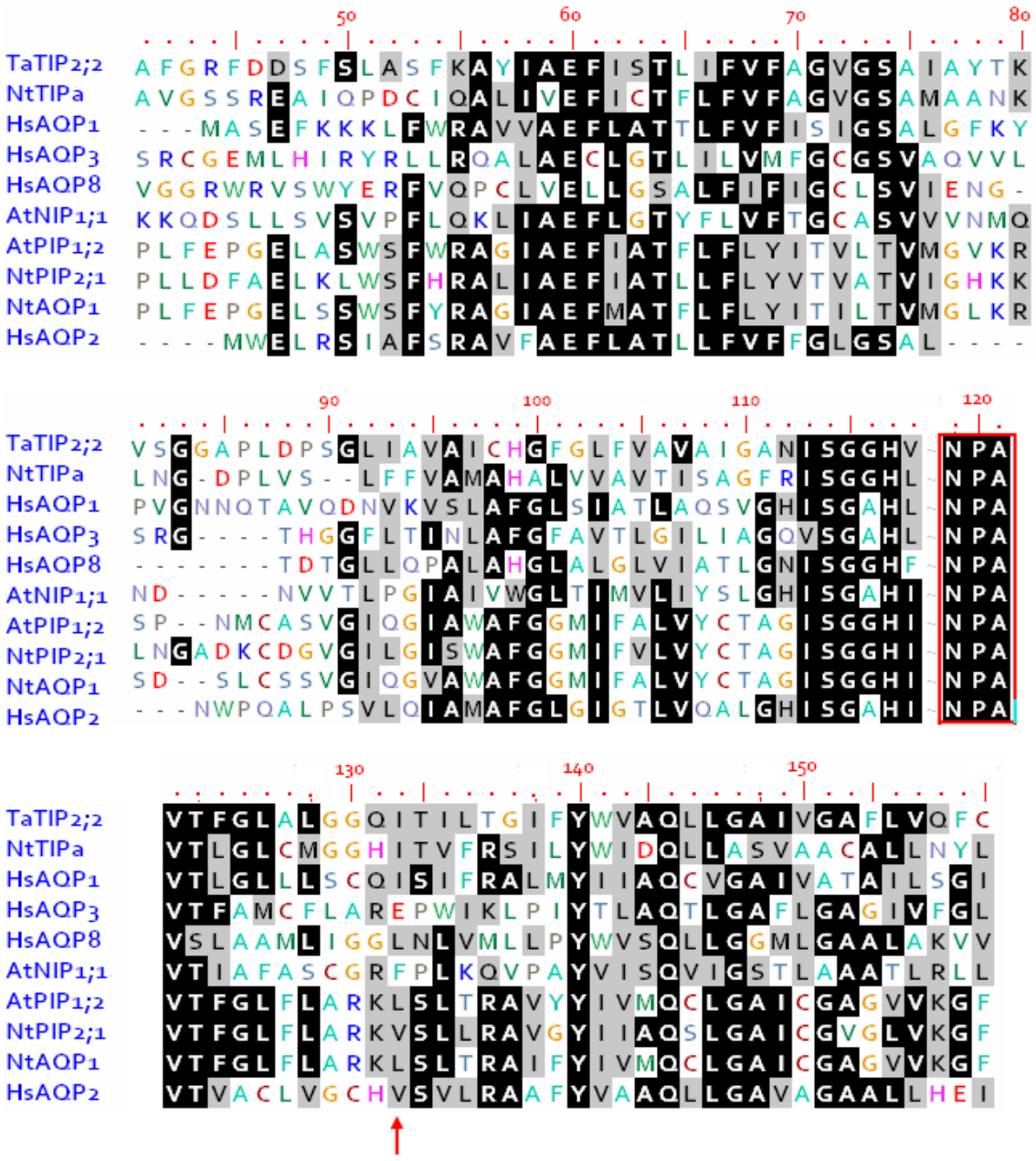

Fig 2.2.1: Sequences of various AQPs, the ammonia permeability of which is already reported, have been aligned. TaTIP2;2, NtTIPa, HsAQP1, HsAQP3, HsAQP8 and AtNIP1;1 are reported to be ammonia transport-facilitating, the rest are non-facilitating. The NPA motifs are boxed in red lines. Red arrows indicate the residues which were distinguished between ammonia transport-facilitating and non-facilitating AQPs. The position indicated by a pink asterisk might be a prospective candidate for future studies to determine the molecular signatures of AQP-facilitated ammonia permeability. The breaks (denoted by ~) represent discontinuity where a blank portion in the alignment was eliminated. Numbering is arbitrary and doesn't represent any of the given sequence. The alignment was generated using the BioEdit software that incorporates the multiple sequence alignment tools of ClustalX.

(Sequence alignment continued from previous page)

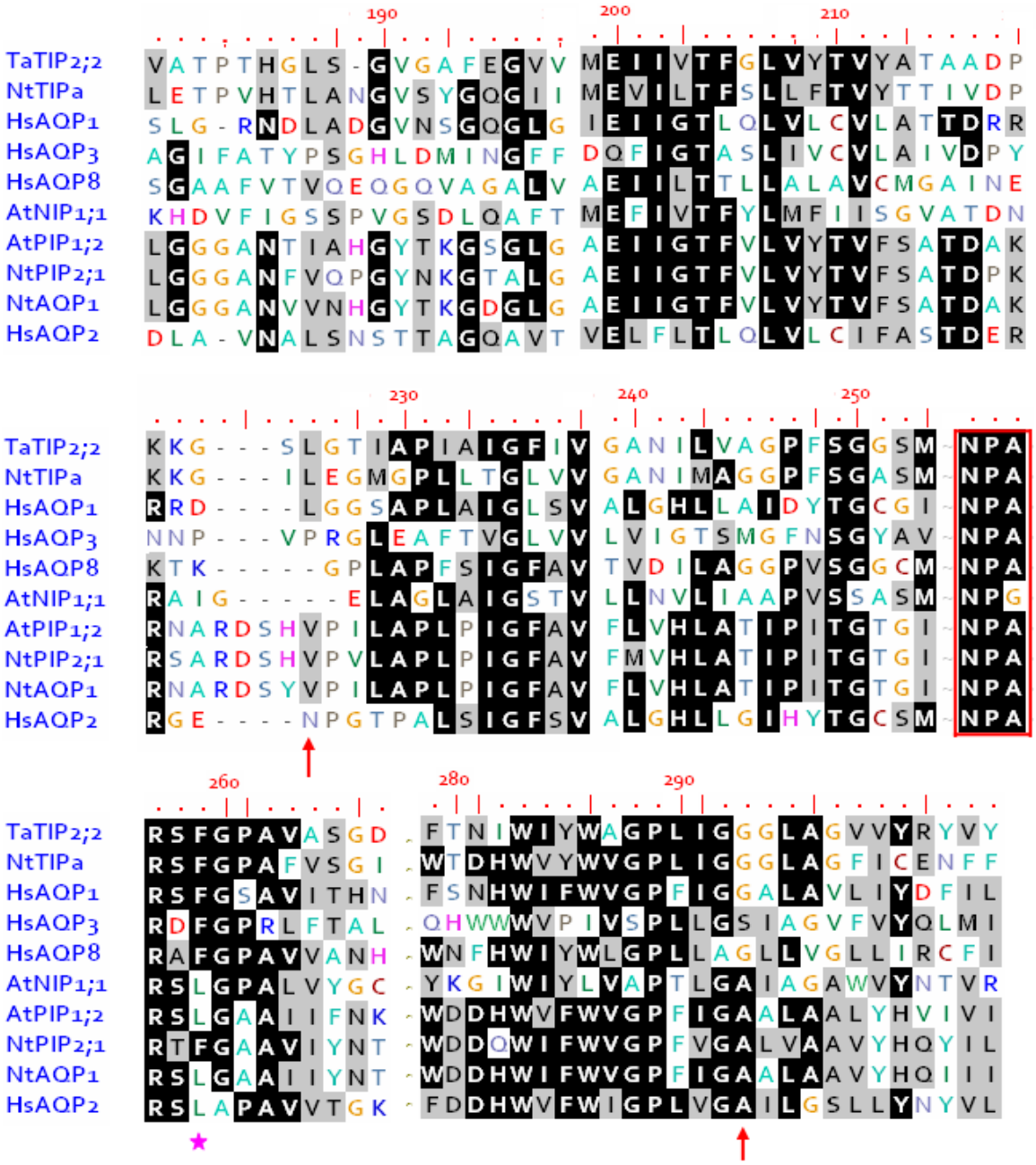

2.2.2 Molecular signatures of selectivity in NtPIP2

2.2.2.1 Mutational analysis

Focusing on the set of amino acid positions as indicated by the sequence alignment, it was attempted to convert the ammonia-tight NtPIP2;1 aquaporin into an ammonia transport facilitating one. This experiment included following point mutations: substitution of Val117 by Ile, Val197 by Leu, and Ala256 by Gly. The mutants Val117 (Position I), Val197 (Position II) and Gly256 (Position III) are located in loop B, loop D and transmembrane helix 6, respectively. Two double mutants that is V117I/V197L and V197L/A256G and a tripe mutant V117I/V197L/A256G were also generated. All the given mutants were devoid of any ammonia permeability; the raw time courses of changes in fluorescence intensity are presented in Fig 2.2.2. The kinetics were not normalized (against each other or against a standard curve) as normalizing the nonfunctional curves elevates the initial brief but fast component (always found in such curves) to several orders of magnitude; a fact which might be considerably misleading in such functional experiments.

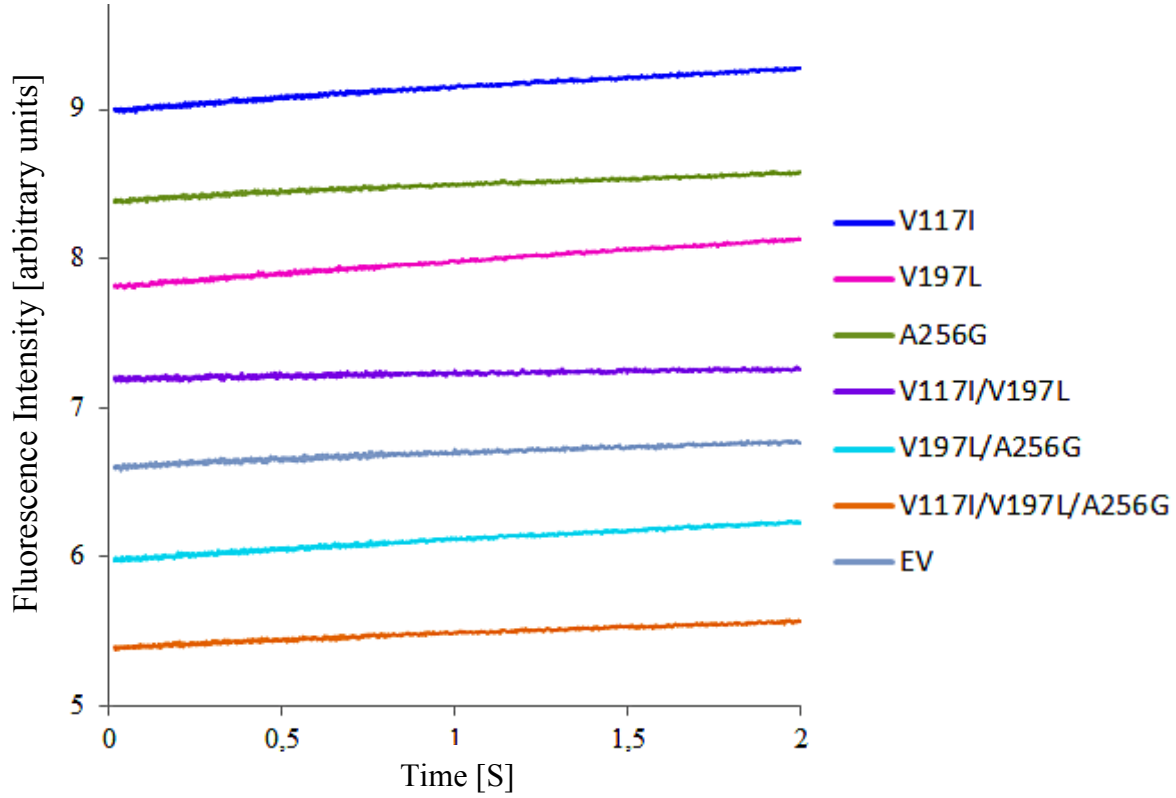

Fig 2.2.2: Time courses of ammonia permeability in various mutants of NtPIP2;1. Each time course is the average of at least 20– 40 kinetics obtained from at least 3 independent experiments. The total number of traces acquired for each construct was at least 50. The raw kinetics are presented without normalization. TaTIP2;2 which is an ammonia-conducting AQP served as positive control in this experiment (data not shown in this figure but given elsewhere).

In contrast to the TaTIP2;2 (results given later in this section), point mutations of homologous residues in NtPIP2 exhibited drastic changes in water permeability. The raw traces (without normalization) are given in Fig 2.2.3. All mutants proved to be different as compared to the wild type PIP2. The osmotic permeability coefficient in V117I was higher (183%), whereas that of the other two point mutations V197L and A256G was much lower (62% and 52%, respectively) than the wild type (Fig 2.2.4). The previously mentioned double mutants were also studied, which included a combination of (i) one faster (compared to WT) and one slower mutant (V117I/V197L) and (ii) both of the slower mutants that is V197L/A256G. The former double mutant V117I/V197L, as expected, was not much different from the wild type (83% of PIP2-WT) and the latter double mutant V197L/A256G was nonfunctional (data not shown). The triple mutant where Val117, Val197 and Ala256 were substituted by Ile, Leu and Gly, respectively, showed a P_f of 30% of the wild type PIP2. See Appendix 1C for detailed P_f values comparison.

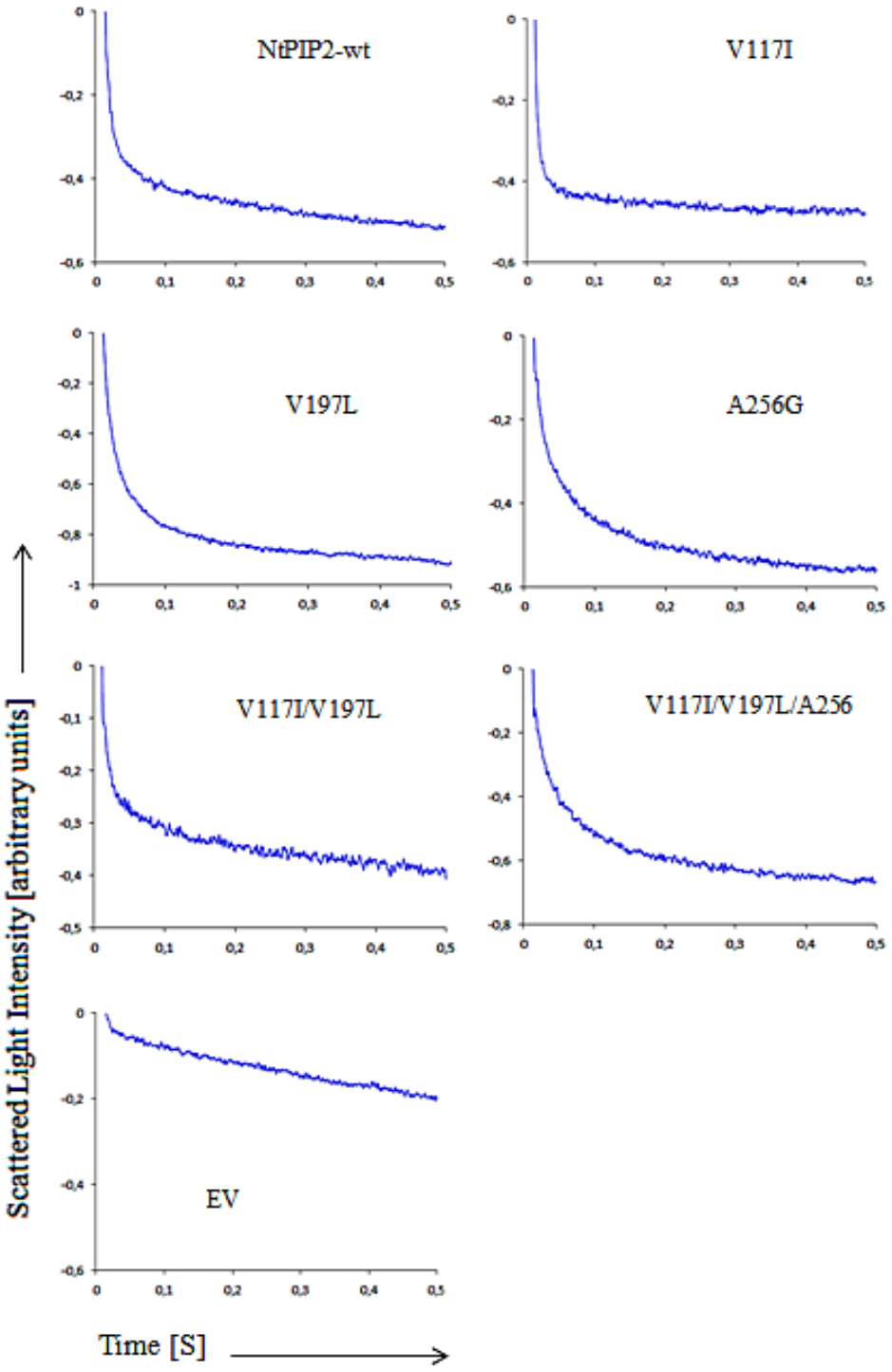

Fig 2.2.3: Water permeability in protoplasts of *Saccharomyces cerevisiae* yeast cells. The figure presents time courses of changes in scattered light intensity in NtPIP2 and its mutants after subjecting the yeast cells to a hypoosmotic shock of 300 mosmol. The raw traces are presented without normalization. Each time course is the average of 20-40 kinetics obtained from 3 individual experiments. The total number of traces acquired for each of the construct was at least 50. Note different scales along the y-axis.

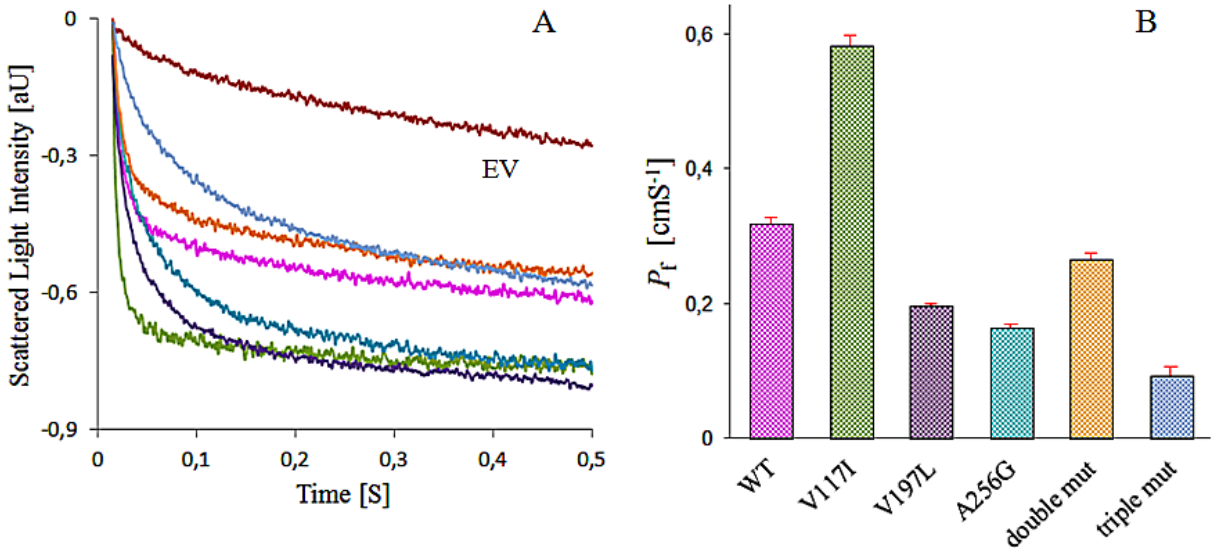

Fig 2.2.4: Water permeability in protoplasts of *Saccharomyces cerevisiae* yeast cells. ***(A)*** Time courses of changes in scattered light intensity in NtPIP2 and its mutants after subjecting the yeast cells to a hypoosmostic shock of 300 mosmol. All the traces are presented after normalization. Each time course is the average of 20-40 kinetics obtained from 3 individual experiments. The total number of traces acquired for each of the constructs was at least 50. ***(B)*** Osmotic permeability coefficients (P_f) are presented as a bar chart for comparison among various mutants. Error bars represent standard error of the mean. WT = wild type NtPIP2;1, double mut = V117I/V197L, triple mut = V117I/V197L/A256G, EV = empty vector. The color scheme in panel A corresponds to the respective bars in panel B.

2.2.2.2 Homology modeling and interpretation of the results

Homology models were drawn to further understand the significance of the above-mentioned residues in water permeability of NtPIP2;1. The coordinates for the model were provided by the online tool namely "SWISS-MODEL" which used the crystal structure of the spinach PIP2 as the template (PDB entry # 2B5F).

Position I: Position I is located in loop B and there is a possibility that the mutation resulted in a displacement of this loop in a way that physical properties of the pore were changed. This position is located close to an aromatic amino acid Phe112 (belonging to TM3) as indicated by the homology model of the protein structure (Fig 2.2.5). As the residue volume of Ile (166.7 Å) is larger as compared to that of Val (140 Å), the distance between Ile117 and Phe112 might have decreased. The homology model indicates that Ile117 is located almost at a van der Waals distance (4.0 Å) from Phe112 (Fig 2.2.5C). The thrust imposed by the presence of a bigger residue close to this Phe may have tilted it towards the pore. Despite the non-reactive side chain of His, cation-π interaction between the aromatic ring of the Phe-112 and water molecules may have resulted into an intense polar contact.

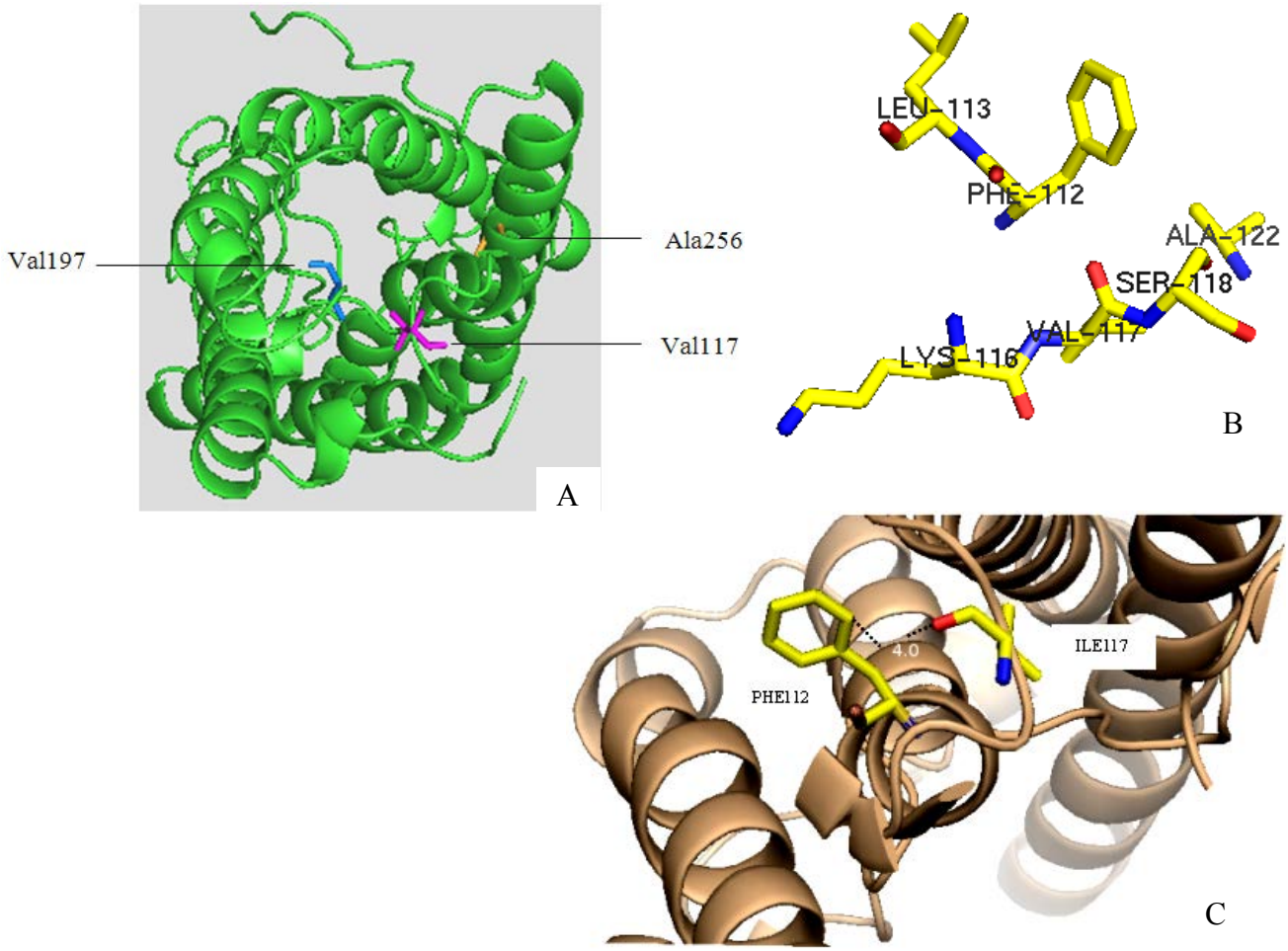

Fig 2.2.5: Homology models of NtPIP2 with the residues of interest shown as a ribbon and stick representation. ***(A)*** A cytoplasmic view of the 3 candidate positions focused in the present study. ***(B)*** The environment around position I is highlighted in a figure showing Cα backbones and the side chains of various amino acids. ***(C)*** A cytoplasmic view of a portion of the PIP2 monomer depicting Val117 (position I) and Phe 112 which are located (almost) at van der Waals distance. The coordinates provided by the online tool "SWISS-MODEL" were used to draw the model in the software PYMOL. SWISS-MODEL used SoPIP2 crystal structure (PDB entry # 2B5F) as template.

Further, the overall atmosphere around the Val117 is highly hydrophobic. A region with such higher hydrophobicity "should have" inclined towards the inner cavity which is not the case according to homology model (Fig 2.2.5B). This mutation may have resulted in conformational changes, as a consequence of which the pore characteristics could possibly have altered. There is also a possibility that one or more residues of this region may have interacted with the pore-forming or the functionally-important residues. Whatever the case may be, the significance of this region in solute permeability shouldn't remain unnoticed because of its location in the loop B which contains one of the two completely conserved NPA motifs in the AQPs.

Position II: The homology model shows that position II is located at the pore mouth (Fig 2.2.6A). Further, it is flanked by the highly reactive imidazole ring of His196 and a non-reactive Pro198 (Fig 2.2.6B). The chances are fair that the remarkable decrease in P_f was because of indirect effects of the mutation on the function. This mutation also involves the substitution by a bigger Leu residue. Although both Pro and Leu possess non-reactive side chains in terms of their role in protein function, the presence of a bigger Leu might have influenced the Pro in a way to jolt the loop into the pore mouth resulting in its partial occlusion. Similarly, Leu may have affected the nearby His (and subsequently the water permeability) in case it has any role in function of the channel. The introduction of a bigger amino acid might have pushed His towards a position unfavorable for the function. Either one or both of the above-mentioned effects may have taken place simultaneously to disfavor the conductance of water.

This position is located in loop D, which is highly versatile in its function and its importance has been signified in the literature (for instance, the role of loop D in gating mechanism). It is quite likely that the mutation at position II had caused some conformational changes leading to a decreased osmotic permeability. Törnroth-Horsefield *et al*. (2006) revealed a gating mechanism in SoPIP2 which involves loop D in opening and closing of the pore. In the closed conformation, loop D folds underneath the pore and a conserved Leu197 located in loop D is inserted into a cavity near the entrance of the channel and occludes it. The residue corresponding to the said Leu197 in case of NtPIP2 is Leu200. Although there is no supporting evidence available, position II may directly interact with Leu200 (Fig 2.2.6B).

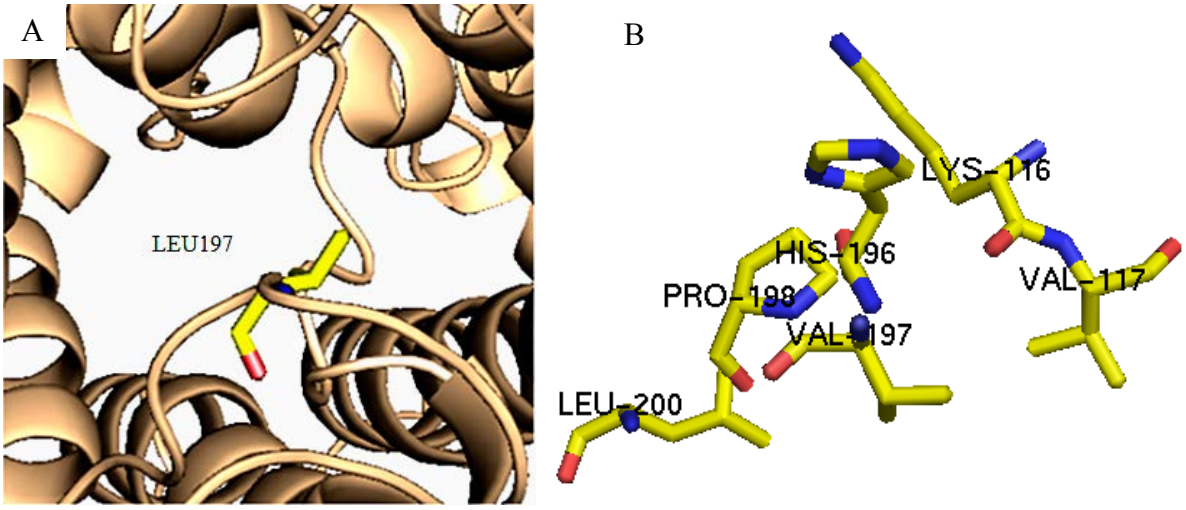

Fig 2.2.6: Homology models to show the environment of position II in NtPIP2. ***(A)*** A cytoplasmic view of the water pore shown as ribbon and stick representation, Leu197 can be

seen protruding into the pore mouth. ***(B)*** The residues around Val197 are highlighted in a figure showing Cα backbones and the side chains of various amino acids. The environment around Val197 is quite versatile. Leu200 which is the residue corresponding to Leu197 (important for gating SoPIP2) is also shown. The coordinates provided by the online tool "SWISS-MODEL" were used to draw the model in the software PYMOL. SWISS-MODEL used the SoPIP2 crystal structure (PDB entry # 2B5F) as the template.

Position III: Positions III is located inside the transmembrane helix 6 which is not known to possess any direct role in solute permeability. The significant decrease in P_f (and no gain of ammonia transport function) by substituting Ala with Gly cannot be thoroughly interpreted with the given results. Probably, the introduction of Gly has destabilized the structure or has inflicted some conformational changes in the protein resulting in altered physical properties of the pore (Lin *et al*., 2006). Either of the above-mentioned situations may reduce the efficiency of the water pore besides keeping the gas pore intact. Apart from the literature, the homology model (Fig 2.2.7) also suggests that this residue itself may not be directly involved in water permeation as the corresponding position is located away from the pore. It is, however, to be noticed that this position lies in a highly hydrophobic atmosphere and is flanked by Ala 259, 260, Pro252 and Phe253. Further, introduction of Gly is known to be even more deleterious for the protein structure (breakage for instance) if its location is inside an α-helix (Kasahara *et al*., 2007).

It is interesting to note that in PIP2, P_f was decreased by substituting Ala whereas in TIP, P_f was increased by introducing Ala. This indicated some role of Ala at this position in facilitating water permeability. It is tempting to speculate that a non-reactive residue at this position is required which is larger in size compared to Gly (Ala has residue volume of 88.6 Å whereas Gly has 60.1 Å). The mutation at the same position in TIP however, didn't bring about any changes in P_{NH_3} which may be attributed to the difference of structure between TIPs and PIPs as well as to the permeation of NH_3 through a separate pore.

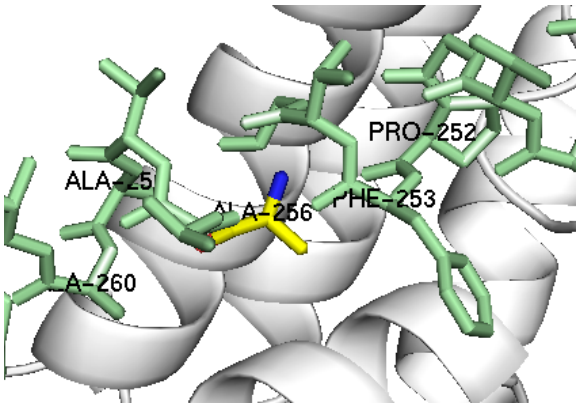

Fig 2.2.7: Position III (Ala256) is located in TM6, a portion of which is modeled as ribbon and stick representation. Ala256 is located in a highly hydrophobic environment and is flanked by Ala 259 and Phe253.

The drastic changes in osmotic permeability of NtPIP2 due to mutations seemed quite surprising particularly because the ammonia transport function in PIP2 (which is otherwise ammonia tight) was not induced at all. Positions I and II involve substitutions among Val, Leu and Ile. The direct involvement of these amino acids in the protein function seems less likely because (i) these possess nonreactive aliphatic side chains (ii) the homology model suggests that these amino acids are located far from the pore (Fig 2.2.5, 2.2.7). Exceptionally, however, position II residue Leu197 in PIP2 is protruding into the pore (Fig 2.2.6). It is not immediately clear as to how Ile and Leu, at the positions I and II of NtPIP2 respectively, perform a role in facilitating water permeability. Probably, the longer size of the aliphatic side chain of Ile and the shorter chain of Val at positions I and II, respectively, are required to maintain the protein conformation (Kasahara *et al*., 2004). In case of TIP, substitution of Ile rather enhanced osmotic permeability. The data regarding position III revealed that the presence of an Ala at this location is required for effective transport of water through the pore. Interestingly however, the presence of either Ala or a Gly had no role in ammonia conductance.

2.2.3 Molecular signatures of selectivity in TaTIP2;2

2.2.3.1 Mutational analysis

This analysis involved three single point mutations as suggested by the sequence alignment i.e. Ile97Leu, Leu168Val and Gly224Ala. Further, a double mutant (Ile97Leu/Leu168Val) and a triple mutant was also generated that substituted native Ile97, Leu168, Gly224 with Leu, Val and Ala, respectively.

The ability to conduct water and ammonia was studied for all the above-mentioned single, double and triple mutants. The time courses of ammonia permeability are presented in Fig 2.2.8 and Fig 2.2.9A, whereas a bar chart showing the comparison of the permeability coefficients among all the mutants is presented in Fig 2.2.9B. The results revealed that none of the single amino acid mutation had any effect on the function of TaTIP2;2 regarding ammonia permeability and all the mutants behaved similar to the wild type TIP (Fig 2.2.9). A slight increase in P_{NH_3} in case of the position II mutant may be due to an experimental artifact. The double mutant was also not an exception. However, the triple mutant where all the native Ile, Leu and Gly were substituted by (respectively) Leu , Val and Ala was 16 % slower than the wild type. The data analysis suggested that there was little variation among the rate constants of individual kinetics of the triple mutant as indicated by low standard error of the mean. The uniformity among the data may indicate that the mutations didn't inflict instability in the protein however, it is not immediately clear if the altered P_{NH_3} was indeed intrinsic to the mutations. See Appendix 1E for a detailed comparison of P_{NH_3} values among all the TIP variants.

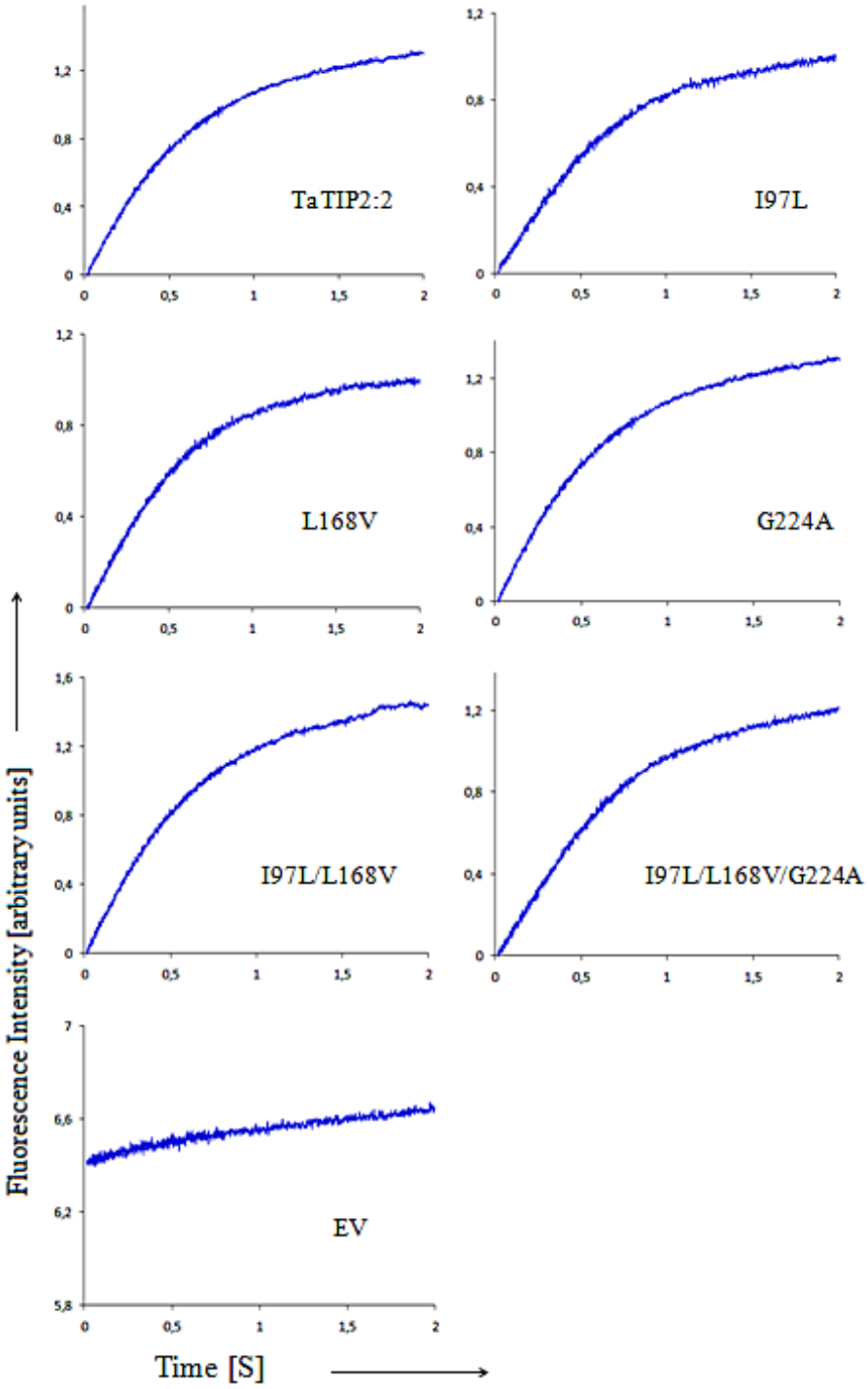

Fig 2.2.8: Ammonia permeability in *Saccharomyces cerevisiae* yeast cells. The figure contains time courses of changes in fluorescence intensity in TaTIP2;2 and its mutants after subjecting the yeast cells to an outer solution containing 25mM NH_4Cl. The raw time courses are presented without normalization. Each time course is the average of 20-40 kinetics obtained from 3 individual experiments. The total number of traces acquired for each of the construct was at least 50. Note different scales along the y-axis.

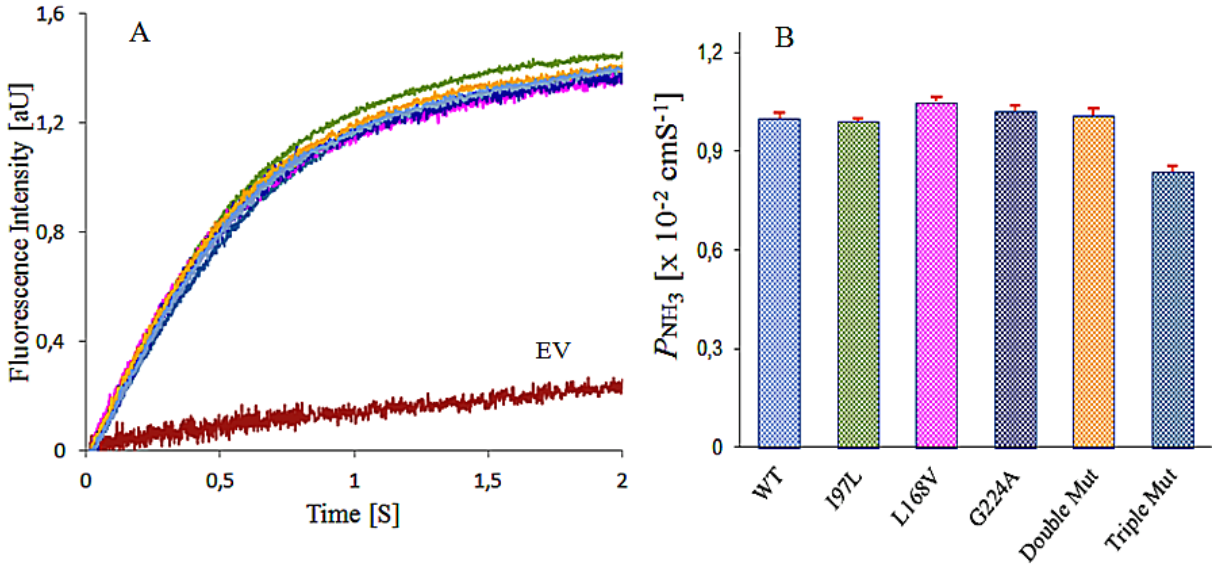

Fig 2.2.9: Ammonia permeability in various mutants of TaTIP2;2. ***(A)*** The time courses represent changes in fluorescence intensity due to rise in pH after subjecting the *Saccharomyces* cells loaded with Fluorescein to an outer solution containing 25mM NH_4Cl. Each time course is the average of 20-40 kinetics obtained from 3 individual experiments. The total number of traces acquired for each of the construct was at least 50. ***(B)*** Coefficients of ammonia permeability are presented in bar chart for comparison among various constructs**.** Error bars represent standard error of the mean. Double Mut = I97L/L168V, Triple Mut = I97L/L168V/G224A, EV = empty vector. The color scheme in panel A corresponds to the respective bars in panel B.

All above-mentioned single, double and triple mutants were also studied for their ability to conduct water. The raw time courses (without normalization) of osmotic permeability for all the constructs are presented in Fig 2.2.10. The functional studies revealed that all the three single mutations were slightly faster in their ability to transport water as compared to wild type TIP (Fig 2.2.11). The double mutant, where the native Ile and Leu were substituted with Leu and Val, respectively, exhibited a significant decrease (24%) in the P_f compared to the wild type. The triple mutant which included additional substitution of Gly by Ala was 18 % slower than the wild type. See Appendix 1D for detailed P_f values comparison among the TIP variants.

Despite varying effects of the mutations on permeabilities in TIP, data of both P_f and P_{NH_3} can be reconciled considering position II and the triple mutants. Both water and ammonia permeabilities were increased (to 5%) in case of position II, whereas the permeabilities were decreased (14-16%) in case of triple mutant.

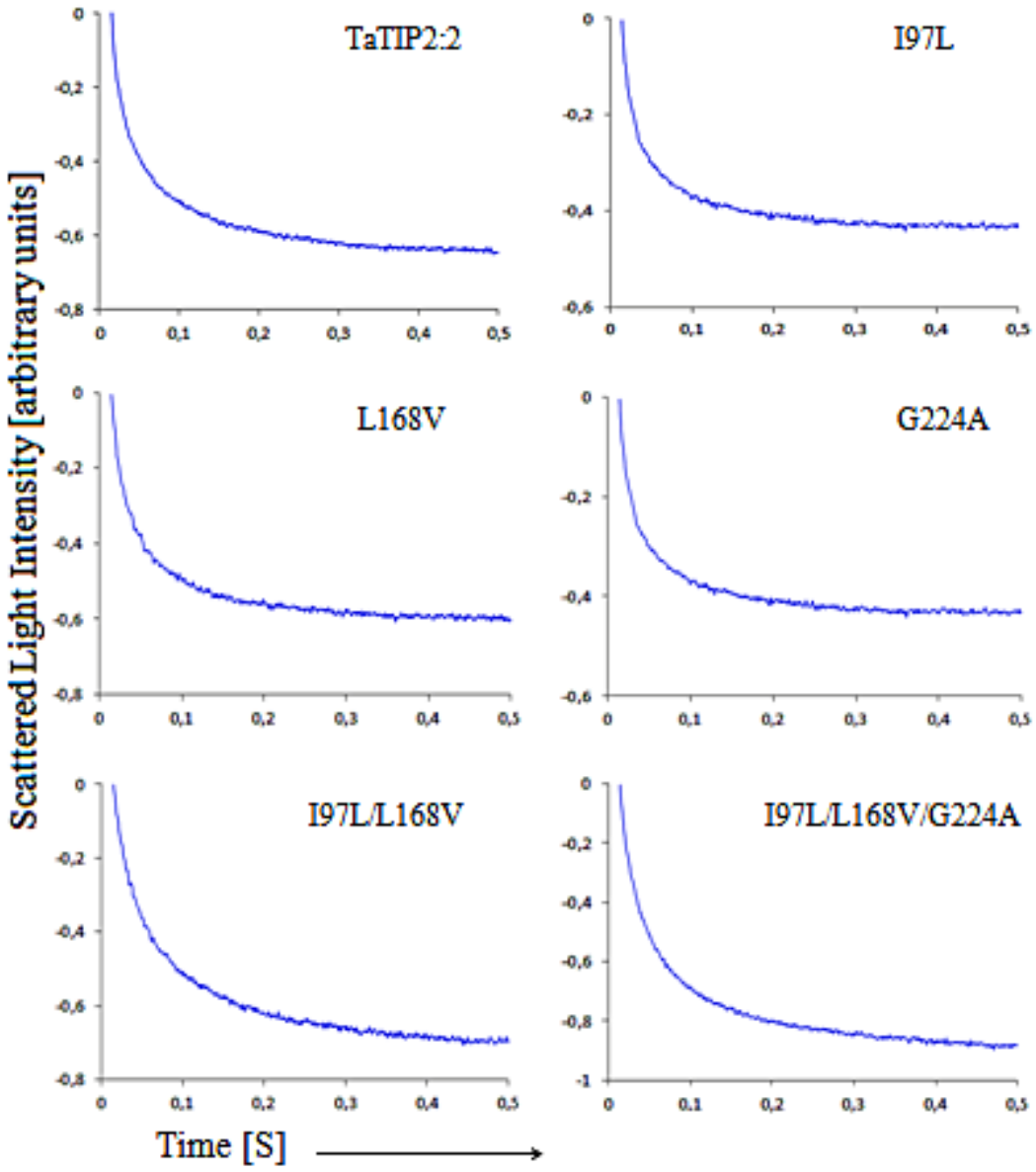

Fig 2.2.10: Water permeability in protoplasts of *Saccharomyces cerevisiae* yeast cells. The figure presents time courses of changes in scattered light intensity in TaTIP2;2 and its mutants after subjecting the yeast cells to a hypoosmotic shock of 300 mosmol. The raw traces are presented without normalization. Each time course is the average of 20-40 kinetics obtained from 3 individual experiments. The total number of traces acquired for each of the construct was at least 50. Note different scales along the y-axis. The time course for the empty vector can be found elsewhere.

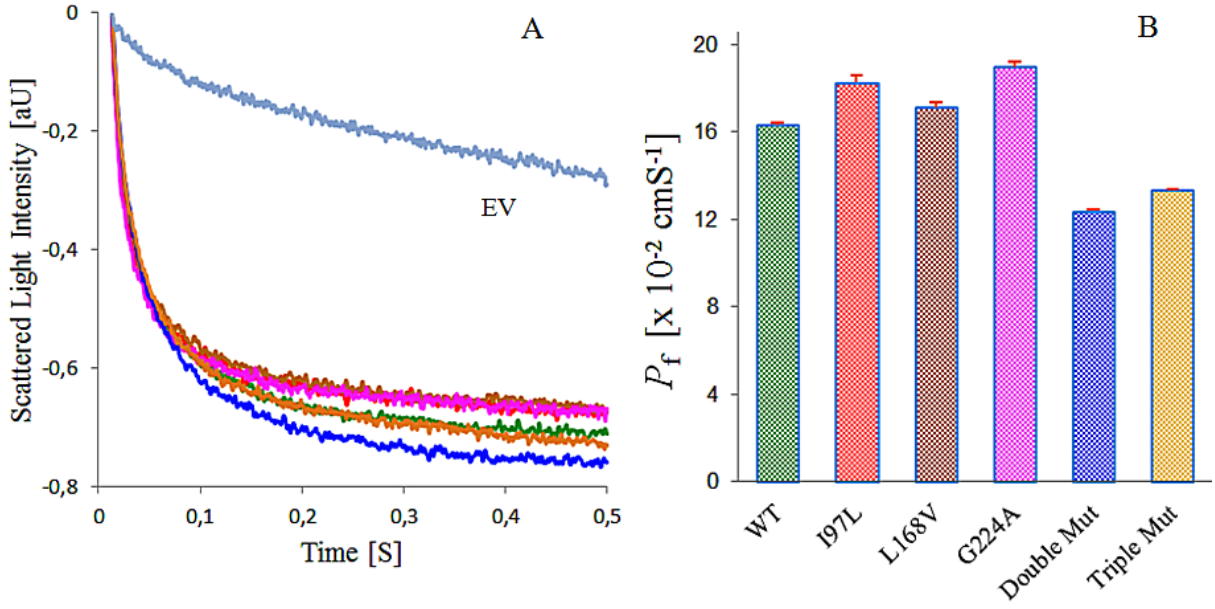

Fig 2.2.11: Water permeability in the protoplasts of *Saccharomyces*. ***(A)*** Time courses of changes in scattered light intensity in TaTIP2;2 and its mutants after subjecting the yeast cells to a hypoosmotic shock of 300 mosmol. All the kinetics are presented after normalization. Each time course is the average of 20-40 kinetics obtained from 3 individual experiments. The total number of traces acquired for each of the construct was at least 50. ***(B)*** Osmotic permeability coefficients (P_f) of various mutants are presented in bar chart for comparison among the constructs. Error bars represent standard error of the mean. WT = wild type TaTIP2;2, Double Mut = I97L/L168V, Triple Mut = I97L/L168V/G224A, EV = empty vector. The color scheme in panel A corresponds to the respective bars in panel B.

2.2.3.2 *Interpretation of the results*

The above-mentioned experiment exhibited a similar decrease in P_f in case of both double and triple mutants, indicating no role of Gly in the function of TaTIP2;2. In comparison to the triple mutant, the double mutant is the one which doesn't involve substitution of Gly. The hypothesis is further supported by the fact that a single Gly to Ala mutation exhibited no effect on P_{NH_3}. The identical variations in P_f and P_{NH_3} in the mutations in position II and the triple mutant might be owing to different protein abundance, however, the present study is too restricted to shed light on this fact. There is readily no concrete interpretation available for the change in osmotic water permeability in case of the mutated positions I and III. Probably, they play some structural role as none of them seems to be accessible to the pore. Once again, the varying effect of the residues on water and ammonia permeability may be attributed to a separate gas pore in AQPs.

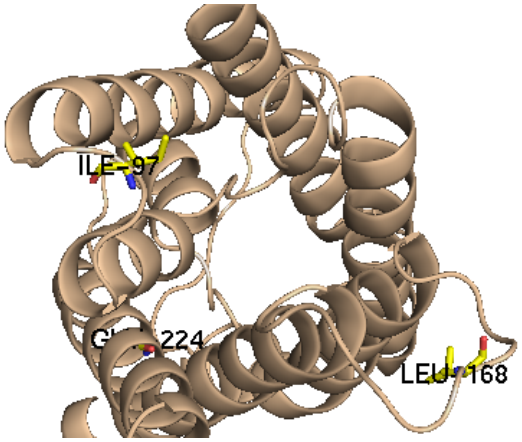

Fig 2.2.12: A cytoplasmic view of the 3 candidate positions in TaTIP2;2 focused in the present study in a ribbon and stick representation.

As it was the Gly to Ala mutation (in triple mutant) which brought about the decrease in P_{NH_3}, it is proposed that Gly (although only in combination with Ile and Leu and not a solo effect) had a role in stability of the structure and the decrease in function was caused by the altered physical properties of the gas pore. Human AQP1, AQP8 and tobacco TIPa also contain a Gly residue at the homologous position (Fig 2.2.1) which signifies its importance in AQPs. Future studies need to be carried out to determine how Gly contributes to ammonia transport facilitation; one approach being mutational analysis in Gly-containing AQPs.

The residues involved in mutational analysis in case of TIP are located far from the pore and the side chains of the concerned residues would be unable to coordinate with the permeating water (according to the homology model in Fig 2.2.12). The Position II, however, is located in the thoroughly investigated loop D. This loop is involved in gating of the aquaporins, including SoPIP2 (Törnroth-Horsefield *et al*., 2006), AQP0 (Nemeth-Cahalan and Hall, 2000) and AQP4 (Zelenina *et al*., 2002). Further the intracellular loop D was reported to be involved in pH sensitivity of PIP2;2 (Tournaire-Roux *et al*., 2003, Fischer and Kaldenhoff, 2008) and AQP3 (Zelenina *et al*., 2003).

2.2.4 General Discussion

Although, the amino acids focused in the present study are not completely conserved throughout a particular category of AQPs (either water or ammonia conducting), their wide occurrence indicates some role in defining the channel properties.

The mutations are located in loop B (Position I), loop D (Position II) and transmembrane helix 6 (Position III), respectively. Both loops are vital for the

function and structural stability in the family of aquaporins. Loop B contains one of the two highly conserved NPA motifs and mutations in this region critically affect the pore function. Also the cysteine residues introduced in this loop usually take the same role as the highly conserved Cys located in loop E (for instance Cys189 in AQP1) of mercury sensitive AQPs (Shi and Verkman, 1996, Jung *et al*., 1994b). The loops B and E were proposed to be confronting each other inside the pore in a so-called "hour glass model" (Jung *et al*., 1994b) and were later verified, through the crystal structure, as the regions containing NPA motifs and taking part in the formation of the water pore (Murata *et al*., 2000).

The residues focused in the present study may inflict only indirect effects on water permeability due to the afore-mentioned reasons. This assumption is supported by a converse mutation (Ile-to-Val) in RsPIP1;3 which increased its transport activity more than 2-fold (Suga and Maeshima, 2004). This mutation was, however, located at a critical region that is close to the second NPA motif. A Val to Ala mutation in TM2 resulted in a drastic reduction of P_f in rice PIPs. The substitution of native Val caused a change in orientation because of indirect effects on constituents of the selectivity filter, ultimately resulting in unfavorable physical changes in the pore (Zhang *et al*., 2010).

Unfortunately, the level of protein expression could not be determined in the present study as an appropriate antibody against the TIP was not available. It was attempted in the present study to produce a monoclonal antibody, but it didn't show any affinity (data not shown). The results have been interpreted, assuming that the protein abundance was the same in all mutants, although this might vary in different mutants after normalizing the P_f data against the protein abundance. It should be noted that, in some instances, single point mutations may indirectly affect protein function through an extensive distortion of the protein structure (Kasahara *et al*., 2006). If proteins are equally abundant in all mutants and the variation in P_f is intrinsic to the mutations, a detailed mutational analysis involving amino acid substitutions of different sizes and secondary structure propensities could further elaborate the significance of said positions in water permeability and mechanism of interaction with the solutes (s). As long as the protein structure is not resolved, other approaches such as cysteine scanning analysis might shed light on access of the concerned residues to the water pore (although less probable).

Besides the mutants focused in the present experiment, some more conserved residues were pointed out in a recent review (Litman *et al*., 2009). The predominantly water permeable AQPs of mammals, i.e. AQP1, 2, 4, 5, 6 and the plant aquaporin PIP2 have a histidine at position 180 (numbers corresponding

to hAQP1 will be referred to hereafter) and an isoleucine at position 184. The aqua-ammoniaporins, i.e. AQP3, 7, 9, 10 in mammals and TIP2;x in plants have got a glycine at positions 180 and 184. At position 190 (arbitrary position 251 in Fig 2.2.1), the exclusive water conducting AQPs contain Ser or Gly, whereas the ammonia conducting ones mostly contain Ala. Interestingly, TIP contains Ser at this position (see Appendix 2 and Fig 2.2.1).

The molecular signatures distinguishing between water conducting aquaporins and the aqua-ammoniaporins are extended beyond the selectivity regions in AQPs. The water conducting AQPs can be converted into water/ammonia conducting pores and vice versa by point mutations. In case of an aqua-ammoniaporin, if the isoleucine corresponding to position 180 of AQP1 is replaced by a histidine and the glycine at position 189 is replaced by a cysteine, the aqua-ammoniaporin would become an exclusive water channel. Likewise, if an AQP1 mutant is generated, in which the histidine at position 180 is replaced by an alanine, the aquaporin becomes ammonia-permeable (Beitz *et al*., 2006).

None of our mutations falls even in the domains suggested by Litman *et al*. (2009) as those are mostly located closer to the second NPA motif. The sequence alignment (Fig 2.2.1) revealed an appealing position 197, which is very close to the second NPA motif. At this location, the hydrophobic residues phenylalanine and leucine are almost equally represented in both, exclusive water channels as well as aqua-ammoniaporins. The dominance of merely these two residues in AQP family needs to be investigated keeping in view the difference of isostericity between Phe and Leu that ambiguates the requirement of hydrophobicity at this position.

2.2.5 Conclusions

Keeping in view the (i) conserved nature of these residues and (ii) drastic changes in P_f by these mutations in PIP2, the concerned positions require further investigation. The following inferences were drawn from the results obtained:

(i) The residues studied in the present experiment didn't appear to play a major role in ammonia selectivity. None of the mutations could induce ammonia permeability in NtPIP2, however, each of the mutations had a strong effect on P_f. Likewise, even the triple mutant in TaTIP2;2 (where all the native residues were substituted with their homologs from NtPIP2), just partially restricted ammonia conductance through the pore. The results provided only little evidence in support of our hypothesis. However, the available experimental data together with the conserved nature (not completely) of these residues lead us to propose their minor role (solo or cumulative

effect) as a part of the selectivity mechanism. A recent study revealed that either of the two essential regions (NPA motif or ar/R region) doesn't suffice alone to impose a selectivity barrier on the potential solutes permeability. It is in fact the cumulative effect of the both as shown by the point mutations in the NPA motif and ar/R region of AQP1 (Wu *et al*., 2009). Therefore, further mutational analyses should be planned in combination with both selectivity regions.

(ii) Nearly all the amino acid substitutions may render the protein unstable to varying degrees. The stability of a protein can be improved by substituting amino acids for those with increased secondary structure propensities. The aromatic amino acids particularly Trp and Phe, which fall in the middle of the propensities scale, significantly stabilize the residual structure (Finnegan and Bowler, 2010). It is recommended that the native Val, Ile and Leu residues are substituted by those with varying secondary structure propensities, but similar molecular volume and side chain properties. Glu and Thr may be good candidates for future studies. The former should receive particular attention because of its highly reactive side chain and increased propensity. The different effect of mutations on P_f and P_{NH3} provides a hint in support of the presence of a central pore.

(iii) Unfortunately the protein expression data is missing in this study. Although less likely because of isosteric similarities in the investigated positions, it would be parsimonious to suggest a normalization of the data against the protein abundance.

(iv) The residues reported here are among those which have been suggested in the alignment comparing ammonia permeable AQPs against the ammonia tight ones. It is recommended that further investigations include even more conserved residue that is Phe in case of aqua-ammoniaporins and Leu in case of water specific AQPs (Fig 2.2.1). Their respective positions in case of TaTIP2;2 and NtPIP2 are 201 and 233 (the corresponding position in case of hAQP1 is 197).

2.3 Molecular determinants of selectivity in AQPs: *Investigations on SF regions and structural domains*

The previous chapter included substitution of several potential molecular signatures that didn't seem to play any important role in ammonia selectivity in AQPs. The investigations were broadened to include the selectivity regions and some of the functionally relevant domains of TaTIP2;2 and NtPIP2 in an attempt to understand the nature of the selectivity barrier imposed by the predominant water conducting channels to hinder the ammonia conductance. These studies involved the same ammonia conducting TaTIP2;2 and non-conducting NtPIP2;1 aquaporins.

2.3.1 Molecular signatures of selectivity in selectivity regions

2.3.1.1 Mutational analysis in the ar/R region

The ar/R region of TaTIP2;2 is a tetrad of His64, Iso179, Gly192 and Arg199 residues, whereas that of NtPIP2,1 is comprising of Phe83, His212, Thr221 and Arg227, which are highly conserved among the PIPs. The positions are designated as H2, H5, LE1 and LE2, respectively. The selectivity filter regions of both TIP and PIP were swapped through sequential mutations in order to study the molecular signatures contributing to ammonia selectivity in AQPs. As to the investigations on TaTIP2;2, the following mutants were generated:

(i) three single mutants, i.e. His64Phe, Ile197His, Gly192Thr
(ii) a double mutant, i.e. His64Phe/Gly192Thr and
(iii) a triple mutant, i.e. His64Phe/Ile197His/Gly192Thr in which the ar/R constriction mimics that of NtPIP2.

All the above-mentioned mutants of TIP proved to be nonfunctional for both water and ammonia transport. The raw time courses (without normalization) of ammonia and water permeability are presented in Fig 2.3.1. It was a surprising outcome as the residues substituted do already exist in water selective AQPs and are highly conserved. Unfortunately, the protein expression of these mutants couldn't be determined due to the lack of an appropriate antibody. An important evidence is however available (see the caption 2.3.1.3 on proton leakage), which confirms that the protein was not expressed in case of the mutant H64F.

In case of tobacco PIP2;1, a predominantly water conducting channel, the individual constituents of the ar/R constriction of TaTIP2;2 were also desired to be replaced. Unfortunately, only one residue at the position LE1, that is Phe83, could be

substituted by His. The other two residues His212 and Thr221 couldn't be substituted, because of failure to accomplish the mutagenesis. The mutant F83H didn't show any function; even the pore lost its ability to conduct water (refer to the general figure 2.3.1 for the raw time courses (without normalization). Immunoblot assay confirmed that it was due to nonexpression of the protein (Fig 2.3.9).

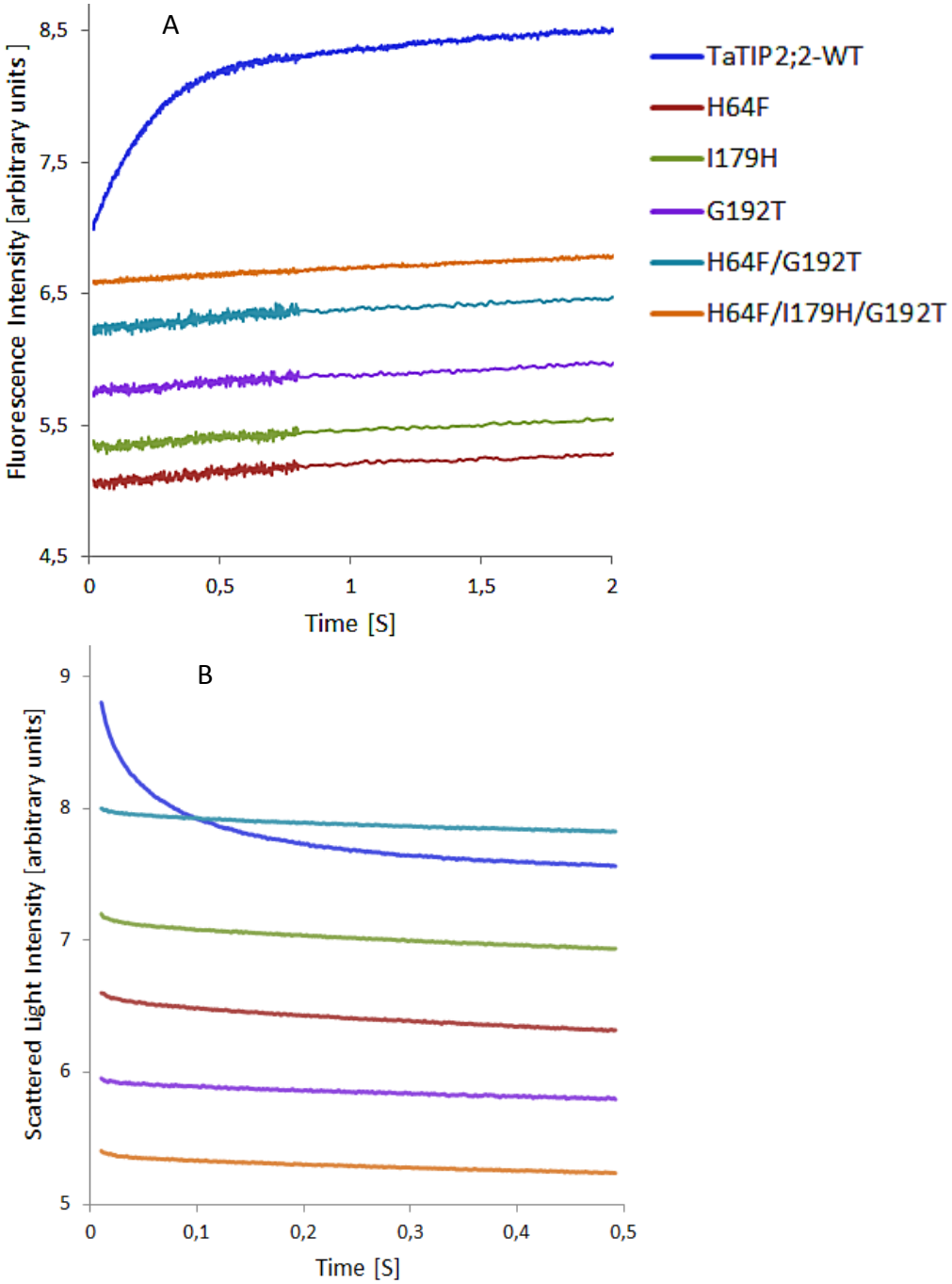

Fig 2.3.1: Ammonia ***(A)*** and water ***(B)*** permeability in various mutants of TaTIP2;2. The time courses for ammonia permeability represent changes in the fluorescence intensity due to rise in pH after subjecting the *Saccharomyces* cells loaded with Fluorescein to an outer

solution containing 25mM NH_4Cl. The time courses for water permeability represent changes in the scattered light intensity after subjecting the yeast cells to a hypoosmotic shock of 300 mosmol. All the time courses are presented in original (without normalization) due to the reason that the normalization elevates the initial brief but faster component by several orders of magnitude. Each time course is the average of 20-40 kinetics acquired from 3 individual experiments. The total number of traces acquired for each of the construct was 50. Note: These kinetics would serve as representative ones for all the nonfunctional constructs following in this section. The color scheme is same in panels A and B.

The wheat TIP2;1 also contains His, Ile and Gly residues at the (respectively) H2, H5 and LE1 positions. All these residues were indispensable for ammonia transport. However, interestingly, yeast complementation performed in the mutated ar/R region (mimicking that of AQP1) of wheat TIP2;1 indicated that the residues constituting the tetrad do not play a vital role in protein folding or trafficking (Jahn *et al*., 2004).

The His and the highly conserved Arg were dispensable for water transport, as observed in AQP1, which implies that water permeability in AQP1 is independent of the polarity at the ar/R constriction (Wu *et al*., 2009). The position H5 of TaTIP2;2 contains a small residue that is Ile, which renders the ar/R region wider in diameter and also makes it more hydrophobic. These are general characteristics of ammonia conducting AQPs (see homology model in figure 2.3.2).

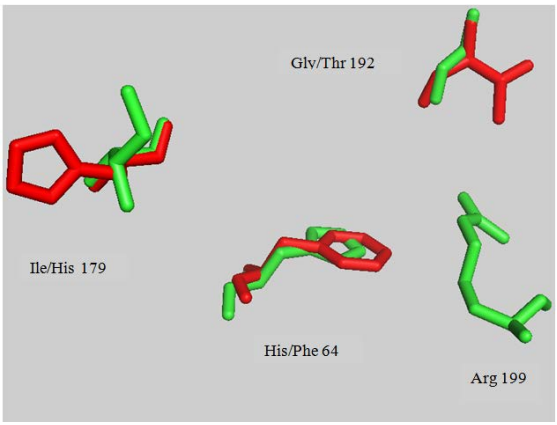

Fig 2.3.2: The residues constituting the ar/R tetrad of TaTIP2;2 derived from the homology model. The native and the mutated residues are superposed on each other and the figure shows their C_α backbones and the side chains to highlight their biochemical properties as well as the effect of mutations on the pore characteristics. The model was drawn in the software PYMOL using the coordinates provided by an online tool SWISS-MODEL. The latter tool used the crystal structure of human AQP4 (PDB entry # 3GD8) as template. Color scheme: native residues are shown in green, mutated residues in red.

In predominant water conducting AQPs, the constriction tetrad is comprised of Phe, His, Cys and Arg. The replacement of native Phe residue (position H2) by a His in MD simulations resulted into blockage of the *Arabidopsis* PIP2 pore (Dynowski *et al*., 2008). The Cys in most of the water, ammonia and glycerol conducting AQPs is replaced by an aromatic functional group carrying amino acid. In case of aquaamoniaporins, the Cys residue is replaced by very small residues like Gly/Ala (reviewed by Litman *et al*., 2009). The His at position H5 is critical for water/ammonia transport specificity. If this His is replaced by Ala in predominantly water permeable channels, the channel would gain the function to transport ammonia (Beitz *et al*., 2006).

The TIP contains the following polar residues in its SF regions: His and Arg (in ar/R region) and Asn (belonging to both NPA motifs). In the ar/R region, the residues Phe and His serve as hydrogen bond donors which could significantly decrease the energetic cost of water transport and hence account for very high intrinsic water transport rates as compared to other AQP isoforms.

2.3.1.2 Mutational analysis in the NPA region

In this experiment, the native Asn from each of the NPA motifs was substituted by His and as a result 2 mutants were generated. The mutants were analysed by stopped-flow spectroscopy to study their ability to facilitate water and ammonia transport. The results revealed that both mutants were nonfunctional. Refer to the general figure for raw time courses (without normalization) given earlier in this section section (Fig 2.3.1).

This study involved the substitution of Asn by His in both the motifs as it was decided to introduce an aromatic ring in the water channel keeping in view the close location of both selectivity regions. The presence of an aromatic ring close to the NPA and the ar/R regions was expected to result in changes in solute permeability without affecting the pore integrity. The loss of function was quite surprising, as both Asn and His are polar residues and may serve as hydrogen bond donors in the context of the requirement for water permeation through the pore. However, His has a positively charged imidazole group and is a particularly reactive amino acid. In molecular dynamics studies, Kong and Ma (2001) also suggested substitution by a His residue because of its size and chemical nature being similar to Asn.

Unfortunately the protein expression data is missing due to the lack of an appropriate antibody against the TIP. There are, however, some supportive evidences (see the caption 2.3.1.3 on proton leakage) available, which confirm that the protein was expressed in both mutants.

Probably, the introduction of an aromatic ring (N-to-H mutations in the motif) has tapered down the constriction and has sterically hindered the passage of heavier molecules of water (2.8 Å) and ammonia (2.9 Å). As previously mentioned, the pore at this region doesn't permit any molecular entity larger than 2.8 Å. Selectivity by size also plays a role to exclude the larger solutes from the pore constriction (Walz *et al*., 2009).

This highly conserved nature of the NPA motifs indicates that each of the residues constituting this motif is inevitable, but the mutational analyses reported so far revealed contrasting effects. Several studies confirmed that the Asn of both NPA motifs are involved in water permeability through H-bonding with water molecules (Sui *et al*., 2001, Yakata *et al*., 2007, Horsefield *et al*., 2008). See a MD simulation (Horsefield *et al*., 2008) presented in figure 2.3.3 which shows interaction between asparagines of the NPA motifs and the water molecules.

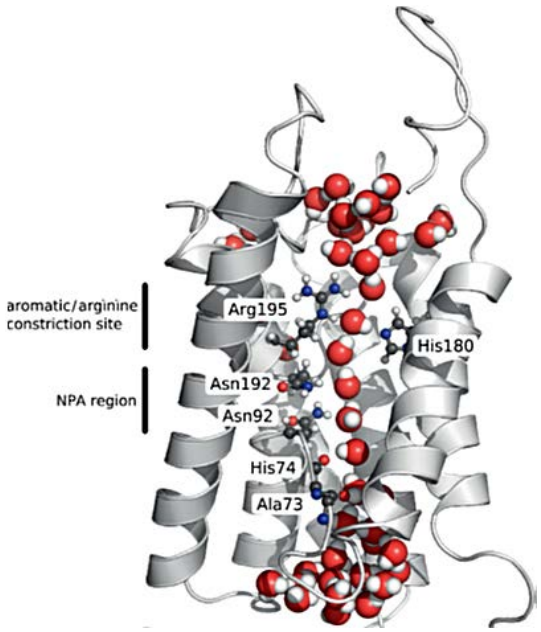

Fig. 2.3.3: Snapshot from an MD simulation of AQP1 showing a single file of water inside the AQP1 channel. Some water-interacting amino acid side chains are shown in ball-and-stick representation. The asparagines of the NPA motifs form strong hydrogen bonds with permeating water molecules (shown as red spheres). Another constriction ar/R region is located at the extracellular exit of channel. (Adopted from Horsefield *et al*., 2008)

The NPA motifs of AQP11 and AQP12 are exceptionally different in the entire family of AQPs. The loop B motif is NPC in AQP11 (Yakata *et al*., 2007) and NPT in AQP12 (Itoh *et al*., 2005). The NPC motif is essentially required for full protein expression, as the exchange of the Cys by an Ala almost abolished water permeability (Ikeda *et al*., 2010). The water permeability in PfAQP (a parasitic

aquaglyceroporin) is even higher than that of orthodox AQPs. It contains NLA and NPS instead of NPA motifs in (respectively) loop B and loop E, but the structural basis for the much higher water permeability or the selectivity mechanism is not provided by the unusual motifs (Hansen *et al*., 2002). Fps1, a glycerol facilitator of yeast and a close homologue of the aquaglyceroporins Glpf, also contains varying motifs that is NPS and NLA in its loops B and E, respectively (Bill *et al*., 2001).

No deletion of NPA motifs in plant AQPs has been reported so far. Deletion of one or both motifs in mammalian AQP4 impaired trafficking, indicating that the NPA motifs play an important role in the plasma membrane expression (Guan *et al*., 2010). The deletion of even both NPA motifs had a little effect on the osmotic permeability and it didn't influence the expression and the intracellular processing of AQP1 at all (Jiang and Ma, 2006). A simulation study in AQP1 indicated that the substitution of native proline of the motif by Leu doesn't affect overall hydrophobicity of the channel. The presence of Leu had a far-reaching effect, but these were compensated by the covalent changes taking place throughout the protein (Newby *et al*., 2008).

Replacing Asn for Asp in the NPA region enabled a low proton permeability in AQP1, but the proton leakage was remarkably higher when the His and the Arg belonging to the ar/R were substituted by Ala and Val, respectively (Wu *et al*., 2009). Some other reports also indicate that a major electrostatic barrier against the transport of solutes originates from the ar/R region in comparison to the NPA motif (Chen *et al*., 2006, Beitz *et al*., 2006). The residues in the NPA region and the helix dipole are not solely responsible for imparting selectivity to the AQPs (Kato *et al*., 2006).

2.3.1.3 Proton leakage through SF variants of TaTIP2;2

This section has described the functional analyses of a number of mutations in the NPA motifs as well as in the ar/R region. All the mutants proved to be nonfunctional and the protein expression in case of the TIP variants couldn't be determined due to the lack of antibody. Therefore, it was decided to confirm the presence of the protein by employing some indirect approach. It was considered most realistic to study the leakage of protons, as any of such mutations is expected to cause changes in the chemical or geometric properties of the selective channel (and less likely breakage of the pore).

Ammonia exists in nature in two forms, the slightly basic NH_3 and the acidic NH_4^+ form. The more acidic the pH, the more is the chemical equilibrium shifted towards the charged form of ammonia, which is ammonium. The Mep family comprises of

the high-affinity ammonium transporters, which act independent of the prevailing pH. According to the Henderson–Hasselbalch equation, almost 80% of the ammonia is available/transported in the form of NH_4^+ at pH of 5.2.

$$\mathrm{pH} = \mathrm{pK}_a + \log \frac{[\mathrm{A}^-]}{[\mathrm{HA}]} \qquad \text{---------- Equation (IIIa)}$$

The data obtained from the given experiment must not be compared with those presented in the section I (concerning to ammonia permeability in the TIP mutants) of this chapter. The reasons are: (i) the pH used in the previous experiments was 8.0 which is different to the one employed in the experiment on proton leakage. (ii) The buffer used in the previous experiments was Tris/HCl whereas it was malate in the present one. In the present experiment, the pH had been varied in the range from 5.2 to 7.2.

This study involved both the afore-mentioned mutations in the NPA region (N84H and N196H) as well as a mutation selected at random from the ar/R region (that is H64F). The results revealed, that the mutations in the NPA motifs, where native Asn was substituted by His had allowed some leakage of protons (Fig 2.3.4). However, the mutation in the ar/R region (H64F) remained non-conducting to the protons (refer to general Fig 2.3.1). The results are presented only as normalized time courses (Fig 2.3.4) and the precise coefficients of proton permeability were not calculated. It is generally believed that the aquaporins conduct ammonia essentially in the form of NH_3 and they don't permit the charged form of ammonia (Holm *et al*., 2005, Saparov *et al*., 2007). It is noteworthy that the function observed in the NPA motifs might be owing to the leakage of some other solute(s). Although this phenomenon was not further investigated, we tempt to speculate that it is probably nothing else but the conductance of the protons.

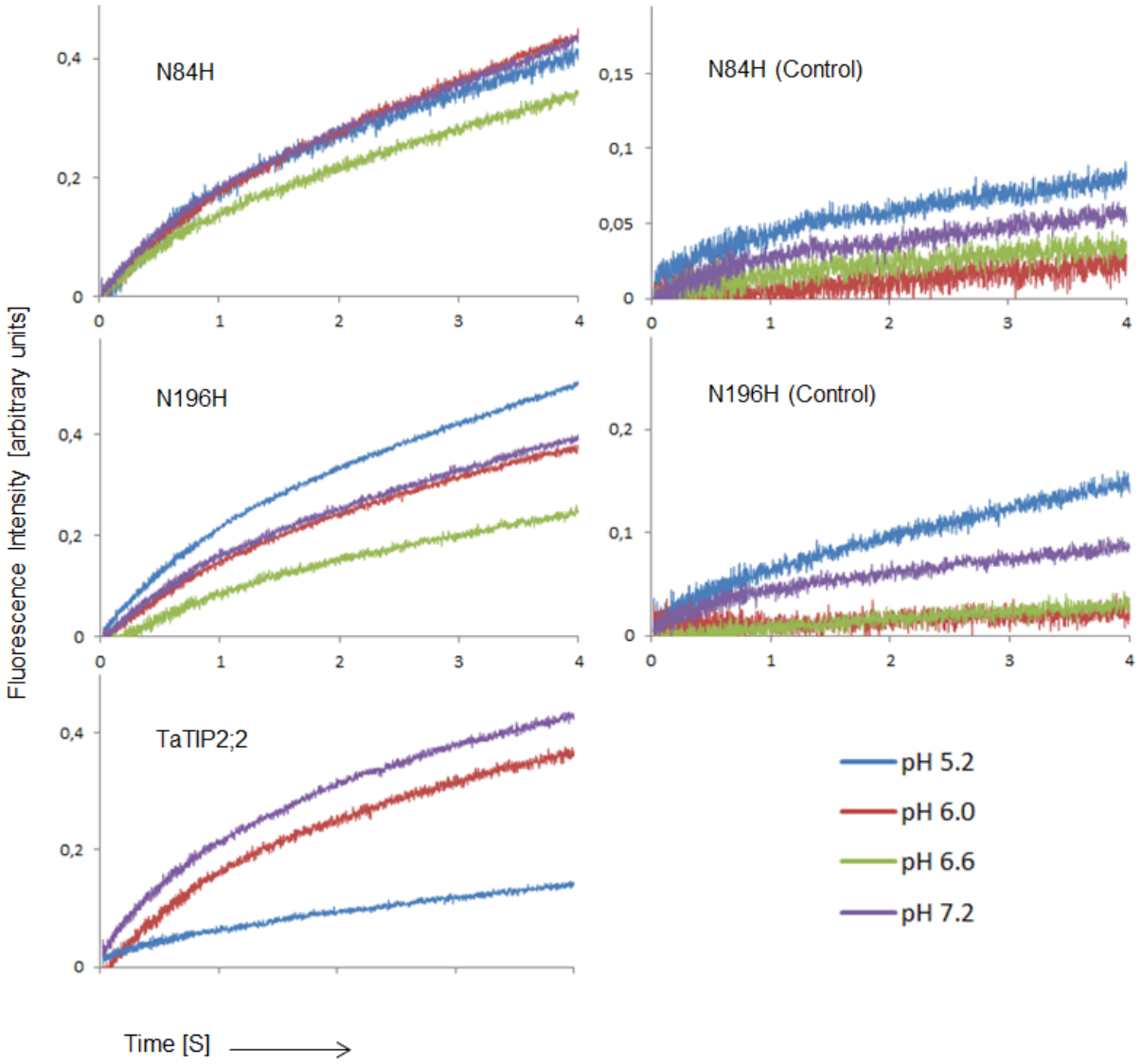

Fig 2.3.4: The presence of varying ammonia species under different pH has been exploited in determining H^+ leakage. The time courses for the leakage of H^+ as indicated by the change in the fluorescence intensity are presented in this figure. The pH of the outer solution containing NH_4Cl was varied from 5.2 to 7.2. Control panels stand for the measurements involving the mutants in which the protein expression was not induced. Each curve is the average of at least 30 traces belonging to 3 independent experiments. The total number of traces acquired for each of the construct was at least 50. Note the different scales along Y-axis. The color scheme is same in all graphs.

Both mutants of the NPA motifs proved to be functional in this experiment unlike their nonfunctionality in the prior studies regarding water and ammonia permeability. The possible explanations might be: (i) The experiments on ammonia were conducted at a pH of 8.0, but the proton permeation was studied in a pH ranging from 5.2 to 7.2. (ii) The buffer used in the proton permeation experiments was maleic acid and the one used for studying water and ammonia permeation was

Tris/HCl. (iii) The fact that the mutation in the ar/R region (H64F) didn't exhibit any proton conductance, further authenticates the present experiment on protons. The results indicate that the loss of ammonia and water transport function in all the previous experiments was intrinsic to the mutations and not because of the non-expression of the protein.

In contrast to the case of the NPA mutants, the mutation in the ar/R region (H64F) exhibited no proton leakage, even at pH 5.2. The kinetics for these mutants are not presented here because of their similarity to other nonfunctional mutants (refer to general figure 2.3.1).

In the present experiment, the conductance of some other cations (and not the protons) can't be ruled out, because of the following reasons: (i) in case of N84H, at pH 7.2, the proton permeability was quite comparable to what was observed at pH 5.2. (ii) In both mutants, the proton leakage is higher at pH 7.2 than at pH 6.6. Unfortunately, these discrepancies can't be reasoned, as comprehensive investigation of this issue is lacking. Once again, the primary objective of this experiment was to determine the protein expression and not to investigate the ability of TaTIP2;2 to facilitate passage of either protons or a solute, other than water/ammonia.

The proton is the smallest and the most mobile cation in aqueous solutions, yet it can't permeate through the selectivity regions of aquaporins. The permeability of solutes in AQPs is determined just partially by the size-restrictive mechanism and the pore size is not the only selectivity barrier against the solute transport (Phongphanphanee *et al*., 2010, Hub and de Groot, 2008, Wang *et al*., 2005). The glycerol facilitator GlpF has the widest pore of 3.3Å diameter (Fu *et al*., 2000), whereas a predominantly water conducting channels like PIP2 have the smallest, that is 2.1Å (Törnroth-Horsefield *et al*., 2006) and the AQP1 has a pore diameter of 2.8Å (Murata *et al*., 2000).

The role of the selectivity regions is not yet fully understood. The electrostatic repulsion generated by the positive charge of Arg in the ar/R region, as well as the size-imposed restriction excludes various ions and protons to permeate (reviewed by Hub *et al*., 2009). Both, the ar/R region as well as the NPA motif hinder the leakage of protons, however the former controls proton exclusion more tightly than the NPA motif (Chen *et al*., 2006, Wu *et al*., 2009).

The Asn of the NPA motif caps the positively charged ends of two short α-helices and a high electrostatic barrier restricts proton leakage through the pore (Li *et al*., 2011, Chakrabarti *et al*., 2004). In contrast, the NPA region prevents more effectively leakage of Na^+ compared to protons. The AQP1 mutants, in which a positive charge in the constriction was removed and the pore was widened by

substituting Arg with Val or His with Ala, exhibited some proton leakage (Beitz *et al*., 2006). The exchange of asparagine for aspartate in the NPA region enabled low proton permeability (Wu *et al*., 2009).

2.3.2 Domain swapping

2.3.2.1 Swapping TM helices & connecting loops between TIP and PIP

The studies were further broadened to determine the molecular signatures responsible for imposing the selectivity barrier to block the ammonia permeation in predominantly water conducting channels (NtPIP2 in our case). Various domains were focused in this experiment; the loops A, D and the transmembrane helices 2, 5 were swapped between TaTIP2;2 and NtPIP2;1 under different arrangements as given in the figure 2.3.5. In the tetrameric view of aquaporins, the transmembrane helices 2 and 5 are oriented towards the central pore (Murata *et al*., 2000). It was expected that any change in the pore characteristics because of the altered TM2 and the TM5 would affect ammonia permeability in case there exists a central pore. All the chimeric proteins were nonfunctional and no protein expression could be determined in case of the altered TIP, because of the lack of an appropriate antibody. In case of NtPIP2, only the chimeric protein containing loop A and TM2 from the TIP was expressed (Fig 2.3.8). The other chimeras containing loop D/TM5 and both the previous swaps combined that is loop A/D as well as TM2/5 from the TIP were nonfunctional. The time courses for permeation are not presented here and were similar to the one given in the general figure 2.3.1 earlier in this section.

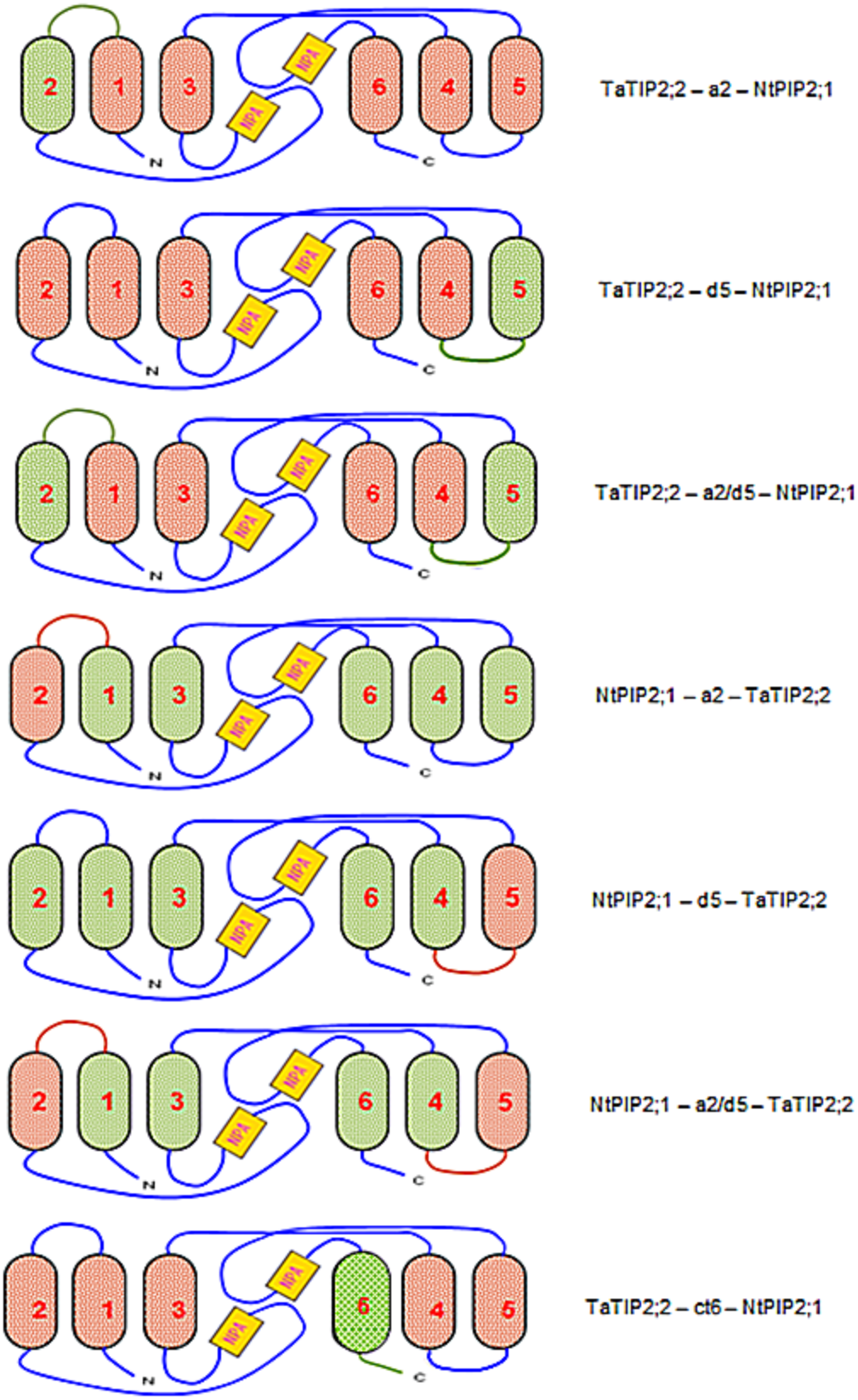

Fig 2.3.5: Topology of the chimeras generated between TaTIP2;2 and NtPIP2. The keys on the right provide the details on the loops and the TM helices swapped; the alphabet in the middle stands for either the loop ("A" or "D") or for the C-terminus ("ct"), and the numeral

digit stands for the TM helix ("2", "5" or "6"). For instance, TaTIP2;2-a2-NtPIP2 would read as the wild type TaTIP2;2 with its loop A and transmembrane helix 2 swapped corresponding to that of NtPIP2. The swaps in the domains of TIP and PIP were accomplished by a method termed as "splicing by overlap extension" (SOE-PCR) which involves a series of PCR reactions. The detailed strategy is explained in the chapter "Materials and Methods".

There is no report available to date involving the domains swapping in plant AQPs. However, in an insect aquaporin AQPcic, the role of the distal part of the TM6 and the C-terminal part was studied by substituting the said domains with those of Glpf and no specific involvement of these regions was observed in tetramerization and channel selectivity (Duchesne *et al*., 2002).

The molecular dynamics simulations (Jensen *et al*., 2008) and the functional data (Nemeth-Cahlan *et al*., 2004) revealed the existence of the pH-sensitive histidines in the extracellular loops A and C of the mammalian AQP0. These His residues contribute to pH-dependent regulation of AQPs, but the exact mechanism is to date unknown. It has been generally proposed in related studies that loop A may possibly undergo slight conformational changes, which are subsequently responsible for gating the pore. Water conductance of spinach PIP2 is regulated by phosphorylation of the two conserved residues, Ser115 and Ser247 (Johansson *et al*., 1996, 1998), and by the protonation of the conserved His residues located in loop D of plant PIP2 (Tournaire-Roux *et al*., 2003, Fischer and Kaldenhoff, 2008). Crystal structures of SoPIP2;1 in the open and the closed pore states further elaborated the involvement of loop D in the gating phenomenon (Törnroth-Horsefield *et al*., 2006).

The contribution of loop D in mercury sensitivity has also been reported. Usually, the Hg sensitive site is located a couple of (usually 3) residues N-terminal to the second NPA motif but in case of AQP4, it is exceptionally located in loop D. The residue at the corresponding position in the orthodox human AQP1 is Thr157 and should be normally inaccessible from the intracellular side (Yukutake *et al*., 2008).

Fig 2.3.6: Partial sequence alignment in which loop A and TM 2 ***(A)*** and loop D and TM5 ***(B)*** domains of TaTIP2;2 and NtPIP2 are compared.

The helices TM2 and TM5 together with the C-terminal halves of the TM1 and TM4 form the major part of the surface of the aqueous pore. The rest of the surface is formed by loops B and E. It is believed that the interaction between the TM2 and the TM5 might be important, especially for the folding of the molecule because, the two helical bundles 1-3 and 4-6 might meet through interaction between TM2 and TM5 (Murata *et al*., 2000). In AQP1, the A loop lies on top of helices 1 and 2, parallel to the side of the monomer. In SoPIP2, however, the position of the helix 1 C-terminus and the helix 2 N-terminus suggested that the loop A was oriented towards the center of the tetrameric topology (Kukulski *et al*., 2005).

The crystal structure of AQP1 showed interaction between the TM2 and 5 by virtue of Gly residues; one each from both TM helices. Both helices are locked together in a so-called "fitting of ridges and grooves" manner (Murata *et al*., 2000). The same positions were later found to be critical for anion permeability. Even minor alterations in the locking interactions of the TM2 and TM5 may cause conformational changes. Any substitution in the first position leads to the conversion of an anion channel into a water-selective channel and the double mutant failed even to traffic to the plasma membrane (Liu *et al*., 2005a).

A. Homology models of a2 and d5 domains of TIP and PIP2

Based on the crystal structure as well as on functional data available to date, the importance of the loops A, D and the TM helices 2 and 5 has been discussed in detail throughout this study. It is quite obvious that even minor changes in the biochemical or the physical properties of these regions may result in noticeable variations in protein function.

The combined domains loop A and TM2 of TaTIP2;2 are 2 amino acids larger and are more hydrophobic than those of NtPIP2;1. An important feature of the given TIP domains is the presence of two proline residues as compared to none in PIP2. The proline rich TM2 indicates the role of this domain in the transport process. Also the two proteins are distantly related and the presence of prolines may be attributed to the conformational variations in these domains (Fig 2.3.6, 2.3.7).

Loop D and TM5 of NtPIP2 is only one amino acid larger and is less hydrophobic than that of TaTIP2;2. An important feature of this region is the presence of two positively charged Arg residues. This domain is enriched with proline residues in both channels, which is probably important because of its highly dynamic loop D. This loop in AQPs is involved in regulating the channels through the so-called gating mechanism. Loop D is capable to sway back and forth resulting into a flip-out mechanism over the pore mouth, which is responsible for its opening and closing. The gating mechanism has been reviewed in detail by Törnroth-Horsefield *et al*. (2010). The domain is also enriched with aromatic rings in case of NtPIP2, which indicates that this domain may play a role in recruitment of transporting solutes (Fig 2.3.6, 2.3.7).

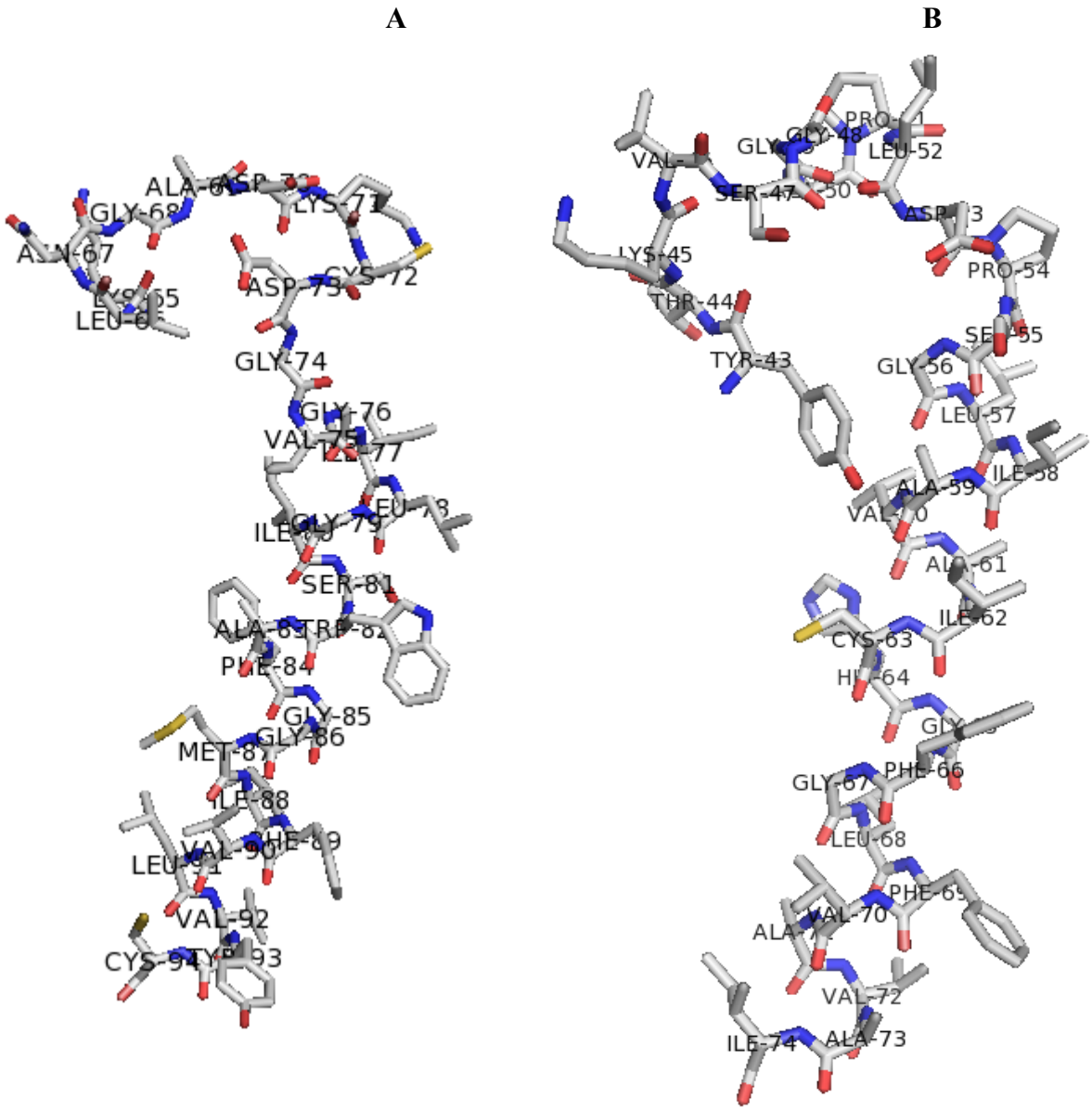

Fig 2.3.7: The structural domains loop A and TM2 shown in this figure were derived from the homology models of the swapped proteins that were drawn to confirm the structural integrity. ***(A)*** NtPIP2;1 ***(B)*** TaTIP2;2. The residues constituting the given domains have been labelled and the figure shows their Cα backbones and the side chains. The coordinates provided by the online tool "SWISS-MODEL" were used to draw the model in the software PYMOL. SWISS-MODEL used human AQP4 (PDB entry # 3GD8) and SoPIP2 crystal structures (PDB entry # 2B5F) as template for TaTIP2;2 and NtPIP2, respectively.

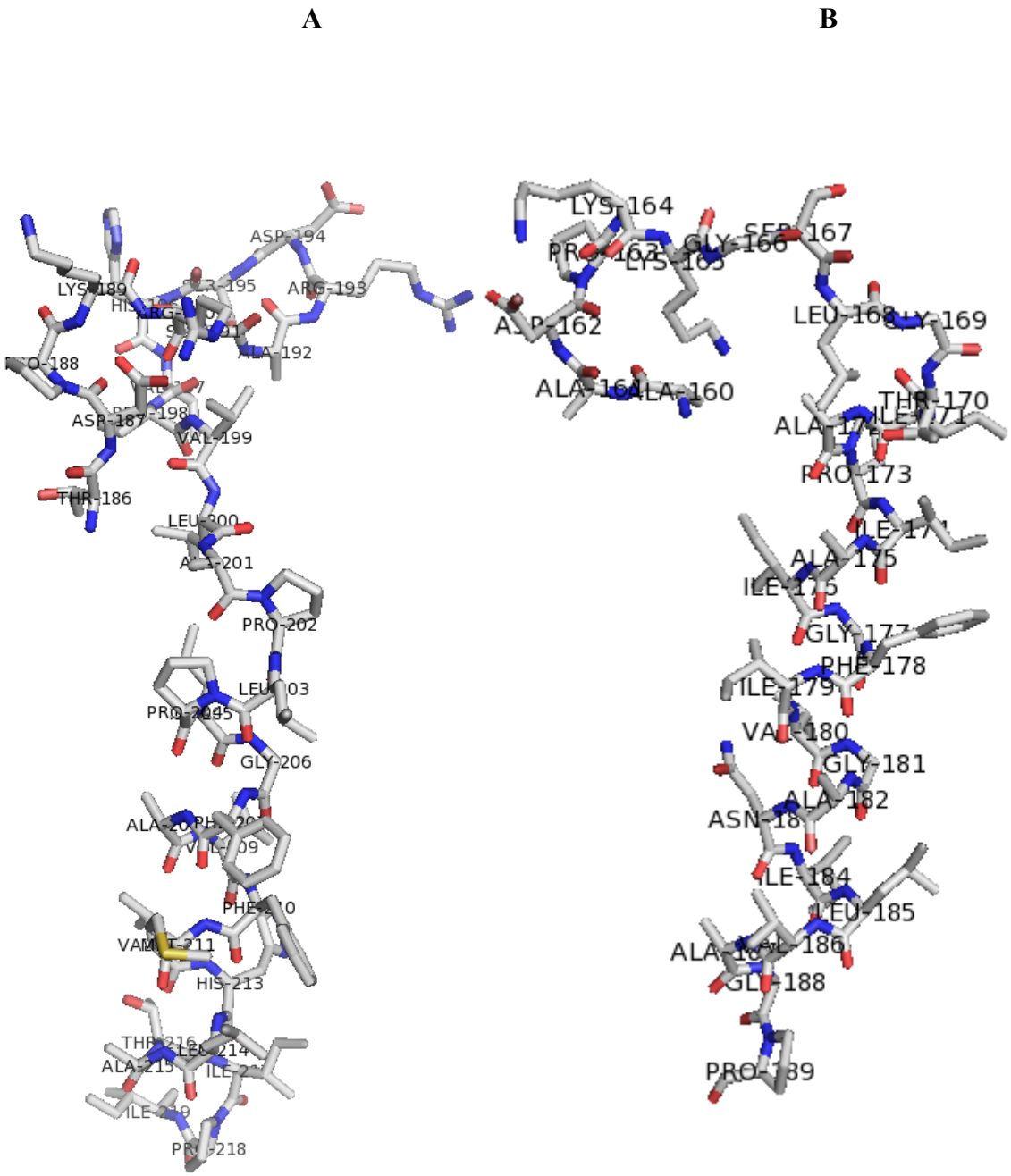

Fig 2.3.8: The structural domains loop D and TM5 shown in this figure were derived from the homology models of the swapped proteins that were drawn to confirm the structural integrity. ***(A)*** NtPIP2;1 ***(B)*** TaTIP2;2. The residues constituting the given domains have been labelled and the figure shows their Cα backbones and the side chains. The coordinates provided by the online tool "SWISS-MODEL" were used to draw the model in the software PYMOL. SWISS-MODEL used human AQP4 (PDB entry # 3GD8) and SoPIP2 crystal structures (PDB entry # 2B5F) as template for TaTIP2;2 and NtPIP2, respectively.

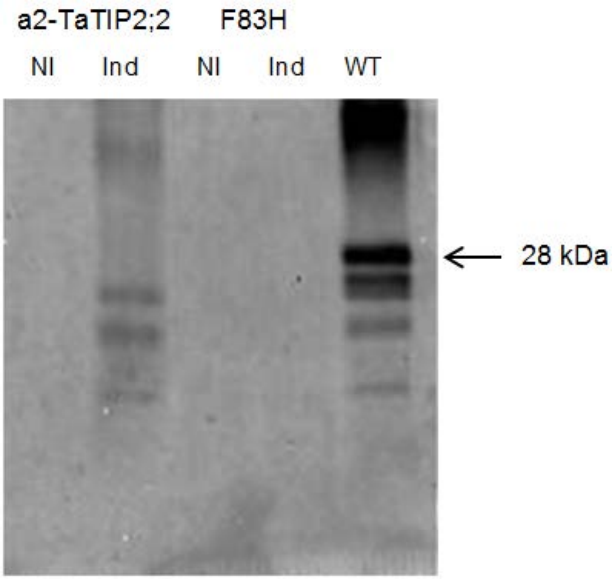

Fig 2.3.9: Western blot analysis of various PIP2 constructs expressed in yeast. F83H is a mutant in which corresponding residues in the ar/R region are substituted. a2-TaTIP2;2 is a NtPIP2 chimera in which loop A and TM2 have been substituted with those of TaTIP2;2. 10 µg of membrane protein from the cells expressing tobacco PIP2;1 were separated by SDS-PAGE and transferred to the nitrocullulose membrane. The wild type (WT) NtPIP2 served as a control.

2.3.2.2 *Swapping the C–terminus together with TM6*

In this experiment, the C-terminus along with the TM6 was attempted to be swapped between TIP and PIP2. These domains were successfully replaced in TIP, but in case of PIP2, the SOE–PCR reactions couldn't be accomplished. The TIP chimera didn't show any water/ammonia transport function (for kinetics, refer to the general figure 2.3.1 given earlier in this section). The result can't be readily interpreted as the protein expression couldn't be determined.

Most MIPs are >300 aa long, but there are examples of much larger proteins in this family, mainly of the eukaryotic origin. The larger size is primarily due to the extended N- and C-terminal domains, the poor conservation in these domains suggesting their involvement in regulation, rather than in function (Ball *et al*., 2003). The role of the C-terminus has been suggested for sorting of the protein in AQP2 (Fushimi *et al*., 1997) and AQP5 (Kosugi-Tanaka *et al*., 2006).

The AQPs regulation by a gating mechanism has been reviewed in detail by Törnroth-Horsefield *et al*. (2010). These are the Ser residues (usually) present in the loop B which are responsible for gating the AQPs as a result of their phosphorylation.

A recent report suggested the involvement of the C-terminal Ser residue in AQP2 regulation that was owing to the conformational changes in the C-terminus to gate the channel (Eto *et al*., 2010). The gating mechanism was thoroughly investigated with the help of the crystal structures in spinach PIP2 (Törnroth-Horsefield *et al*., 2006) and in AQP5 (Horsefield *et al*., 2008). Unusually, gating of a yeast aquaporin (Aqy1) was reported to take place by virtue of a N-terminal Tyr residue (Fischer *et al*., 2009).

It is now well-established that membrane accumulation of AQP2 can be controlled by phosphorylation of the C-terminus. The modification of the C-terminus may interfere the trafficking of AQP5 (Ohashi *et al*., 2008) and several studies have been reported to signify this role of the C-terminus in AQP2 (Moeller *et al*., 2010) and AQP5 (Kosugi-Tanaka *et al*., 2006). A couple of Ser residues are closely located in the C-terminus, out of which only one could be phosphorylated favouring the protein export from the endoplasmic reticulum in case of AtPIP2;1 (Prak *et al*., 2008) and AQP2 (Hoffert *et al*., 2008).

Hedfalk *et al*. (2004) reported a novel function for the C-terminal domain of Fps1p, an atypical member of the MIP family. The C-terminus regulated the channel as explained by the properties of the 12 residues constituting a part of the C-terminus right next to the last TMD.

The presence of Val276-Val-His-Val-Ile280 in the C-terminus was indispensible for targeting of AQP4 to the plasma membrane (Nakahama *et al*., 2002). The C-terminal region has been proposed to be involved in AQP1 regulation, because it carries a consensus sequence for Ca^{2+} binding (Fotiadis *et al*., 2002).

2.3.3 Overview of the section

The present study gives supportive evidence for the importance of the two selectivity regions. The ar/R region of TaTIP2;2 was sequentially mutated so that it mimicked that of NtPIP2;1. Surprisingly, even the single mutations in the ar/R region of TIP were impermeable to ammonia/water/protons. Unfortunately, only one of the mutants (that is F83H) in the ar/R region of both TIP and PIP2 was confirmed to be without any protein expressed. The results are in contrast to previous reports. A couple of the ar/R filter mutants reported so far (Beitz *et al*., 2006) were functional (although they drastically changed the pore characteristics) and their association with protein sorting has not been established.

The previous reports suggest that protons are excluded by both the selectivity regions however, the main electrostatic barrier originates from the ar/R region. At the NPA

region, a positive electrostatic field originates from the two short α–helices, which restricts alkali cations (partially proton leakage too) through the pore. The removal of Asn at the NPA region and the alteration of the ar/R filter to increase its hydrophobicity reduce the electrostatic barrier and allow proton leakage through the pore. The ability of the NPA mutants in the present study to conduct protons is in agreement with the previous reports. However, there is readily no interpretation available for the loss of water/ammonia transport functions.

The crystal structure data as well as the results from the functional experiments have revealed the significance of some of the transmembrane helices and the connecting loops in AQP structure and function. TM helices 2, 5 and the loops A, D were swapped between ammonia conducting TaTIP2;2 and the predominantly water conducting channel NtPIP2;1 in a sequential manner. Further, it was also attempted to swap the C-terminus between the two channels. All the chimeric proteins were found to be nonfunctional for ammonia as well as for water transport. Among the PIP chimeras, protein was expressed only in case of the one with the swapped loop A and TM2. Unfortunately, no protein expression could be determined in case of the corresponding TIP chimeras due to the afore-mentioned reasons. The results imply remarkable structural differences between the two channels. Furthermore, no major alterations in the structural domains can be tolerated; any change would result in deleterious effects on structure/function of the AQPs.

3. MATERIAL & METHODS

3.1 Procedures and manipulations of DNA

3.1.1 Restriction endonuclease digestion of DNA

The restriction digestion was performed according to the instructions of the enzyme manufacturer (MBI Fermentas). One unit of enzyme (per µg of DNA) was added to the reaction mix and the DNA was digested in the recommended buffer. The digestion was allowed to occur for 4 hours to overnight at 37°C.

3.1.2 Agarose gel electrophoresis

Conventional agarose gels contained 0.8% agarose prepared in bidest water and ethidium bromide (0.05 µg/ml) was added to visualize the DNA. The gel was submerged into a chamber containing the running buffer (1x TAE buffer). The DNA samples were mixed with 1x loading buffer and loaded onto the gel. The electrophoresis was performed at a current of 35-45 mA (50–100 V). The DNA bands could be visualized by placing the gel under the UV light (302nm).

50 x TAE (1 L)	242 g	Tris, pH 8.0
	57.1 ml	Glacial acetic acid
	0.5 M	EDTA pH 8.0
5 x Loading Buffer	2 %	Ficoll 400
	0.5 %	SDS
	50 mM	EDTA
	0.2 %	Orange G
	10 %	Glycerin

3.1.3 Isolation / Purification of DNA fragments from agarose gels

Purification of PCR products/DNA fragments by directly using the kit was avoided, rather the following two-steps strategy was adopted: **(i)** The digested DNA (or the required DNA fragment) was isolated from the agarose gel by electrophoresis. The required band was cut using a sharp scalpel as it became visible under the UV light (302 nm) due to prior staining with ethidium bromide. The pieces of agarose gels were collected in a 1.5ml reaction tube. **(ii)** In order to isolate the required DNA fragment from the agarose, the gel extraction kit manufactured by Qiagen was used and the procedure recommended by the manufacturer was followed. At the final step, DNA was eluted into 20µl of TE buffer (10 mM Tris-HCl, 1 mM EDTA, pH 8.0).

3.1.4 Determination of nucleic acid concentration

The DNA samples were diluted (1:50) and the absorption was measured at 260 nm and 280 nm on a photometer. The relative amount of the protein contamination in the sample was determined by calculating A_{260}/A_{280} ratio. A pure DNA preparation was desired to achieve a ratio between 1.8 and 1.9.

3.1.5 Polymerase Chain Reaction (PCR)

All PCR reactions were performed on the "Biometra T-Gradient" thermal cycler. A standard PCR reaction contained the following components:

50 ng	Template DNA
5 µl	10x Reaction buffer (Biotherm)
1 µl	dNTP-Mix (10 mM)
0.8 pmol	Sense-Primer (10 pmol/µl)
0.8 pmol	Antisense-Primer (10 pmol/µl)
1.5 mM	$MgCl_2$
0.5 U	Taq-Polymersase (Biotherm, 5U/µl)
	Bidest. H_2O to 50 µl

Standard PCR program:

1. Initial denaturation	95°C	2 min
2. Denaturation	95°C	30 s
3. Annealing	55°C	30 s
4. Extension	72°C	6 min (1 min for every 1 kb)
25x Cycle from step 2 to step 4		
5. Final extension	72°C	10 min
	4°C hold	

3.1.6 Gene splicing by overlap extension (gene SOEing)

The principle of splicing by overlap extension (SOE) is based on the rejoining of two halves of the same gene with the "overlap" containing the altered sequence, or the joining of two unrelated sequences. This method is useful for joining even three segments. This recombination involves a series of PCR reactions as illustrated in Fig 3.1. It is accomplished in three separate polymerase chain reactions: (i) During two independent PCRs, the splices AB and CD are generated using the primers a, b and c, d, respectively. The primers add the sequences at the fusing ends of the products AB and CD so that the products are complementary to each other. (ii) After purification of both fragments, a final PCR is performed; splices AB and CD would produce the recombinant product AD. The recombinant product is cloned into the vector using the appropriate restriction sites, which are introduced into the recombinant product by the outer primers (a and d).

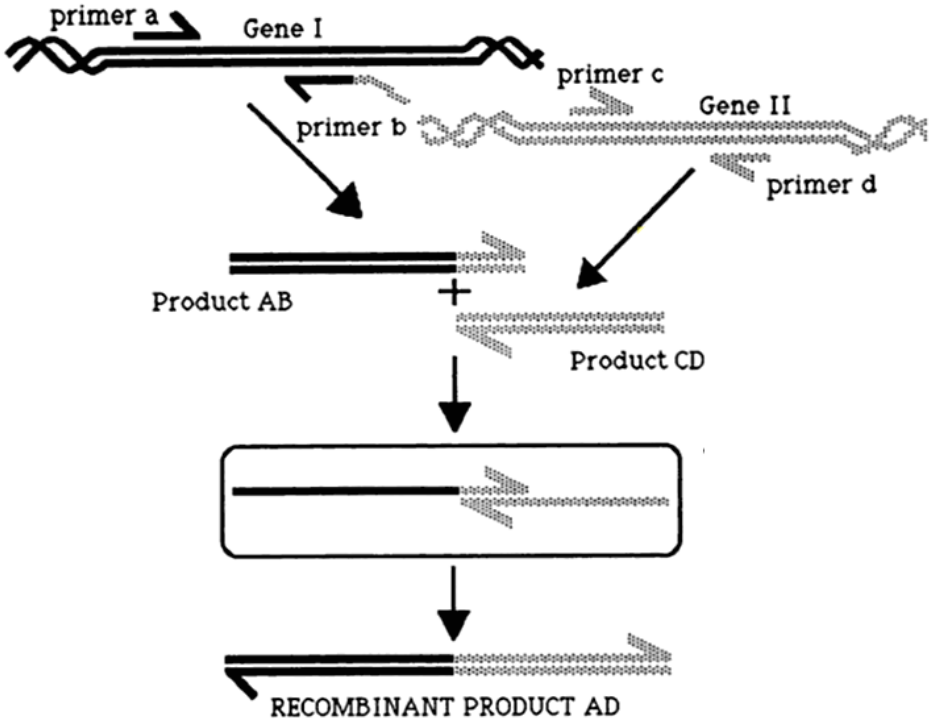

Fig 3.1: Schematics for of the general procedure of gene splicing by overlap extension (SOEing). Adopted from: Horton (1993).

3.1.7 Site-directed Mutagenesis

Site-directed (or specific) mutagenesis is a molecular biology technique in which a mutation is created at a defined site in a DNA molecule, usually a plasmid. For accomplishing site-directed mutagenesis in the DNA sequences, a "QuickChange® Site-Directed Mutagenesis Kit" was used. The procedure recommended by the kit manufacturer (Stratagene) was followed.

The thermal cycling reaction was set as follows:

Template DNA	50 ng
10x buffer	5 µl
dNTP's (10mM)	1 µl
Forward Primer (5 pmol)	1 µl
Reverse Primer (5 pmol)	1 µl
Pfu polymerase (3 U/ml)	0.5 µl
Bidest. H_2O to 50 µl	

The thermal cycling program was as follows:

1. Initial denaturation	95°C	2 min
2. Denaturation	95°C	30 s

3. Annealing	55°C	30 s
4. Extension	72°C	6 min (1 min for every 1 kbp)
5. *Cycle from step 2 to step 4*		25x
6. Final extension	72°C	10 min
	4°C hold	

After thermal cycling, the reaction was cooled down on ice for 2 min. The restriction enzyme DpnI (10U) was added to the reaction tube to digest the methylated, non-mutated, double stranded DNA. The digested reaction was incubated at 37ºC for 1 hour.

3.1.8 Ligation of DNA fragment

The final reaction volume for ligation was set at 10 µl. 50 ng vector DNA along with the required amount of insert DNA (in a molar ratio ranging from 1:1 up to 1:5) were added into the ligation reaction. The amount of insert DNA was determined with the help of the following formula:

$$DNA[pmol] = \frac{2 \times 10^{-6} \times DNA[\mu g]}{DNA[bp] \times 660Da}$$

The following reaction was set:

Linearized vector DNA	50 ng
DNA Insert	x ng
10x T4 Ligase buffer	1 µl
T4 DNA Ligase	0.5 U
H_2O to 10 µl	

The reaction mixture was incubated at 16°C for 6 hours to overnight. As a control, a reaction was set exactly as mentioned above but without the insert DNA. Almost 5µl of the ligated mixture was used for transforming the bacterial cells.

3.1.9 Sequencing of DNA fragments

The DNA sequencing required highly pure DNA. The commercial services of Seqlab and Starseq (based respectively in Göttingen and Mainz, Germany) were used for DNA sequencing and the reactions were prepared according to the instructions. The recommended amount of DNA along with the primer specific to the PCR product were added into a 200 µl reaction tube to prepare the sample.

3.2 Procedures and manipulations of *E. coli*

3.2.1 *E. coli* strains used in the study

Strain	Genotyp	Supplied by
XL1 blue	recA1 endA1 gyrA96 thi-1 hsdR17 supE44 relA1 lac [F´ proAB laclqZΔM15 Tn10 (Tetr)]	Protagen
DH5α	F´- endAI hsdRJ7 (r-, mit) supE44 thi-1 λ- recAl gyrA96 relAI deoR A(lacZYA-argF)- U169 Φ80dlacZΔM15	Invitrogen

3.2.2 Media for cultivation and transformation of *E. coli*

LB Medium*	1% Trypton 0.5% Yeast extract 0.5% NaCl set pH at 7.5 *Volume raised to 1 L with bidest H_2O*
Antibiotic for selection:	50 µg/µl Ampicilin
SOC Medium*	2% Tryptone 0.5% Yeast extract 10 mM NaCl 2.5 mM KCl 10 mM $MgCl_2$ 10 mM $MgSO_4$ 20 mM Glucose set pH at 7.0

*1% agar was added for semi-solid media

3.2.3 Preparation of chemically competent *E. coli* cells

A single bacterial colony was picked to inoculate 3 ml of the LB media. The bacteria were grown overnight in a test tube placed on a shaking incubator set at 37°C. The bacterial pre-culture was diluted with 400 ml of the LB media in a large 2 L flask to have a good ratio between the surface and the volume and was grown with vigorous shaking until OD_{550} = 0.48 (2-2.5 h). Then bacterial suspension was poured into 50 ml falcon tubes, chilled on ice for 15 min and centrifuged at 4,000 rpm for 10 min at 4°C. All further steps were performed in a cold room and on ice. The harvested bacterial cells were resuspended in 20 ml of 0.1 M $CaCl_2$ solution, incubated on ice for 2 hours and centrifuged again as mentioned above. The pellet was resuspended in 43 ml of 0.1 M $CaCl_2$ and 7 ml of sterile glycerol. Finally the cells were dispensed

into aliquots of 250 µl and were shock-frozen using liquid nitrogen before storage at –70°C.

3.2.4 Heat-shock transformation of E. coli cells

For transforming the *E. coli* with the required construct, 50 µl of the competent cells were thawed on ice. Either 5 ng of the sample DNA or 5 µl of the ligation reaction mixture was added to the competent cells in the reaction tube and gently mixed by swirling. The tubes were incubated on ice for 20 min. Cells were heat-shocked in a 42°C water bath for 45 sec and immediately cooled on ice for 2 min.

The transformed bacterial cells were then mixed with 1 ml SOC medium and the tubes were transferred to the shaking incubator set at approx. 225 rpm at 37°C for 45 min. Finally, the transformed bacteria (100-200 µl) were plated on a petri dish containing semi solid LB medium supplemented with the antibiotic (100 µg/ml ampicillin) required for positive selection and incubated at 37°C for 18 hrs.

3.2.5 Plasmid isolation from *E. coli* cells (miniprep)

3 ml of LB Media was inoculated with a single bacterial colony. The culture was grown overnight in a test tube. The cells were transferred into 1.5 ml reaction tubes and harvested by centrifugation at 13,000 rpm for 30 seconds. The supernatant was completely removed and the cells were resuspended in 300 µl of the Resuspension Buffer. 300 µl of the Lysis buffer was added into the reaction tube and the bacterial suspension was gently mixed by inverting it 10-15 times. The cell lysis required 5 minutes of incubation at RT. The neutralization of the cell lysate was achieved by adding 300µl ice-cold Buffer III. The suspension was again gently mixed and incubated for 10 min on ice.

The samples were centrifuged at 13,000 rpm for 10 min at RT. The genomic DNA as well as the proteins were pelleted during this centrifugation step. Almost 700 µl of the supernatant volume was transferred to a 1.5 ml reaction tube containing 800 µl of isopropanol. The DNA pellet was washed twice with 70% ethanol in order to remove the salts. The pellet was air-dried at RT and the DNA was eluted with 20 µl of bidest water. The plasmid preparation was stored at -20°C.

Solution I (Cell Resuspension buffer)

50 mM	Tris/HCl pH 8.0
10 mM	EDTA
100 µg/ml	RNaseA

Solution II (Alkaline Lysis Solution)

200 mM	NaOH
1%	SDS

Solution III (Neutralization Solution)
3 M Potassium acetate pH 5.5

3.3 Procedures and manipulations of yeast

3.3.1 *Saccharomyces cerevisiae* strains used in the study

The *Saccharomyces cerevisiae* strain 31019b (if not otherwise mentioned) was used in the present study which had the following genotype:
MATa, ura3, mep1Δ, mep2Δ::LEU2 mep3Δ::kanMX2 (Marini *et al*., 1997)

3.3.2 Cultivation of yeast cultures

Culturing yeast for various purposes:

The non-transformed yeast cells were cultivated in either liquid or semi-solid YPD medium for various purposes. The yeast cultures meant for permeability measurements on the stopped-flow spectrometer were grown for a definite induction period using the appropriate selection medium [SC + gal (-Ura)]. When no induction of the protein expression was required, the media contained glucose instead of galactose. The time taken for the yeast to attain the NtPIP2 expression at its peak was already determined in the lab. Regarding TaTIP2;2, preliminary experiments had to be performed but the data are not presented. The ells were grown under continued shaking at 225 rpm at a temperature of 30^{o}C.

Media Composition:

YPD medium*	1% Bacto yeast extract 2% Bacto peptone 2% Glucose
SC+gal (-Ura) Medium* (1l)	0,17% Yeast Nitrogen Base 0,5% Ammonium sulfate 0,115% -Ura Amino acids Mix 2% Galactose
SC+glu (-Ura) Medium* (1l)	As above, except the Galactose was substituted with 2% Glucose
10 x amino acids mix (– Ura)	**0.01%** Adenine, Arginine, Cysteine, Lysine, Threonine, Leucine **0.005%** Aspartate, Histidine, Isoleucine, Methionine, Phenylalanine, Proline, Serine, Tyrosine, Valine

* To prepare the semi-solid media, 1.5% agar was added

3.3.3 Isolation of plasmid DNA from yeast

The procedure of Robzyk and Kassir (1992) was followed. 1.5 ml of the overnight culture was grown in a selection medium. The cells were harvested and resuspended in 100 µl STET solution. 0.2 g glass beads (ø 0.5 mm, Sigma) were added to the cell suspension. The cells were vigorously vortexed for 5 minutes before another 100 µl of STET solution were added and the reaction tube was incubated in boiling water bath for 3 min. After brief cooling, the tube was centrifuged at 13,000 rpm for10 min at 4°C. 100 µl of the supernatant were transferred to a fresh tube containing 50 µl of 7.5 M ammonium acetate, incubated at -20°C for 1 hour, and centrifuged for 10 minutes at 4°C. 100 µl of the supernatant were added to 200 µl of ice-cold ethanol. Cells were spun down, washed with ethanol and resuspended in 20 µl of bidest water. 10 µl of this solution were used to transform the competent bacteria.

STET Solution	8 %	Saccharose
	50 mM	Tris/ HCl pH 8.0
	50 mM	EDTA
	5 %	Triton-X 100

3.3.4 Biolistic transformation of yeast cells

The yeast cells were transformed with the required plasmid DNA through the biolistic method following the protocol of Sanford *et al*. (1993). A particle delivery system (PDS) 1000/He (Bio-Rad Labs, USA) was used for this purpose. Briefly, a single colony was inoculated on a petri dish containing semi-solid YPD media and grown for 48 hours at 30°C. The microcarriers (Tungsten particles) were washed with ethanol through a series of steps and could be stored for a period of 2 weeks at 4^{o}C. The DNA coating was accomplished by mixing 50 µl of microcarriers, 5 µg (in 5 µl volume) of plasmid DNA, 50 µl of 2.5 M $CaCl_2$ and 20 µl of 100 mM freshly prepared spermidine solution. The particles had to undergo a series of washing steps using ethanol before these were ready for bombardment. The suspension of 10 µl DNA-coated gold particles was placed on the microcarrier plate and air-dried. The overnight wild-type yeast culture was harvested by centrifugation at 3,000 rpm for 3 min. After washing with bidest water, the cells were again resuspended in water. 80 µl of the cell suspension was spread on the petri dish containing an appropriate selection media. After drying, the plates were placed at a recommended distance from the microcarriers inside the vacuum chamber of the particle gun. The particles were finally bombarded on the yeast cells using a helium pressure of 1100 psi under a vacuum of 3.6 MPa.

3.3.5 Estimation of cytosolic pH in yeast cells

The ratiometric pH determination method (Slavik, 1982) was followed to determine the cytosolic pH. The technique is based on the selective excitation of 2 forms of

fluorescein, basic (monoanionic) and acidic (dianionic). Each of these forms possesses different fluorescence properties. The proportion of these 2 forms is pH-dependent and may be monitored by the ratio of fluorescence intensities observed following excitation at 435 nm and 490 nm.

The ratiometric pH determination is particularly reliable in case of turbid solutions where fluorescence intensity fluctuates due to excitation and emission light scattering. The advantage of this method is that the ratio of fluorescence intensity is not sensitive to fluctuations of light scattering.

3.3.5.1 The fluorescent dye "Fluorescein diacetate" (FDA)

Fluorescein is an aromatic heterocyclic molecule the applications of which range from forensics to microscopy utilizing its fluorescence properties. An important use of Fluorescein is measurement of intracellular pH. As the Fluorescein leaks out of the cells rapidly, highly charged derivatives are recommended (Lakowicz, 2006). Fluorescein has a pK_a of 6.4, and its ionization equilibrium leads to pH-dependent absorption and emission over the range of 5 to 9. The absorption and emission spectra of fluorescein are shown in Fig 4.2.

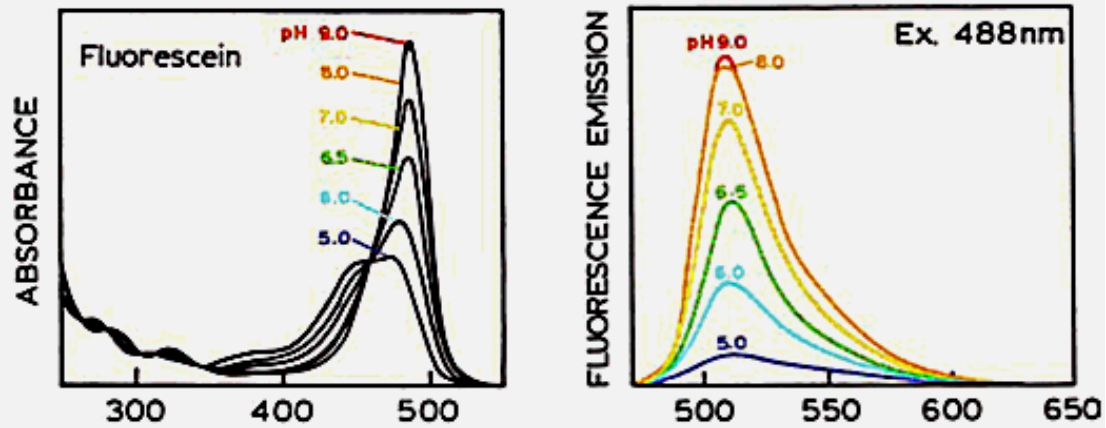

Fig 4.2: Absorption and emission spectra of Fluorescein. Adopted from Lakowicz (2006)

Fluorescein is a complex fluorophore which, depending on pH, exists in one or more of four different prototropic forms that is cation, neutral, monoanion and dianion. However, in the pH range 6-10, only the monoanion-dianion equilibrium prevails. Only these two forms of fluorescein are fluorescent and their maximum excitation occurs at 494 nm and emission at 521 nm (probes.invitrogen.com). In aqueous solutions with pH above 9, its phenol and carboxylic acid functional groups are both totally ionized. Upon acidification, first the phenolic group is protonated to yield the monoanion (pK_a ≈6.4) followed by the carboxylic acid (pK_a < 5) yielding neutral fluorescein species. Upon further acidification, a cation form (pK_a < 2.1) will be generated (Bamfield, 2001).

3.3.5.2 Plotting a calibration curve

For measuring the apparent changes in cytosolic pH of *Saccharomyces cerevisiae* cells, a colorless membrane permeable diacyl derivative of Fluorescein (Fluorescein diacetate; Sigma catalog no. F7378) was used, because of the following reasons: (i) It does not show fluorescence as such but, only after decomposition to fluorescein through intracellular esterases. (ii) Fluorescein shows low membrane permeability and data can be comfortably recorded for several minutes without risk of dye leakage out of the cell.

For each pH, the emission intensity was detected at 520 nm. A ratio of light emission at 520nm was determined for excitation at ~490 nm versus the excitation at its isosbestic point of ~435 nm. The ratio of these two intensities ($I_{490/435}$) was plotted against pH on a logarithmic scale (see Fig 2.1.10 in results section). The data were fitted with a second-order polynomial function (see Fig 2.1.10 in results section). The results were used to generate an equation that converted recorded fluorescence ratio in case of yeast cells to apparent pH_i values.

For obtaining data for the calibration curve, McIlvaine buffers were prepared with pH varying from 5 to 9.

McIlvaine Buffer	0,2M	Disodium hydrogen phosphate (Na_2HPO_4)
	0,1M	Citric acid ($C_6H_8O_7$)

3.3.5.3 Estimation of cytosolic pH

Yeast cells from an overnight culture (20ml) were harvested by centrifugation and loaded with Fluorescein. 5ml of loading buffer and Fluorescein diacetate (at an end concentration of 50µM) were added to the yeast cells (pellet) and were placed on a shaking incubator set at 125 rpm for 15 min at 30°C. The cells were washed twice with bidest water and resuspended in the incubation buffer (as given under the caption 3.4.2.3, ammonia permeability buffers). Fluorescence intensities ($I_{490/435}$) were recorded before and immediately after addition of 25mM NH_4Cl, in order to obtain apparent values for starting and final pH, used for calculating P_{NH_3} values.

3.4 Determination of Permeabilities

3.4.1 Stopped Flow Spectrophotometer

A schematic diagram of the stopped-flow spectrophotometer is given in Fig 3.3. The two syringes of the apparatus are filled with yeast cells (suspended in incubation buffer) and the mixing buffer (represented as solution A and B, respectively in the Fig 3.3). The solutions inside the syringes are compressed to force their mixing in a cuvette (observation cell). From here, the mixed solutions are forced out to pass into the stop syringe. The plunger of the stop syringe hits the stopping block to terminate the mixing process. The flow fills the stop-syringe, until the plunger hits the trigger-

switch. This simultaneously stops the flow and starts the data acquisition. The progress of the reaction is monitored in the observation cell using the emission measured at a 90° angle to the excitation beam (Nalefski and Newton, 2003).

An important feature of the stopped-flow technique is to record the absorbance within milliseconds of mixing the two reactants. In addition, the stop syringe assures for a steady rate of flow so that the reactants can be added to the solution and the products are formed at a consistent rate.

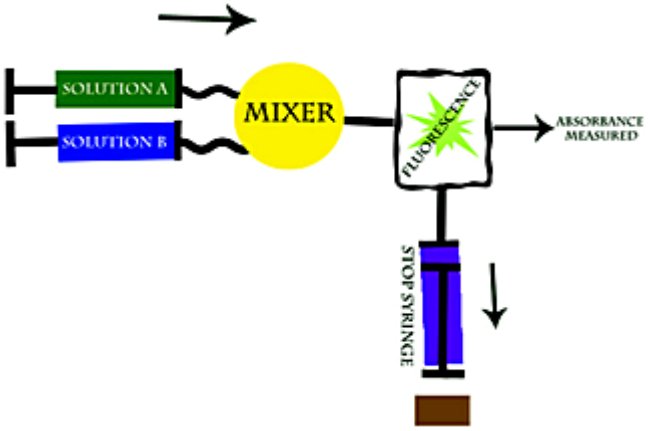

Fig 3.3: Schematic diagram of the stopped-flow apparatus.
Adopted from: http://chemwiki.ucdavis.edu/

3.4.2 Determination of Ammonia Permeability

3.4.2.1 Principle

According to the Henderson-Hasselbalch equation, at pH 8.0 more than 80% of ammonia will be in the NH_3 form (which is a slightly basic ammonia species). Therefore, the intracellular pH will increase as a result of ammonia uptake through the membrane. The change in intracellular pH corresponds to changes in the fluorescence intensity which are recorded by the stopped-flow spectrophotometer and are shown graphically on the Biokine software.

3.4.2.2 Loading of yeast cells with Fluorescein diacetate (FDA)

20 ml of the overnight culture was raised and the cells were harvested at 3,000 rpm for 3 min at RT in a table-top centrifuge. The pellet was washed twice with bidest water. After the final centrifugation, cells were resuspended in 5 ml of loading solution and were placed on a shaking incubator set at 125 rpm and 30°C. After 15 minutes, cells were loaded with fluorescein, giving them a yellow color. The cells were quickly spun down at 3,000 rpm at 4°C. The loading solution was completely removed and the cells were resuspended in the appropriate incubation buffer. The cells were kept on ice until the measurements were started.

Loading Solution	50 mM	HEPES/NaOH	pH 7.0
	5 mM	2-Deoxy-D-Glucose	
	50 µM	FDA	

3.4.2.3 Experimental Conditions

All the measurements were performed at a temperature of 10°C, that was maintained by using a circulating water-bath. The yeast cells loaded with fluorescein were mixed with an equal volume (100 µl) of the mixing buffer. The velocity of the flow was set to 10 ml/s. The instrument's dead time was estimated to be 1.6 ms. The dead time is defined as the time from mixing the reactants to the beginning of the recording.

Light source	λex: 490 nm		
Time base 1 =	20 µs/data point	for	4000 data points
Time base 2 =	200 µs/data point	for	2000 data points
Time base 3 =	2 ms/data point	for	1000 data points
Filter	300 µs		

Ammonia permeabilities were analysed by measuring pH dependent fluorescence changes using a 515 nm cut-off-filter for light emission and excitation at 490 nm.

Buffer Composition:

Incubation Buffer	50 mM	NaCl	
	10 mM	Tris/HCl	pH 8.0
	5 mM	$CaCl_2$	
Mixing Buffer	50 mM	NH_4Cl	
	10 mM	Tris/HCl	pH 8.0
	5 mM	$CaCl_2$	

3.4.3 Determination of Water Permeability

3.4.3.1 Principle:

The measurement of water transport was based on changes in the volume of the yeast protoplasts and the subsequent effect on the intensity of the scattered light. An osmotic gradient of 300mOsmol was generated across the plasma membrane by mixing the protoplast suspension with the hypotonic solution (mixing buffer) resulting in water influx and swelling of the protoplasts. The incident light after striking with the protoplasts surface is scattered and the photomultiplier detects the scattered light intensity from a right angle (Fig 3.3). More the cells are swollen, more would be the surface area of protoplasts and less would be the scattering of light.

3.4.3.2 Preparation of yeast protoplasts:

The procedure reported by Bertl *et al*. (1998) was adopted to prepare the yeast protoplasts. The cell wall was digested by using Zymolyase. Zymolyase, derived from *Arthrobacter luteus*, is a purified mixture of β-glucanases and proteases. The ingredients of this mixture work in conjunction for an efficient cell wall degradation. As the Zymolyase may damage the membrane proteins, bovine serum albumin (BSA) was added which acts as a competitive substrate for the proteases. The procedure for protoplast preparation was as follows:

10 ml from an overnight yeast culture were harvested at 3,000 rpm for 3 min in a Beckmann tabletop centrifuge at RT. The cells were washed with distilled water, resuspended in 3 ml of incubation buffer and placed on a shaking incubator set at 200 rpm and 30°C for 15 min. After that, 4 ml of the protoplast buffer was added to the suspension along with zymolyase 20T and BSA (end concentration are given below). The suspension was incubated for 45 min and 30°C on a shaker set to 200 rpm. The protoplast suspension was centrifuged at 3,000 rpm for 3 min at RT and resuspended in the appropriate incubation buffer for subsequent stopped-flow measurements.

Incubation buffer	50 mM	KH_2PO_4 (pH 7.2 adjusted with KOH)
	0.2%	β-Mercaptoethanol
Protoplast buffer	Incubation buffer with 2.4 M Sorbitol	
	0.01-0.03 mg/ml	Zymolyase (20T)
	25 mg/ml	BSA

3.4.3.3 Experimental Conditions:

Water transport was measured using light source set at a wavelength of 436nm. The other experimental conditions were same as previously mentioned for the ammonia measurements.

Incubation Buffer	1.8 M	Sorbitol	
	50 mM	NaCl	
	5 mM	$CaCl_2$	
	10 mM	Tris/HCl	pH 8.0
Mixing Buffer	Same as above except Sorbitol concentration was 1.2 M		

3.4.4 Data Analysis

3.4.4.1 Calculation of osmotic permeability coefficient (P_f)

For each of the constructs, at least 50 time courses were obtained from at least three independent stopped-flow measurements, which involved independent batches of yeast cultures. The traces were analyzed using the software "Biokine" version 4.27 (Bio-Logic Science Instruments, France). Using this software, the kinetics were analyzed by fitting them using single exponential function. The data fitting provided rate constants (*ki*) required to calculate the permeability coefficients, which can be used to compare (transport) function of various constructs. For water transport curves, data were analyzed for a time period of 100 ms after its beginning (see Fig 3.4 for further details). The software employed "Simplex" algorithm to fit the time courses. The equation is given as:

$$Y = at + b + \sum_{i=1}^{N} c_i e^{-k_i t}$$

In this equation, the portion (at + b) represents the linear component of the reaction whereas the remaining portion represents the sum of exponential functions.

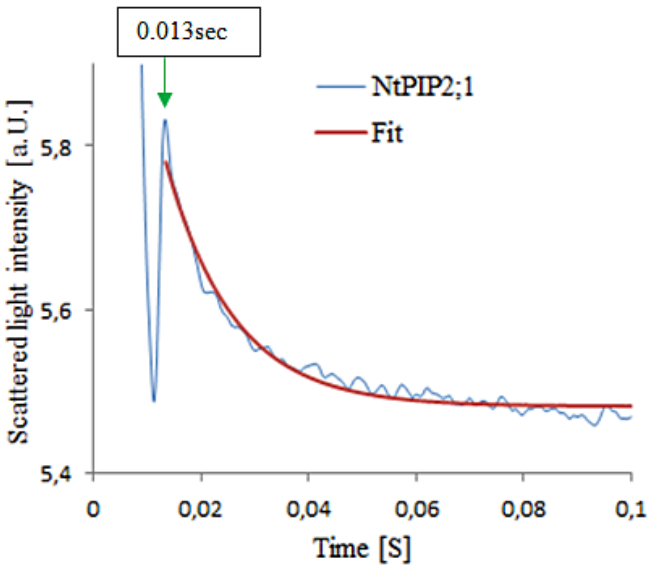

Fig 3.4: Graphic representation of the exponential fit of a typical water transport curve. The arrow indicates the starting point for the "fit" procedure. Only that part of the time course is shown that was used to calculate the rate constant (*ki*).

The coefficients of the ammonia (P_{NH_3}) and the osmotic permeability (P_f) serve as the unit for the transport efficiency [cm/s] of the respective solutes through a membrane. Using the *ki* values, the coefficients of osmotic permeability were calculated by the following equation (van Heeswijk and van Os, 1986):

$$P_f = k_i \cdot \frac{V_o}{S_o \cdot V_w \cdot C_{out}}$$

In the above equation, k is the fitted exponential rate constant, V_W is the molar volume of H_2O, V_0 and S_0 are the initial mean volume und the initial mean surface area of the protoplasts, respectively. C_{out} is the external osmolarity.

3.4.4.2 Calculation of ammonia permeability coefficient (P_{NH_3})

For ammonia transport curves, the data were fitted using single exponential function for the time period of 2 seconds (see Fig 3.5 for further details). The coefficients of the ammonia permeability were calculated by the following equation (Yang *et al.*, 2000):

$$P_{NH_3} = \frac{1}{\tau}\left[\left(\frac{S}{V}\right)/10^{(pH_f - pK_a)}\right]^{-1}$$

(Units are cm/s)

In this equation, S is the surface ($S = \pi r^2$) and V is the volume ($V = 4/3.\ \pi r^3$) of the yeast protoplast. τ is the time constant, pH_f is the final pH and pK_a of ammonia is 9.24. Surface and volume of the cells were calculated from the cell diameter (5µm) determined through microscopical measurement.

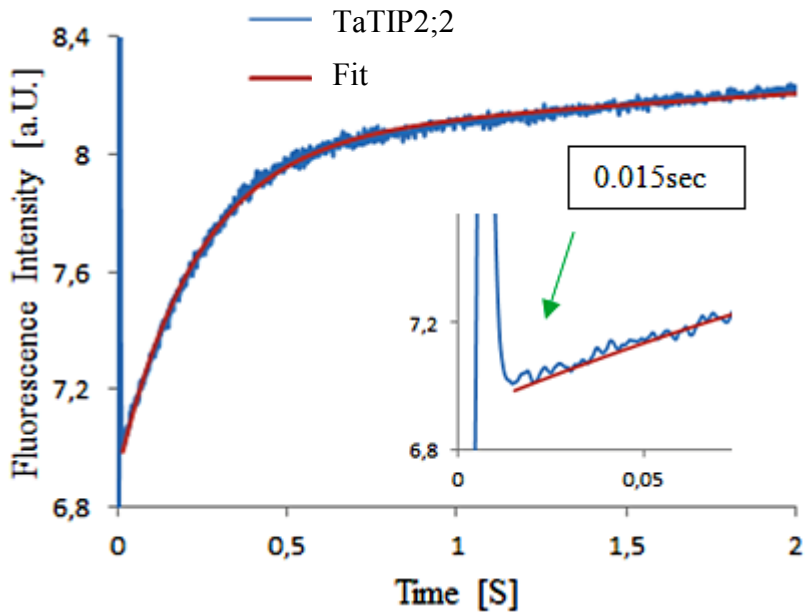

Fig 3.5: Graphic representation of the exponential fit of a typical ammonia transport curve. The arrow (inside the inset) indicates starting point for the "fit" procedure. Only that part of the time course is shown that was used to calculate the rate constant (*ki*).

3.5 Procedures and manipulations of proteins

3.5.1 Isolation of membrane proteins from yeast

Yeast cells from an overnight culture were harvested by centrifuging at 500 *xg* for 3 min at RT and washed with bidest water. For each gram of yeast cells, 3 ml of homogenization buffer and an equal volume of chilled and acid-washed glass beads (ø 0.5 mm, Sigma) were required. The cells were vortexed for a total of 20 min with repeated vortexing and subsequent cooling on ice, each for 1 min periods.

The homogenate was centrifuged at 2,500 *xg* at 4°C for 5 min to remove cell debris. In order to sediment the membranes, the supernatant was centrifuged in an ultracentrifuge (Sorvall Discovery M120) at 50,000 *xg* at 15°C for 15 min. The membrane pellet was resuspended in 250µl of TB buffer.

Homogenization Buffer

50mM	Na_3PO_4	pH 7.5
1mM	EDTA	
5%	Glycerin	
1µg/ml	Leupeptin	
1µg/ml	Pepstatin	

TB Buffer

10mM	Tris/HCl	pH 7.5
1mM	DTT	

3.5.2 Determination of protein concentration

Protein concentration was determined according to the Bradford method (Bradford, 1976), which exploits the deprotonation of the "Coomassie Brilliant Blue G-250" (CBBG) dye upon binding to protein. The dye exists either in the cationic form (red color) or in the anionic form (blue color). Under the acidic environment of the reagent, the coomassie dye changes its color from brown to blue in proportion to the amount of the protein. Protein binding (primarily with arginine, lysine and histidine) results into a spectral shift from the reddish form of the dye (absorbance maximum at 465nm) to its blue form (absorbance maximum at 595nm). The increase of absorbance at 595 nm is proportional to the amount of dye bound with the protein which indicates the amount of the protein present in the sample.

Protein concentration in the sample is determined by comparison to the color response of the protein assay standards, usually prepared as a series of known dilutions of bovine serum albumin (BSA). Bovine serum albumim (BSA) in 0.5 M NaOH was used as the standard. For determination of the protein concentration in an unknown sample, 1 ml of Bradford reagent (Carl Roth GmbH) was mixed with 1µl of the sample, incubated for 5 min at room temperature and the absorbance was

determined at 595 nm. A standard curve was obtained by plotting the absorbance (595 nm) of the standards (y-axis) versus their concentration in µg/ml (x-axis).

3.5.3 SDS-Polyacrylamide gel electrophoresis (SDS PAGE)

Sodium dodecyl sulfate (SDS) is an amphipathic detergent. SDS causes proteins to denature and disassociate from each other. SDS-treated proteins have very similar charge-to-mass ratios and similar shapes. During PAGE, the rate of migration of the SDS-treated proteins is effectively determined by the molecular weight. In the presence of SDS, the intrinsic charge of a protein is masked. Resolving the proteins in a discontinuous SDS-PAGE offers the advantage, that the proteins migrate quickly through the stacking gel and are squeezed down to a thin layer at the interface between the two gels before these are actually separated in the resolving gel.

The Laemmli (1970) method was used for the electrophoretic separation of proteins. Thin layer polyacrylamide gels of 1.5 mm thickness were prepared by using an assembly fitted with the glass plates. The protein samples (prepared in Laemmli buffer followed by boiling at 95°C for 5 min) were separated on 12.5% SDS-PAGE gels. The gels were run in an electrophoresis chamber purchased from Hoefer Inc, USA (model name: Mighty Small II SE 250).

The gels were prepared by mixing the chemicals as listed below and were polymerized by the addition of APS and TEMED. After complete polymerization, an equal amount of protein extract (10 µg) in an equal volume of the buffer (10 µl) was loaded. A current of 30 mA was continuously supplied for an initial 15 minutes, followed by 80mA for the rest of the running period. The current supply was disconnected immediately after the tracking dye Bromophenol blue left the running buffer.

The protein samples were mixed with 0.25 x volume of 4 x sample buffer and were heated at 95°C for 5 min. After cooling, the samples were loaded onto the stacking gel. The PageRuler prestained protein ladder (MBI Fermentas, Germany) was used as a marker for the molecular weight determination.

Stacking gel (4%)

4%	Acrylamid/Bis-acrylamid (29:1)
125mM	Tris/HCl pH 6.8
0.2%	SDS
0.1%	TEMED
0.6%	APS

Resolving gel (12,5%)

12.5%	Acrylamid/Bis-acrylamid (29:1)
375mM	Tris/HCl pH 8.8

0.2%	SDS	
0.05%	TEMED	
0.33%	Ammonium persulfate	

Running Buffer

129mM	Glycin	
0.1%	SDS	
25mM	Tris	pH 8.3

4 x Sample Buffer

250mM	Tris/HCl	pH 6.8
200mM	DTT	
8%	SDS	
40%	Glycerin	
0.01%	Bromo phenol blue	

3.5.4 Coomassie-Staining of Proteins

The stacking gel was removed and the running gel was soaked into the Coomassie staining solution (Sambrook and Gething, 1989) to stain the proteins separated in the polyacrylamide gel. The gel was incubated in the staining solution for 1 hour on a rocking platform at RT. The gel was washed with bidest water and again incubated with the destaining solution for 1 hour at RT. The protein bands were now clearly visible.

Coomassie – Staining solution

10%	Acetic acid
7%	Methanol
1%	Coomassie Briliant Blue R-250

Destaining solution

10%	Acetic acid
7%	Methanol

3.5.5 Western blotting

3.5.5.1 Transfer on a nitrocellulose membrane

The proteins in a polyacrylamide gel were transferred to a nitrocellulose membrane (Protran BA 83 Cellulose nitrate, Schleicher und Schuell) using a Biorad transfer tank. The transfer was carried out at 120 V for 2 h, while maintaining 10^{o}C temperature of the transfer bath. SDS-coated negatively charged proteins are transferred to the membrane when the voltage is applied. The protein transfer on nitrocellulose membrane was checked by staining with Ponceau S for 1 min.

The membrane was washed twice with 15 ml of wash buffer (PBS-Tween), each for 10 min with gentle shaking on a rocking platform.

3.5.5.2 Immunodetection of proteins through Chemiluminescence

The membrane was incubated overnight in blocking solution at 4°C to reduce unspecific binding. The membrane was washed in PBS-Tween buffer on a rocking platform and incubated in the primary antibody solution (diluted in blocking solution) for 1 h at RT. The membrane was washed again three times in the wash buffer for 10 min each and was incubated in the secondary antibody solution with shaking for 1 hour at RT. The membrane was washed thrice (for 10 min each) with wash buffer and then washed twice with Assay buffer. The membrane was ready for chemiluminescent detection.

The chemiluminescent detection is based on the interaction of a chemiluminescent substrate with an enzyme that has been conjugated to an antibody. As the enzyme-antibody conjugate binds to the substrate, a reaction is catalyzed resulting in light emission. In the present study, a chemiluminescent kit (Western-Star™ System, Applied Biosystems) was used for the detection of the blot according to the instructions of the kit manufacturer. The enzymatic dephosphorylation of the substrate CDP-Star® through the alkaline phosphatase conjugated to the secondary antibody emitted light signals which were captured by the gel documentation system (ChemiDoc XRS System, BioRad) equipped with a CCD camera.

Blocking Solution	5 % Skimmed milk in PBS-Tween buffer		
10 x PBS Buffer	82.3 g	Na_2HPO_4,	
	23.5 g	NaH_2PO_4	
	40 g	NaCl	
	volume raised to 1 L with bidest. H_2O		
10 x Assay Buffer	200 mM	Tris-HCl	pH 9.8
	20 mM	$MgCl_2$	
Washing Buffer	1x	PBS	
	0.5%	Tween 20	
Chemi-luminescent Substrate (1ml)			
	20mM	Tris/HCl	pH 9.8
	1mM	$MgCl_2$	
	0.25mM	CDP-Star®	
	1x	Nitro Block II™ (20x)	
Primary antibody	Anti-NtPIP2;1 from rabbit		
	Dilution 1:500 in Blocking solution		

Secondary antibody Anti-rabbit IgY (Sigma)
Dilution 1:30,000 in Blocking solution

3.6 Software/Tools used in the present study

3.6.1 Homology modelling

The coordinates required for drawing the homology models were provided by the online tool "SWISS-MODEL" (Arnold *et al*., 2006, Kiefer *et al*., 2009, Peitsch, 1995). The models were drawn in the software PYMOL version 1.4. SWISS-MODEL comparative given protein with the crystal structures available in the Protein Data Bank (PDB). It selected hAQP4 crystal structure (PDB entry # 3GD8) as template in case of TaTIP2;2 whereas it used spinach PIP2 crystal structure (PDB entry # 2B5F) as template in case of NtPIP2;1.

3.6.2 Primer designing Tools

The commercial program Vector NTI was generally used to design the primers. However, for site-directed mutagenesis, the online primer-designing tool provided by Stratagene was also used for counter-checking.

3.6.3 Sequence alignments

Sequence alignments were generated using BioEdit software version 7.0.9 (Hall, 1999) that incorporates multiple sequence alignment tools of ClustalX.

3.6.4 Verification of sequencing quality

The program Chromas Lite version 2.0 was used to open the histograms provided by the sequencing service and the sequencing quality was determined.

3.7 Synthetic Oligonucleotides

All the primers were synthesized by Eurofins MWG Operon, Germany.

3.7.1 Primers for sequencing TaTIP2;2 and NtPIP2;1

Table 4.1: Primers for sequencing of cDNA in yeast expression vectors pYes 2.1/TOPO or pYes2/CT.

TaTIP2;2	Sequence 5´-3´	Melting-Temperature (Tm) [°C]
TaTIP2;2–C63A_for	TGCCATCGCCTACACTAAGGTGAGCGG	70.7
TaTIP2;2–A118C_for	TCACCGGCATCTTCTATTGGG	62.6
TaTIP2;2–C237A_for	TCCATGAACCCTGCACGCTCCTTC	68
TaTIP2;2–C123A_rev	ATGTTGGCGCCGACGATGAAG	64.5

NtPIP2;1		
NtPIP2-F83H_for	GAAGGATTACGTGGACCCACCACCAGCT	70.5
NtPIP2-H212I_for	GTGCAACCTGGTTATAACAAGGGCACAGC	68.9

3.7.2 Primers for loop A & TM2 swapping in TaTIP2;2

Table 4.2: Primers for generating a TaTIP2;2 chimera in which its loop A and TM2 were exchanged with those from NtPIP2;1.

Name	Sequence 5´-3´	Melting-Temp (Tm) [°C]
TIP2;2-EcoRI_for	AAAGAATTCATGCCGGGCTCCATC	64.6
TIP2;2-XbaI_rev	AAATCTAGATTAGTAGTCGTTGCCGGC	64.6
TIP2-SegI_rev	GCACCATTCAACTTCTTGTGGGCGATGGCA GAGCC	74.1
TIP2-SegII_for	TGATTTTTGTTCTTGTTTACTGCGGCGCCAA CATCTCCG	71.6
PIP2-Seg_for	GGCTCTGCCATCGCCCACAAGAAGTTGAAT GGTGC	74.1
PIP2-Seg_rev	CGGAGATGTTGGCGCCGCAGTAAACAAGAA CAAAAATCA	71.6

3.7.3 Primers for loop A & TM2 swapping in NtPIP2;1

Table 4.3: Primers for generating a NtPIP2;1 chimera in which its loop A and TM2 were exchanged with those from TaTIP2;2.

Name	Sequence 5´-3´	Melting-Temp (Tm) [°C]
PIP2;1-EcoRI_for	AAAGAATTCATGTCAAAGGACGTGATTGAAG	63.3
PIP2;1-XbaI_rev	AAATCTAGATTAGTTGGTTGGGTTACTGCG	64.6
PIP2-SegI_rev	CGCCGCTCACCTTAGTGTAACCAATTACAGTTGCA ACAGTG	72.7
PIP2-SegII_for	GTCGCGGTCGCCATCACTGCCGGTATCTCTGGTG	76.7
TIP-Seg_for	CACTGTTGCAACTGTAATTGGTTACACTAAGGTG AGCGGCG	72.7
TIP-Seg_rev	CACCAGAGATACCGGCAGTGATGGCGACCGCGAC	76.7

3.7.4 Primers for loop D & TM5 swapping in TaTIP2;2

Table 4.4: Primers for generation of a TaTIP2;2 chimera in which its loop D and TM5 were exchanged with those from NtPIP2;1.

Name	Sequence 5´-3´	Melting-Temperature (Tm) [°C]
TIP2;2EcoRI_for	AAAGAATTCATGCCGGGCTCCATC	64.6
TIP2;2-XbaI_rev	AAATCTAGATTAGTAGTCGTTGCCGGC	64.6
TIP2-SegI_rev	GGCACTTCTTTTAGGGTCAGTGGTGGCGTACACGGTG	74.7

TIP2-SegII_for	CATGGTTCATTTGGCTACTTTCTCCGGCGGGTCC	73.1
PIP2-Seg_for	CACCGTGTACGCCACCACTGACCCTAAAAGAAGTGCC	74.7
PIP2-Seg_rev	GGACCCGCCGGAGAAAGTAGCCAAATGAACCATG	73.1

3.7.5 Primers for loop D & TM5 swapping in NtPIP2;1

Table 4.5: Primers for generation of a NtPIP2;1 chimera in which its loop D and TM5 were exchanged with those from TaTIP2;2

Name	Sequence 5´-3´	Melting-Temperature (Tm) [°C]
PIP2;1-EcoRI_for	AAAGAATTCATGTCAAAGGACGTGATTGAAG	63.3
PIP2;1-XbaI_rev	AAATCTAGATTAGTTGGTTGGGTTACTGCG	64.6
PIP2-SegI_rev	TTGGGGTCGGCGGCAGCAGAGAAAACAGTGTAAACAAG	73.3
PIP2-SegII_for	CTCGTTGCCGGCCCCATTCCTATTACTGGAACTGGTA	73.6
TIP2-Seg_for	CTTGTTTACACTGTTTTCTCTGCTGCCGCCGACCCCAA	73.3
TIP2-Seg_rev	TACCAGTTCCAGTAATAGGAATGGGGCCGGCAACGAG	73.6

3.7.6 Primers for C-terminus swapping in TaTIP2;2

Table 4.6: Primers for generation of a TaTIP2;2 chimera in which its C-terminus was exchanged with that from NtPIP2;1.

Name	Sequence 5´-3´	Melting-Temp (Tm) [°C]
TIP2;2-EcoRI_for	AAAGAATTCATGCCGGGCTCCATC	64.6
PIP2;1-XbaI_rev	AAATCTAGATTAGTTGGTTGGGTTACTGCG	64.6
PIP2-Seg_for	GGCGACTTCACCAACATCTGGATTTTCTGGGTTGGAC	72.5
TIP2-Seg_rev	GTCCAACCCAGAAAATCCAGATGTTGGTGAAGTCGCC	72.5

3.7.7 Primers for Site-Directed Mutagenesis

Table 4.7: Primers for generating point mutations in TaTIP2;2 and NtPIP2;1 through site-directed mutagenesis.

Name	Sequence 5´-3´	Melting-Temperature (Tm) [°C]
TaTIP2;2-C63A_s	GCCGTGGCGATAGCCCACGGGTTCGGGC	83.3
TaTIP2;2-C63A_as	GCCCGAACCCGTGGGCTATCGCCACGGC	83.3
TaTIP2;2-C123A_s	CCTCGTCCAGTTCGCCACCGGCGTGGCG	84.3
TaTIP2;2-C123A-as	CGCCACGCCGGTGGCGAACTGGACGAGG	84.3

TaTIP-A117C_s	GTGCCATCGTCGGCTGCTTCCTCGTCCAGT	73.6
TaTIP-A117C_as	ACTGGACGAGGAAGCAGCCGACGATGGCAC	73.6
TaTIP2;2 N84H_s	GCGGCCACGTGCACCCTGCCGTC	78.1
TaTIP2;2 N84H_as	GACGGCAGGGTGCACGTGGCCGC	78.1
TaTIP2;2 N196H_s	GGCGGGTCCATGCACCCTGCACGCT	78.4
TaTIP2;2 N196H_as	AGCGTGCAGGGTGCATGGACCCGCC-	78.4
TaTIP2;2 I97L_s	CCTCGGCGGCCAGCTCACCATCCTCAC	80.1
TaTIP2;2 I97L_as	GTGAGGATGGTGAGCTGGCCGCCGAGG	80.1
TaTIP2;2 L168V_s	CAAGAAGGGTTCCGTCGGCACCATCGC	78.6
TaTIP2;2 L168V_as	GCGATGGTGCCGACGGAACCCTTCTTG	78.6
TaTIP2;2 G224A_s	GCTCATCGGCGCTGGCCTCGCCG	79.9
TaTIP2;2 G224A_as	CGGCGAGGCCAGCGCCGATGAGC	79.9
NtPIP2;1 V117I_s	TTTGGGTTGTTCTTAGCAAGAAAAATCTCATTGTTAAGAGCAGTGGG	78.6
NtPIP2;1 V117I_as	CCCACTGCTCTTAACAATGAGATTTTTCTTGCTAAGAACAACCCAAA	78.6
NtPIP2;1 V197L_s	TGCCCGTGACTCCCATCTCCCTGTTTTGG	78.8
NtPIP2;1 V197L_as	CCAAAACAGGGAGATGGGAGTCACGGGCA	78.8
NtPIP2;1 A256G_s	GTTGGACCATTTGTGGGAGGTTTGGTAGCAGCAGTATATC	79.1
NtPIP2;1 A256G_as	GATATACTGCTGCTACCAAACCTCCCACAAATGGTCCAAC	79.1
TaTIP2;2 H64F_s	CCGTGGCGATATGCTTCGGGTTCGGGCTGT	78.3
TaTIP2;2 H64F_as	ACAGCCCGAACCCGAAGCATATCGCCACGG	78.3
TaTIP2;2 I179H_s	CGTCGGCGCCAACCACCTCGTTGCCGGC	79.5
TaTIP2;2 I179H_as	GCCGGCAACGAGGTGGTTGGCGCCGACG	79.5
TaTIP2;2 G192T_s	GCCCCTTCTCCGGCACGTCCATGAACCCTG	79.7
TaTIP2;2 G192T_as	CAGGGTTCATGGACGTGCCGGAGAAGGGGC	79.7
NtPIP2;1 F83H_s	GGTTGGTATTCTTGGTATTTCTTGGGCTCATGGTGGCATGATTTT	78.5
NtPIP2;1 F83H_as	AAAATCATGCCACCATGAGCCCAAGAAATACCAAGAATACCAACC	78.5

4 SUMMARY

The plant aquaporin TaTIP2;2 investigated in this study is permeable to both water and ammonia. Based on previous findings that in TaTIP2;2 ammonia transport is mercury sensitive, but water transport is mercury insensitive, a detailed study was planned to get a deeper insight into the coordination site(s) for Hg. Further, this study was aimed to shed light on the mechanism of metal inhibition, and provide evidence for the function of the tetrameric pore.

The mutational analyses involve substitutions of the native Cys residues and introduction of an already known Hg-sensitive site belonging to another TIP isoform. The results reveal that the presence of a Cys at a particular site in TM3 of the plant TIPs would render them Hg-sensitive. A consensus region of metal sensitivity in plant AQPs (similar to the one in mammalian AQPs) has also been proposed for accommodating a Hg-sensitive Cys. However, in case of plants, the PIPs are well-characterized aquaporins and in this family too, no report of Hg sensitivity is available to date. The consensus region may be located at different positions in different families of plant AQPs. In case of the TIP family, it is located in TM3.

The issue of the different Hg sensitivities of water and ammonia transport function in TIP could not be resolved and still remains controversial. As the decrease in P_{NH_3} may take place because of ammonia-mercury complex formation (and not because of Cys-Hg coordination), further investigations have been suggested to solve this issue. Particular attention may be laid on acquiring some stoichiometric data that determines the decrease in ammonia concentration available to enter the pore mouth versus the decrease of ammonia inside the pore because of the mercury inhibition. The application of selective inhibitors for water transport and for the putative central pore of AQPs would also be useful, if the gases are indeed conducted through the central pore. This study doesn't provide any further evidence on the presence of a separate gas pore.

Another part of this study involved a functional approach to investigate the molecular determinants of ammonia selectivity in AQPs. The sequence alignment including predominantly water conducting AQPs in comparison to the ammonia conducting ones suggested a couple of amino acids which were distinguishable between the two AQP categories. The residues identified in NtPIP2 are Val, Val and Ala positioned at 117, 197 and 256 respectively. The corresponding residues in case of TaTIP2;2 are Ile, Leu and Gly.

The failure in inducing ammonia conductance in PIP2 and no effect of the mutations on TIP in turning it into a water channel indicate their insignificant role in ammonia permeability in AQPs. However, a drastic effect on water permeability in PIP2 (and

not in TIP) suggests their role in the water transport function of the protein. It is tempting to speculate that the above-mentioned residues are part of the mechanism facilitating the water conductance in AQPs, either by direct interaction with the water molecules or by physical effects on the pore. The varying effects of the given residues may be attributed to the difference in structure between TIPs and PIPs besides pointing towards the presence of a central pore in AQPs.

Although the protein abundance in various mutants could not be determined because of the lack of an appropriate antibody, the isosteric similarities among the substituted residues lead to consider it as less likely. This study also suggests another position among the AQPs which is rather more conserved and should be considered in future work.

A remarkable part of the present work encompasses the generation of a number of protein chimeras and the mutations in the essential pore structures of AQPs. It was attempted to completely swap the ar/R region between TaTIP2;2 and NtPIP2;1. Furthermore, Asn of both the NPA motifs were also mutated to His. Surprisingly, in case of the former mutations, none of those were permeable to either water or ammonia. The latter mutants were also nonfunctional, however, proton leakage was observed which indicated that the mutations didn't hinder the protein expression.

Some domains of structural and functional importance were also swapped between TIP and PIP. These included exchange of loops A, D; the transmembrane helices 2, 5 and the C-terminus. None of the chimeric proteins showed any ammonia/water transport function. Unfortunately, in case of the TIP chimeras, the protein expression couldn't be determined because of the lack of an appropriate antibody. Also, in case of TIP, there is readily no interpretation available for the loss of ammonia/water transport function after swapping its loop A and TM2 with those of PIP2.

Zusammenfassung

In dieser Arbeit wurde das Aquaporin TaTIP2;2 untersucht, welches eine Permeabilität sowohl für Wasser als für Ammoniak zeigte. Basierend auf vorherigen Erkenntnissen, dass in TIP2.2 Ammoniaktransport, aber nicht Wassertransport durch Quecksilber inhibiert werden kann, war eine detaillierte Studie geplant, um einen tieferen Einblick in die Angriffstelle(n) für Hg zu bekommen. Desweiteren war das Ziel, den Mechanismus der Quecksilberinhibierung näher zu beleuchten und Evidenz für die Funktion der zentralen Pore im Tetramer zu finden.

Mutationsanalysen beinhalten den Austausch von Aminosäuren der natürlich vorhandenen Cysteinreste, sowie das Einbringen eines Quecksilber sensitiven Abschnitts welcher zu einer anderen TIP Isoform gehört. Die Ergebnisse offenbaren, dass die Anwesenheit von Cystein an einer bestimmten Stelle in TM3 der pflanzlichen TIP Isoformen diese Hg sensitiv machen. Es wurde vorgeschlagen, dass eine metallsensitive Konsensus Region in pflanzlichen Aquaporinen (ähnlich zu den AQPs in Säugetieren) ein Hg-sensitives Cystein enthält. Allerdings wurde in pflanzlichen PIPs, die zu einer sehr gut charakterisierten Familie von Aquaporinen gehören, bisher nicht über Hg-Sensitivität berichtet. Die Konsensus Region könnte an verschiedenen Positionen in den unterschiedlichen Familien der pflanzlichen Aquaporine lokalisiert sein. Im Fall der TIP Familie ist es inTM3 lokalisiert.

Das Problem der unterschiedlichen Quecksilber-Empfindlichkeit der Wasser- bzw. Ammoniak-Leitfähigkeit von TIP konnte nicht gelöst werden und ist nach wie vor kontrovers. Die Abnahme von P_{NH_3} könnte durchaus aufgrund einer Komplexbildung zwischen Ammoniak und Quecksilber zu Stande kommen (und nicht aufgrund einer Cys-Hg Wechselwirkung). Um dieses Problem zu lösen wurden weiterführende Experimente vorgeschlagen. Dabei könnte ein besonderes Augenmerk darauf liegen, stöchiometrische Daten bezüglich der Ammoniak-Verfügbarkeit und dessen Abnahme am Poren-Eingang im Vergleich zur Abnahme innerhalb der Pore aufgrund der Quecksilber-Inhibierung zu erhalten. Indem man selektive Inhibitoren für die Wasser- sowie die putative Tetramer-Pore des Aquaporins verwendet, könnten ebenfalls hilfreiche Untersuchungen durchgeführt werden, gesetzt den Fall, dass das Gas tatsächlich durch die zentrale Pore tritt. Die vorliegende Arbeit bietet keinen weiteren Beleg für die Existenz einer separaten Gas-Pore.

Ein weiterer Teil der vorliegenden Arbeit schloss die Untersuchung der molekularen Grundlagen der Ammoniak-Selektivität von Aquaporinen mit Hilfe eines funktionellen Ansatzes mit ein. Die Sequenz-Vergleiche von hauptsächlich wasserleitfähigen im Gegensatz zu Ammoniak-leitfähigen Aquaporinen ergaben, dass sich einige Aminosäuren innerhalb der jeweiligen Aquaporin-Gruppe unterschieden. Bei den identifizierten

Aminosäuren in NtPIP2 handelt es sich um Val, Val und Ala an den Positionen 117, 197 und 256. Die entsprechenden Aminosäuren im Fall von TaTIP2;2 sind Ile, Leu und Gly.

Der Umstand, dass Ammoniak-Leitfähigkeit in PIP2 nicht induziert, bzw. in TIP nicht unterbunden werden konnte, zeigt, dass PIP2 Aquaporine prinzipiell für Ammoniak-Transport nicht von Bedeutung sind. Allerdings unterstreicht der drastische Effekt auf die Wasserpermeabilität im Falle von PIP2, nicht jedoch bei TIP, deren Bedeutung für den Wassertransport. Daher liegt es nahe anzunehmen, dass die oben angesprochenen Aminosäure-Positionen ein Teil des Wassertransport-Mechanismus in Aquaporinen sind, entweder durch direkte Interaktion mit den Wasser-Molekülen, oder durch physikalischer Effekte im Porenbereich. Die unterschiedlichen Effekte bestimmter Aminosäurepositionen können sich außer aus der Anwesenheit einer zentralen Pore noch aus weiteren strukturellen Unterschieden zwischen TIP und PIP Aquaporinen ergeben.

Obwohl für zahlreiche Mutanten aufgrund des Fehlens geeigneter Antikörper die Menge exprimierten Proteins nicht bestimmt werden konnte, erscheint diese Möglichkeit aufgrund der isosterischen Ähnlichkeiten unter den ausgetauschten Aminosäure jedoch weniger wahrscheinlich. Die vorliegende Studie weist auf eine weitere Aminosäure-Position hin, die höher konserviert ist und in zukünftigen Studien betrachtet werden sollte.

Ein großer Teil dieser Arbeit beschäftigt sich mit der Herstellung verschiedener Proteinchimären und Mutationen in essentiellen Porenstrukturen von AQPs. Ziel war es, die komplette ar/R-region zwischen TaTIP2;2 und NtPIP2;1 auszutauschen. Es wurden auch die Asn beider NPA Motive zu His mutiert. Erstere waren erstaunlicherweise weder für Wasser noch für Ammoniak permeabel. In Letzteren konnten Protonen Leckströme beobachtet werden, ein Hinweis darauf, dass die Mutationen die Proteinexpression nicht unterdrückten.

Manche für Aufbau und Funktion wichtigen Domänen wurden ebenfalls zwischen TIP und PIP ausgetauscht. Dies umfasste den Austausch der Loops A, D; die Transmembranhelices 2 und 5 sowie den C-Terminus. Keine dieser Proteinchimären zeigte eine Funktion bezüglich Wasser- oder Ammoniakleitfähigkeit. Leider konnte im Falle der TIP-Chimären keine Expression des Proteins nachgewiesen werden, da ein passender Antikörper fehlte. Auch im Falle von TIP kann momentan keine Deutung für den Funktionsverlust bezüglich Ammoniak/Wasser vorgenommen werden, nachdem der Loop A und TM2 mit denen von PIP2 ausgetauscht wurde.

5 BIBLIOGRAPHY

Abdoun K, Stumpff F, Wolf K, Martens H (2005) Modulation of electroneutral Na transport in sheep rumen epithelium by luminal ammonia. Am J Physiol Gastrointest Liver Physiol. 289(3): G508-G520.

Agre P, King LS, Yasui M, Guggino WB, Ottersen OP, Fujiyoshi Y, Engel A, Nielsen S (2002) Aquaporin water channels-from atomic structure to clinical medicine. J Physiol. 542(Pt 1): 3-16.

Akgun U, Khademi S (2011) Periplasmic vestibule plays an important role for solute recruitment, selectivity and gating in the Rh/Amt/MEP superfamily. Proc Natl Acad Sci USA. 108(10): 3970-5.

Alexandersson E, Fraysse L, Sjövall-Larsen S, Gustavsson S, Fellert M, Karlsson M, Johanson U, Kjellbom P (2005) Whole gene family expression and drought stress regulation of aquaporins. Plant Mol Biol. 59(3): 469-484.

Arnold K, Bordoli L, Kopp J, Schwede T (2006). The SWISS-MODEL Workspace: A web-based environment for protein structure homology modeling. Bioinformatics. 22(2): 195-201.

Bai L, Fushimi K, Sasaki S, Marumo F (1996) Structure of aquaporin-2 vasopressin water channel. J Biol Chem. 271(9): 5171-6.

Ball LE, Little M, Nowak MW, Garland DL, Crouch RK, Schey KL (2003) Water permeability of C-terminally truncated aquaporin 0 (AQP0 1-243) observed in the aging human lens. Invest Ophthalmol Vis Sci. 44(11): 4820-8.

Bamfield P, Hutchings MG (2010) Phenomena involving absorption of energy followed by emission of light. In: Chromic phenomena: Technological applications of colour chemistry. pp. 234-365. The Royal Soc Chem, UK.

Banaszak LJ (2000) Foundations of structural biology. In: Metal Ions Bound to Proteins. pp. 137-147. Academic Press, UK.

Banci L, Bertini I, Cantini F, Della-Malva N, Migliardi M, Rosato A (2007) The different intermolecular interactions of the soluble copper-binding domains of the Menkes protein, ATP7A. J Biol Chem. 282(32): 23140-6.

Banci L, Bertini I, Cantini F, Massagni C, Migliardi M, Rosato A (2009) An NMR study of the interaction of the N-terminal cytoplasmic tail of the Wilson disease protein with copper(I)-HAH1. J Biol Chem. 284(14): 9354-60.

Bansal A, Sankararamakrishnan R (2007) Homology modeling of major intrinsic proteins in rice, maize and *Arabidopsis*: comparative analysis of transmembrane helix association and aromatic/arginine selectivity filters. BMC Struc Biol. 7: 27.

Bar-Or D, Curtis G, Rao N, Bampos N, Lau E (2001) Characterization of the Co(2+) and Ni(2+) binding amino-acid residues of the N-terminus of human albumin. An insight into the mechanism of a new assay for myocardial ischemia. Eur J Biochem. 268(1): 42-47.

Beitz E, Pavlovic-Djuranovic S, Yasui M, Agre P, Schultz JE (2004) Molecular dissection of water and glycerol permeability of the aquaglyceroporin from *Plasmodium falciparum* by mutational analysis. Proc Natl Acad Sci USA. 101(5): 1153-8.

Beitz E, Wu B, Holm LM, Schultz JE, Zeuthen T (2006) Point mutations in the aromatic/arginine region in aquaporin 1 allow passage of urea, glycerol, ammonia, and protons. Proc Natl Acad Sci USA. 103(2): 269-274.

Bertl A, Kaldenhoff R (2007) Function of a separate NH_3-pore in aquaporin TIP2;2 from wheat. FEBS Lett. 581(28): 5413-7.

Bertl A, Bihler H, Reid JD, Kettner C, Slayman CL (1998) Physiological characterization of the yeast plasma membrane outward rectifying K^+ channel, DUK1 (TOK1), *in situ*. J Mem Biol. 162(1): 67-80.

Bill RM, Hedfalk K, Karlgren S, Mullins JG, Rydström J, Hohmann S (2001) Analysis of the pore of the unusual major intrinsic protein channel, yeast Fps1p. J Biol Chem. 276(39): 36543-9.

Biela A, Grote K, Otto B, Hoth S, Hedrich R, Kaldenhoff R (1999) The *Nicotania tabacum* plasma membrane aquaporin NtAQP1 is mercury-insensitive and permeable for glycerol. Plant J. 18(5): 565–570.

Bondi A (1964) van der Waals volumes and radii. J. Phys. Chem. 68(3): 441-451.

Bremner I, Beattie JH (1990) Metallothionein and the trace minerals. Ann Rev Nutrition. 10: 63-83.

Brooks HL, Regan JW, Yool AJ (2000) Inhibition of aquaporin-1 water permeability by tetraethylammonium: involvement of the loop E pore region. Mol Pharmacol. 57(5): 1021–6.

Chakrabarti N, Tajkhorshid E, Roux B, Pomès R (2004) Molecular basis of proton blockage in aquaporins. Structure. 12(1): 65-74.

Chen H, Ilan B, Wu Y, Zhu F, Schulten K, Voth GA (2007) Charge delocalization in proton channels, I: The aquaporin channels and proton blockage. Biophys J. 92(1): 46–60.

Chen H, Ilan B, Wu Y, Zhu F, Schulten K, Voth GA (2007) Charge delocalization in proton channels, I: the aquaporin channels and proton blockage. Biophys J. 92(1): 46–60.

Cousins RJ (1995) Trace element micronutrients. In: RA Mayers (ed.), Moelcular biology and biotechnology: A comprehensive desk reference. pp. 898-902. Wiley-VCH, Inc, USA.

Daniels MJ, Chaumont F, Mirkov TE, Chrispeels MJ (1996) Characterization of a new vacuolar membrane aquaporin sensitive to mercury at a unique site. Plant Cell. 8(4): 587-599.

Daniels MJ, Mirkov TE, Chrispeels MJ (1994) The plasma membrane of *Arabidopsis thaliana* contains a mercury-insensitive aquaporin that is a homolog of the tonoplast water channel protein TIP. Plant Physiol. 106(4): 1325-33.

de Groot BL, Engel A, Grubmüller H (2003) The Structure of the Aquaporin-1 Water Channel: A Comparison between Cryo-electron Microscopy and X-ray Crystallography. J Mol Biol. 325(3): 485-493.

de Groot BL, Grubmüller H (2001) Water permeation across biological membranes: mechanism and dynamics of aquaporin-1 and GlpF. Science. 294(5550): 2353-7.

de Groot BL, Grubmüller H (2005) The dynamics and energetics of water permeation and proton exclusion in aquaporins. Curr Opin Struct Biol. 15(2): 176-83.

Desrochers PJ, Duong DS, Marshall AS, Lelievre SA, Hong B, Brown JR, Tarkka RM, Manion JM, Holman G, Merkert JW, Vicic DA (2007) Nickel-cysteine binding supported by phosphine chelates. Inorg Chem. 46(22): 9221-33.

Detmers FJM, De Groot BL, Muller EM, Hinton A, Konings IBM, Sze M, Flitsch SL, Grubmüller H, Deen PMT (2006) Quaternary ammonium compounds as water channel blockers - specificity, potency, and site of action. J Biol Chem. 281(20): 14207-14.

Dixon NE, Gazzola C, Watters JJ, Blakely RL, Zerner B (1975) Jack bean urease (EC 3.5.1.5). Metalloenzyme. Simple biological role for nickel. J Am Chem Soc. 97(14): 4131–3.

Doig AJ, Williams DH (1991) Is the hydrophobic effect stabilizing or destabilizing in proteins? The contribution of disulphide bonds to protein stability. J Mol Biol. 217(2): 389-398.

Duchesne L, Pellerin I, Delamarche C, Deschamps S, Lagree V, Froger A, Bonnec G, Thomas D, Hubert JF (2002) Role of C-terminal domain and transmembrane helices 5 and 6 in function and quaternary structure of major intrinsic proteins: analysis of aquaporin/glycerol facilitator chimeric proteins. J Biol Chem. 277(23): 20598-604.

Duncan KE, Ngu TT, Chan J, Salgado MT, Merrifield ME, Stillman MJ (2006) Peptide folding, metal-binding mechanisms, and binding site structures in metallothioneins. Exp Biol Med (Maywood). 231(9): 1488-99.

Dynowski M, Mayer M, Moran O, Ludewig U (2008) Molecular determinants of ammonia and urea conductance in plant aquaporin homologs. FEBS Lett. 582(16): 2458-62.

Ermler U, Grabarse W, Shima S, Goubeaud M, Thauer RK (1998) Active sites of transition-metal enzymes with a focus on nickel. Curr Opin Struct Biol. 8(6): 749-58.

Eto K, Noda Y, Horikawa S, Uchida S, Sasaki S (2010) Phosphorylation of aquaporin-2 regulates its water permeability. J Biol Chem. 285(52): 40777-84.

Finnegan ML, Bowler BE (2010) Propensities of aromatic amino acids versus leucine and proline to induce residual structure in the denatured-state ensemble of Iso-1-cytochrome c. J Mol Biology. 403(4): 495-504

Fischer M, Kaldenhoff R (2008) On the pH regulation of plant aquaporins. J Biol Chem. 283(49): 33889-92.

Fischer G, Kosinska-Eriksson U, Aponte-Santamaría C, Palmgren M, Geijer C, Hedfalk K, Hohmann S, de Groot BL, Neutze R, Lindkvist-Petersson K (2009) Crystal structure of a

yeast aquaporin at 1.15 angstrom reveals a novel gating mechanism. PLoS Biol. 7(6): e1000130.

Fotiadis D, Suda K, Tittmann P, Jenö P, Philippsen A, Müller DJ, Gross H, Engel A (2002) Identification and structure of a putative Ca^{2+}-binding domain at the C terminus of AQP1. J Mol Biol. 318(5): 1381-94.

Freedman RB, Hirst TR, Tuite MF (1994) Protein disulphide isomerase: Building bridges in protein folding. Trends Biochem Sci. 19(8): 331-336.

Fu D, Libson A, Miercke LJ, Weitzman C, Nollert P, Krucinski J, Stroud RM (2000) Structure of a glycerol-conducting channel and the basis for its selectivity. Science. 290(5491): 481-6.

Fujiyoshi Y, Mitsuoka K, de Groot BL, Philippsen A, Grubmüller H, Agre P, Engel A (2002) Structure and function of water channels. Curr. Opin. Struct. Biol. 12(4): 509–515.

Fushimi K., Sasaki S, Marumo F (1997) Phosphorylation of serine 256 is required for cAMP-dependent regulatory exocytosis of the aquaporin-2 water channel. J Biol Chem. 272(23): 14800-14804.

Glusker JP, Katz AK, Bock CW (1999) Metal ions in biologcal systsems. The Rigaku J. 16 (2): 8-16

Gruswitz F, Chaudhary S, Ho JD, Schlessinger A, Pezeshki B, Ho CM, Sali A, Westhoff CM, Stroud RM (2010) Function of human Rh based on structure of RhCG at 2.1 Å. Proc Nat Acad Sci USA. 107(21): 9638-43.

Guan XG, Su WH, Yi F, Zhang D, Hao F, Zhang HG, Liu YJ, Feng XC, Ma TH (2010) NPA motifs play a key role in plasma membrane targeting of aquaporin-4. IUBMB Life. 62(3): 222-226.

Gupta AB, Sankararamakrishnan R (2009) Genome-wide analysis of major intrinsic proteins in the tree plant *Populus trichocarpa*: characterization of XIP subfamily of aquaporins from evolutionary perspective. BMC Plant Biol. 9: 134.

Hall TA (1999) BioEdit: a user-friendly biological sequence alignment editor and analysis program for Windows 95/98/NT. Nucl Acids Symp Ser. 41: 95-98.

Hansen M, Kun JFJ, Schultz JE, Beitz E (2002) A single, bi-functional aquaglyceroporin in blood-stage *Plasmodium falciparum* malaria parasites. J Biol Chem. 277(7): 4874–82.

Hasegawa H, Ma T, Skach W, Matthay MA, Verkman AS (1994) Molecular cloning of a mercurial-insensitive water channel expressed in selected water-transporting tissues. J Biol Chem. 269(8): 5497-500.

Hazama A, Kozono D, Guggino WB, Agre P, Yasui M (2002) Ion permeation of AQP6 water channel protein. Single channel recordings after Hg_2^+ activation. J Biol Chem. 277(32): 29224–30.

Hazes B, Dijkstra BW (1988) Model building of disulfide bonds in proteins with known three-dimensional structure. Protein Engg. 2(2): 119-125.

Hedfalk K, Bill RM, Mullins JG, Karlgren S, Filipsson C, Bergstrom J, Tamás MJ, Rydström J, Hohmann S (2004) A regulatory domain in the C-terminal extension of the yeast glycerol channel Fps1p. J Biol Chem. 279(15): 14954-60.

Hirano Y, Okimoto N, Kadohira I, Suematsu M, Yasuoka K, Yasui M (2010) Molecular mechanisms of how mercury inhibits water permeation through aquaporin-1: understanding by molecular dynamics simulation. Biophys J. 98(8): 1512–9.

Ho JD, Yeh R, Sandstrom A, Chorny I, Harries WE, Robbins RA, Miercke LJ, Stroud RM (2009) Crystal structure of human aquaporin 4 at 1.8 Å and its mechanism of conductance. Proc Natl Acad Sci USA. 106(18): 7437-42.

Hoffert JD, Fenton RA, Moeller HB, Simons B, Tchapyjnikov D, McDill BW, Yu MJ, Pisitkun T, Chen F, Knepper MA (2008) Vasopressin-stimulated increase in phosphorylation at Ser269 potentiates plasma membrane retention of aquaporin-2. J Biol Chem. 283(36): 24617-27.

Holm LM, Jahn TP, Moller AL, Schjoerring JK, Ferri D, Klærke DA, Zeuthen T (2005) NH_3 and NH_4^+ permeability in aquaporin-expressing *Xenopus* oocytes. Pflügers Arch - Eur J Physiol. 450(6): 415–428.

Horsefield R, Nordén K, Fellert M, Backmark A, Törnroth-Horsefield S, Terwisscha van Scheltinga AC, Kvassman J, Kjellbom P, Johanson U, Neutze R (2008) High-resolution x-ray structure of human aquaporin 5. Proc Natl Acad Sci USA. 105(36): 13327-32.

Howitt SM, Udvardi MK (2000) Structure, function and regulation of ammonium transporters in plants. Biochim et Biophys Acta. 1465(1-2): 152-170.

Hub JS, de Groot BL (2008) Mechanism of selectivity in aquaporins and aquaglyceroporins. Proc Natl Acad Sci USA. 105(4): 1198-203.

Hub JS, Grubmüller H, de Groot BL (2009) Dynamics and energetics of permeation through aquaporins. What do we learn from molecular dynamics simulations? In: E Beitz (ed.), Aquaporins: Handb Exp Pharmac. (190): 57-76. Springer-Verlag Berlin-Heidelberg.

Ikeda M, Andoo A, Shimono M, Takamatsu N, Taki A, Muta K, Matsushita W, Uechi T, Matsuzaki T, Kenmochi N, Takata K, Sasaki S, Ito K, Ishibashi K (2011) The NPC motif of aquaporin-11, unlike the NPA motif of known aquaporins, is essential for full expression of molecular function. J Biol Chem. 286(5): 3342-50.

Ishibashi K, Kuwahara M, Gu Y, Tanaka Y, Marumo F, Sasaki S (1998) Cloning and functional expression of a new aquaporin (AQP9) abundantly expressed in the peripheral leukocytes permeable to water and urea, but not to glycerol. Biochem Biophys Res Commun. 244(1): 268–274.

Ishibashi K, Morinaga T, Kuwahara M, Sasaki S, Imai M (2002) Cloning and identification of a new member of water channel (AQP10) as an aquaglyceroporin. Biochim Biophys Acta. 1576(3): 335-340.

Ishibashi K, Kuwahara M, Gu Y, Kageyama Y, Tohsaka A, Suzuki F, Marumo F, Sasaki S (1997) Cloning and functional expression of a new water channel abundantly expressed in the testis permeable to water, glycerol, and urea. J Biol Chem. 272(33): 20782-6.

Ishikawa F, Suga S, Uemura T, Sato MH, Maeshima M (2005) Novel type aquaporin SIPs are mainly localized to the ER membrane and show cell-specific expression in *Arabidopsis thaliana*. FEBS Lett. 579(25): 5814-20.

Itoh T, Rai T, Kuwahara M, Ko SB, Uchida S, Sasaki S, Ishibashi K (2005) Identification of a novel aquaporin, AQP12, expressed in pancreatic acinar cells. Biochem Biophys Res Commun. 330(3): 832-8.

Jahn TP, Moller AL, Zeuthen T, Holm LM, Klaerke, DA, Mohsin B, Kuhlbrandt W, Schjoerring JK (2004) Aquaporin homologues in plants and mammals transport ammonia. FEBS Lett. 574(1-3): 31-36.

Jakob U, Muse W, Eser M, Bardwell JC (1999) Chaperone activity with a redox switch. Cell 96: 341–352.

Jensen MØ, Dror RO, Xu H, Borhani DW, Arkin IT, Eastwood MP, Shaw DE (2008) Dynamic control of slow water transport by aquaporin 0: implications for hydration and junction stability in the eye lens. Proc Natl Acad Sci USA. 105(38): 14430-5.

Jensen MR, Petersen G, Lauritzen C, Pedersen J, Led JJ (2005) Metal binding sites in proteins: identification and characterization by paramagnetic NMR relaxation. Biochemistry. 44(33): 11014-23.

Jiang Y, Ma T (2006) Importance of NPA motifs in the expression and function of water channel aquaporin-1. Chinese Sci Bull. 52(6): 771-776.

Johanson U, Karlsson M, Johansson I, Gustavsson S, Sjövall S, Fraysse L, Weig AR, Kjellbom P (2001) The complete set of genes encoding major intrinsic proteins in *Arabidopsis* provides a framework for a new nomenclature for major intrinsic proteins in plants. Plant Physiol. 126(4): 1358–69.

Johansson I, Larsson C, Ek B, Kjellbom P (1996) The major integral proteins of spinach leaf plasma membranes are putative aquaporins and are phosphorylated in response to Ca^{2+} and apoplastic water potential. Plant Cell. 8(7): 1181-1191.

Johansson I, Karlsson M, Shukla VK, Chrispeels MJ, Larsson C, Kjellbom P (1998) Water transport activity of the plasma membrane aquaporin PM28A is regulated by phosphorylation. Plant Cell. 10(3): 451-459.

Jung JS, Bhat RV, Preston GM, Guggino WB, Baraban JM, Agre P (1994a) Molecular characterization of an aquaporin cDNA from brain: candidate osmoreceptor and regulator of water balance. Proc Nat Acad Sci USA. 91(26): 13052–6.

Jung JS, Preston GM, Smith BL, Guggino WB, Agre P (1994b) Molecular structure of the water channel through aquaporin CHIP. The hourglass model. J Biol Chem. 269(20): 14648-54.

Kasahara T, Ishiguro M, Kasahara M (2004) Comprehensive chimeric analysis of amino acid residues critical for high affinity glucose transport by Hxt2 of *Saccharomyces cerevisiae*. J Biol Chem. 279 (29): 30274-8.

Kasahara T, Ishiguro M, Kasahara M (2006) Eight amino acid residues in transmembrane segments of yeast glucose transporter Hxt2 are required for high-affinity transport. J Biol Chem. 281(27): 18532-8.

Kasahara T, Maeda M, Ishiguro M, Kasahara M (2007) Identification by comprehensive chimeric analysis of a key residue responsible for high affinity glucose transport by yeast HXT2. J Biol Chem. 282(18): 13146-50.

Kato M, Pisliakov AV, Warshel A (2006) The barrier for proton transport in aquaporins as a challenge for electrostatic models: The role of protein relaxation in mutational calculations. Proteins. 64(4): 829–844.

Khademi S, O'Connell J III, Remis J, Robles-Colmenares Y, Miercke LJ, Stroud RM (2004) Mechanism of ammonia transport by Amt/MEP/Rh: structure of AmtB at 1.35 Å. Science. 305(5690): 1587-94.

Khademi S, Stroud RM (2006) The Amt/MEP/Rh Family: Structure of AmtB and the mechanism of ammonia gas conduction. Physiology. 21: 419-429.

Kiefer F, Arnold K, Künzli M, Bordoli L, Schwede T (2009) The SWISS-MODEL repository and associated resources. Nucl Acids Res. 37: D387-D392.

Kim Y, Choi I, Kang SK, Lee J, Yi J (2006) Multi-functionalization of organosilanes on submicron-sized island-type electrodes for the selective detection of metal ions. Appl Physics Lett. 88(1): 013113.

Kjellbom P, Larsson C, Johansson I, Karlsson M, Johanson U (1999) Aquaporins and water homeostasis in plants. Trends Plant Sci. 4(8): 308-314.

Kong Y, Ma J (2001) Dynamic mechanisms of the membrane water channel aquaporin-1 (AQP1). Proc Natl Acad Sci USA. 98(25): 14345-9.

Kosugi-Tanaka C, Li X, Yao C, Akamatsu T, Kanamori N, Hosoi K (2006) Protein kinase A-regulated membrane trafficking of a green fluorescent protein-aquaporin 5 chimera in MDCK cells. Biochim Biophys Acta. 1763(4): 337-44.

Kozlowski H, Decock-Le Révérend B, Ficheux D, Loucheux C, Sovago I (1987) Nickel(II) complexes with sulfhydryl containing peptides. Potentiometric and spectroscopic studies. J Inorg Biochem. 29(3): 187-197.

Kuang K, Haller JF, Shi G, Kang F, Cheung M, Iserovich P, Fischbarg J (2001) Mercurial sensitivity of aquaporin 1 endofacial loop B residues. Protein Sci. 10(8): 1627-34.

Kukulski W, Schenk AD, Johanson U, Braun T, de Groot BL, Fotiadis D, Kjellbom P, Engel A (2005) The 5Å structure of heterologously expressed plant aquaporin SoPIP2;1. J Mol Biol. 350(4): 611-6.

Kuwahara M, Gu Y., Ishibashi K, Marumo F, Sasaki S (1997) Mercury-sensitive residues and pore site in AQP3 water channel. Biochem. 36(46): 13973–8.

Laemmli UK (1970) Cleavage of structural proteins during the assembly of the head of bacteriophage T4. Nature. 227(5259): 680-685.

Lagree V, Pellerin I, Hubert JF, Tacnet F, Le Caherec F, Roudier N, Thomas D, Gouranton J, Deschamps S (1998) A yeast recombinant aquaporin mutant that is not expressed or mistargeted in *Xenopus* oocyte can be functionally analyzed in reconstituted proteoliposomes. J Biol Chem. 273(20): 12422-6.

Lakowicz JR (2006) Multiphoton excitation and microscopy. In: Principles of Fluorescence Spectroscopy. pp. 607-622. Springer Science and Business Media, USA.

La Mendola D, Pietropaolo A, Pappalardo G, Zannoni C, Rizzarelli E (2008) Prion proteins leading to neurodegeneration. Curr Alzheimer Res. 5(6): 579-90.

Lamoureux G, Klein ML, Bernèche S (2007) A stable water chain in the hydrophobic pore of the AmtB ammonium transporter. Biophys J. 92(9): L82-4.

Lamoureux G, Javelle A, Baday S, Wang S, Bernèche S (2010) Transport mechanisms in the ammonium transporter family. Transfusion Clinique et Biologique. 17(3): 168-175.

Le Cahérec F, Deschamps S, Delamarche C, Pellerin I, Bonnec G, Guillam MT, Thomas D, Gouranton J, Hubert JF (1996) Molecular cloning and characterization of an insect aquaporin: Functional comparison with aquaporin 1. Eur J Biochem. 241(3): 707–715.

Lee J, Kozono D, Remis J, Kitagawa Y, Agre P (2005) Structural basis for conductance by the archaeal aquaporin AqpM at 1.68 Å. Proc Natl Acad Sci USA. 102(52): 18932–7.

Li H, Chen H, Steinbronn C, Wu B, Beitz E, Zeuthen T, Voth GA (2011) Enhancement of proton conductance by mutations of the selectivity filter of aquaporin-1. 407(4): 607-620.

Li X, Guo M, Fan J, Tang W, Wang D, Ge H, Rong H, Teng M, Niu L, Liu Q, Hao Q (2006) Crystal structure of 3-hydroxyanthranilic acid 3,4-dioxygenase from *Saccharomyces cerevisiae*: a special subgroup of the type III extradiol dioxygenases. Protein Sci. 15(4): 761-73.

Lin Y, Cao Z, Mo Y (2006) Molecular dynamics simulations on the *Escherichia coli* ammonia channel protein AmtB: mechanism of ammonia/ammonium transport. J Am Chem Soc. 128(33): 10876–84.

Litman T, Søgaard R, Zeuthen T (2009) Ammonia and urea permeability of mammalian aquaporins. In: E Beitz (ed.), Aquaporins: Handb Exp Pharmac. (190): 327-58. Springer-Verlag Berlin-Heidelberg.

Liu LH, Ludewig U, Gassert B, Frommer WB, von Wirén N (2003) Urea transport by nitrogen-regulated tonoplast intrinsic proteins in Arabidopsis. Plant Physiol. 133(3): 1220-8.

Liu K, Kozono D, Kato Y, Agre P, Hazama A, Yasui M (2005a) Conversion of aquaporin 6 from an anion channel to a water-selective channel by a single amino acid substitution. Proc Nat Acad Sci USA. 102 (6): 2192-7.

Liu K, Nagase H, Huang CG, Calamita G, Agre P (2005b) Purification and functional characterization of aquaporin-8. Biol Cell. 98(3): 153–161.

Liu Z, Chen Y, Mo R, Hui C, Cheng JF, Mohandas N, Huang CH (2000) Characterization of human RhCG and mouse Rhcg as novel nonerythroid Rh glycoprotein homologues predominantly expressed in kidney and testis. J Biol Chem. 275(33): 25641-51.

Loitto VM, Forslund T, Sundqvist T, Magnusson KE, Gustafsson M (2002) Neutrophil leukocyte motility requires directed water influx. J Leucoc Biol. 71(2): 212–222.

Loque D, Ludewig U, Yuan L, von Wiren N (2005) Tonoplast intrinsic proteins AtTIP2;1 and AtTIP2;3 facilitate NH_3 transport into the vacuole. Plant Physiol. 137(2): 671-680.

Loque D, von Wiren N (2004) Regulatory levels for the transport of ammonium in plant roots. J Exp Bot. 55(401): 1293–305.

Ludewig U, Wilken S, Wu B, Jost W, Obrdlik P, El Bakkoury M, Marini AM, André B, Hamacher T, Boles E, von Wirén N, Frommer WB (2003) Homo- and hetero-oligomerization of ammonium transporter-1 NH_4^+ uniporters. J Biol Chem. 278(46): 45603-10.

Ludewig U, von Wirén N, Frommer WB (2002) Uniport of NH_4^+ by the root hair plasma membrane ammonium transporter LeAMT1;1. J Biol Chem. 277(16): 13548–55.

MacIver B, Cutler CP, Yin J, Hill MG, Zeidel ML, Hill WG (2009) Expression and functional characterization of four aquaporin water channels from the European eel (*Anguilla anguilla*). J Exp Biol. 212(17): 2856-63.

Marini AM, Soussi-Boudekou S, Vissers S, Andre B (1997) A family of ammonium transporters in *Saccharomyces cerevisiae*. Mol Cell Biol. 17(8): 4282-93.

Marini AM, Vissers S, Urrestarazu A, André B (1994) Cloning and expression of the MEP1 gene encoding an ammonium transporter in *Saccharomyces cerevisiae*. EMBO J. 13(15): 3456-63.

Marking GA, Hanko JA, Kanatzidis MG (1998) New quaternary thiostannates and thiogermanates $A_2Hg_3M_2S_8$ (A=Cs, Rb; M=Sn, Ge) through molten A_2S_x. Reversible glass formation in $Cs_2Hg_3M_2S_8$. Chem Mater. 10: 1191-9.

Maurel C, Reizer J, Schroeder JI, Chrispeels MJ (1993) The vacuolar membrane protein γ-TIP creates water specific channels in *Xenopus* oocytes. EMBO J. 12(6): 2241-7.

Mayer M, Schaaf G, Mouro I, Lopez C, Colin Y, Neumann P, Cartron JP, Ludewig U (2006) Different transport mechanisms in plant and human AMT/Rh-type ammonium transporters. J Gen Physiol. 127(2): 133-144.

Miller AJ, Cookson SJ, Smith SJ, Wells DM (2001) The use of microelectrodes to investigate compartmentation and the transport of metabolized inorganic ions in plants. J Exp Bot. 52(356): 541-9.

Mitani, N, Yamaji N, Ma JF (2008) Characterization of substrate specificity of a rice silicon transporter, Lsi1. Pflügers Arch - Eur J Physiol. 456(4): 679–686.

Moeller HB, Praetorius J, Rützler MR, Fenton RA. Moeller HB, Praetorius J, Rützler MR, Fenton RA (2010) Phosphorylation of aquaporin-2 regulates its endocytosis and protein-protein interactions. Proc Natl Acad Sci USA. 107(1):424-9.

Montalvetti A, Rohloff P, Docampo R (2004) A functional aquaporin co-localizes with the vacuolar proton pyrophosphatase to acidocalcisomes and the contractile vacuole complex of *Trypanosoma cruzi*. J Biol Chem. 279(37): 3867-82.

Mulrooney SB, Hausinger RP (2003) Nickel uptake and utilization by microorganisms. FEMS Microbiol Rev. 27(2-3): 239-61.

Müller EM, Hub JS, Grubmüller H, de Groot BL (2008) Is TEA an inhibitor for human aquaporin-1? Pflügers Arch - Eur J Physiol. 456(4): 663-9.

Murata K, Mitsuoka K, Hirai T, Walz T, Agre P, Heymann JB, Engel A, Fujiyoshi Y (2000) Structural determinants of water permeation through aquaporin-1. Nature. 407(6804): 599-605.

Nakahama K, Fujioka A, Nagano M, Satoh S, Furukawa K, Sasaki H, Shigeyoshi Y (2002) A role of the C-terminus of aquaporin 4 in its membrane expression in cultured astrocytes. Genes Cells. 7(7): 731-741.

Nakhoul NL, Hering-Smith KS, Abdulnour-Nakhoul SM, Hamm LL (2001) Transport of NH_3/NH_4^+ in oocytes expressing aquaporin-1. Am J Physiol Renal Physiol. 281(2): F255–F263.

Nakamoto RK, Rao R, Slayman CW (1991). Expression of the yeast plasma membrane H^+-ATPase in secretory vesicles. A new strategy for directed mutagenesis. J Biol Chem. 266(12): 7940-9.

Nalefski EA, Newton AC (2003) Use of stopped-flow fluorescence spectroscopy to measure rapid membrane binding by protein kinase C. Methods Mol Biol. 233: 115-28.

Németh-Cahalan KL, Kalman K, Froger A, Hall JE (2007) Zinc modulation of water permeability reveals that aquaporin 0 functions as a cooperative tetramer. J Gen Physiol. 130(5): 457-64.

Németh-Cahalan KL, Hall JE (2000) pH and calcium regulate the water permeability of aquaporin 0. J Biol Chem. 275(10): 6777–82.

Németh-Cahalan KL, Kalman K, Hall JE (2004) Molecular basis of pH and Ca^{2+} regulation of aquaporin water permeability. J Gen Physiol. 123(5): 573–580.

Newby ZE, O'Connell J , Robles-Colmenares Y, Khademi S, Miercke LJ, Stroud RM (2008) Crystal structure of the aquaglyceroporin PfAQP from the malarial parasite *Plasmodium falciparum*. Nat Struct Mol Biol. 15(6): 619-25.

Niemietz CM, Tyerman SD (2002) New potent inhibitors of aquaporins: silver and gold compounds inhibit aquaporins of plant and human origin. 531(3): 443-447.

Niemietz CM, Tyerman SD (2000) Channel-mediated permeation of ammonia gas through the peribacteroid membrane of soybean nodules. FEBS Lett. 465 (2-3): 110-114.

Ninnemann O, Jauniaux JC, Frommer WB (1994) Identification of a high affinity NH_4^+ transporter from plants. EMBO J. 13(15): 3464–71.

Nollert P, Harries WE, Fu D, Miercke LJ, Stroud RM (2001) Atomic structure of a glycerol channel and implications for substrate permeation in aqua(glycero)porins. FEBS Lett. 504(3): 112-7.

Nozaki K, Ishii D, Ishibashi K (2008) Intracellular aquaporins: clues for intracellular water transport? Pflügers Arch – Eur J Physiol. 456(4): 701-707.

Nygaard TP, Rovira C, Peters GH, Jensen MØ (2006) Ammonium recruitment and ammonia transport by *E. coli* ammonia channel AmtB. Biophys J. 91(12): 4401-12.

Ohashi Y, Tsuzaka K, Takeuchi T, Sasaki Y, Tsubota K (2008) Altered distribution of aquaporin 5 and its C-terminal binding protein in the lacrimal glands of a mouse model for Sjögren's syndrome. Curr Eye Res. 33(8): 621-9.

Okubo-Kurihara E, Sano T, Higaki T, Kutsuna N, Hasezawa S (2009) Acceleration of vacuolar regeneration and cell growth by overexpression of an aquaporin NtTIP1;1 in tobacco BY-2 cells. Plant Cell Physiol. 50(1): 151-60.

Oliva R, Calamita G, Thornton JM, Pellegrini-Calace M (2010) Electrostatics of aquaporin and aquaglyceroporin channels correlates with their transport selectivity. Proc Nat Acad Sci USA. 107(9): 4135-40

Park W, Scheffler BE, Bauer PJ, Campbell BT (2010) Identification of the family of aquaporin genes and their expression in upland cotton (*Gossypium hirsutum* L.). BMC Plant Biol. 10: 142.

Peitsch MC (1995) Protein modeling by E-mail. Nature Biotech. 13: 658-660.

Pelis RM, Dangprapai Y, Wunz TM, Wright SH (2007) Inorganic mercury interacts with cysteine residues (C451 and C474) of hOCT2 to reduce its transport activity. Am J Physiol Renal Physiol. 292(5): F1583-F1591.

Perez-Garcia O, Escalante FM, de-Bashan LE, Bashan Y (2011) Heterotrophic cultures of microalgae: metabolism and potential products. Water Res. 45(1):11-36.

Phongphanphanee S, Yoshida N, Hirata F (2010) Molecular selectivity in aquaporin channels studied by the 3D-RISM theory. J Phys Chem B. 114(23): 7967-73.

Podsiadlo P, Komiyama T, Fuller RS, Blum O (2004) Furin inhibition by compounds of copper and zinc. J Biol Chem. 279: 36219–27.

Prak S, Hem S, Boudet J, Viennois G, Sommerer N, Rossignol M, Maurel C, Santoni V (2008) Multiple phosphorylations in the C-terminal tail of plant plasma membrane aquaporins: role in subcellular trafficking of AtPIP2;1 in response to salt stress. Mol Cell Proteomics. 7(6):1019-30.

Prasad GV, Coury LA, Finn F, Zeidel ML (1998) Reconstituted aquaporin-1 water channels transport CO_2 across membranes. J Biol Chem. 273(50): 33123-6.

Preston BM, Carroll TP, Guggino WB, Agre P (1992) Appearance of water channels in *Xenopus oocytes* expressing red cell CHIP28 protein. Science. 256(5055): 385–387.

Preston GM, Jung JS, Guggino WB, Agre P (1993) The mercury-sensitive residue at cysteine 189 in the CHIP28 water channel. J Biol Chem. 268(1): 17-20.

Raina S, Preston GM, Guggino WB, Agre P (1995) Molecular cloning and characterization of an aquaporin cDNA from salivary, lacrimal, and respiratory tissues. J Biol Chem. 270(4): 1908-12.

Ralle M, Lutsenko S, Blackburn NJ (2004) Copper transfer to the N-terminal domain of the Wilson disease protein (ATP7B): X-ray absorption spectroscopy of reconstituted and chaperone-loaded metal binding domains and their interaction with exogenous ligands. J Inorg Biochem. 98(5): 765-74.

Reizer J, Schroeder JI, Chrispeels MJ (1993) The vacuolar membrane protein γ-TIP creates water specific channels in *Xenopus* oocytes. EMBO J. 12(6): 2241-7

Rivers RL, Dean RM, Chandy G, Hall JE, Roberts DM, Zeidel ML (1997) Functional analysis of Nodulin 26, an aquaporin in soybean root nodule symbiosomes. J Biol Chem. 272(26): 16256-61.

Robzyk K, Kassir Y (1992) A simple and highly efficient procedure for rescuing autonomous plasmids from yeast. Nucl Acids Res. 20(14): 3790.

Rothberg BS, Shin KS, Phale PS, Yellen G (2002) Voltage-controlled gating at the intracellular entrance to a hyperpolarization-activated cation channel. J Gen Physiol. 119(1): 83-91.

Sambrook J, Gething MJ (1989) Protein structure. Chaperones, paperones. Nature. 342(6247): 224-225.

Sandrin TR, Hoffman DR (2007) Bioremediation of organic and metal contaminated environments: Effects of metal toxicity, speciation, and bioavailability on biodegradation. In: SN Singh and RD Tripati (ed.), Environmental bioremediation technologies. pp. 1-34. Springer-Verlag Berlin Heidelberg.

Sanford JC, Smith FD, Russel JA (1993) Optimizing the biolistic process for different biological applications. Methods Enzymol. 217: 483-509.

Santos CRA, Estêvão MD, Fuentes J, Cardoso JCR, Fabra M, Passos AL, Detmers FJ, Deen PMT, Cerdà J, Power DM (2004) Isolation of a novel aquaglyceroporin from a marine teleost (*Sparus auratus*): function and tissue distribution. J. Exp. Biol. 207(Pt 7): 1217-27.

Saparov MS, Liu K, Agre P, Pohl P (2007) Fast and selective ammonia transport by aquaporin-8. J Biol Chem. 282(8): 5296–5301.

Savage DF, Stroud RM (2007) Structural basis of aquaporin inhibition by mercury. J Mol Biol. 368(3): 607-17.

Savage DF, O'Connell JD III, Miercke LJ, Finer-Moore J, Stroud RM (2010) Structural context shapes the aquaporin selectivity filter. Proc Natl Acad Sci USA. 107(40): 17164-9.

Savage DF, Egea PF, Robles-Colmenares Y, O'Connell JD III, Stroud RM (2003) Architecture and selectivity in aquaporins: 2.5Å x-ray structure of aquaporin Z. PLoS Biol. 1(3): 334-340.

Schumacher V, Schärer K, Wühl E, Altrogge H, Bonzel KE, Guschmann M, Neuhaus TJ, Pollastro RM, Kuwertz-Bröking E, Bulla M, Tondera AM, Mundel P, Helmchen U, Waldherr R, Weirich A, Royer-Pokora B (1998) Spectrum of early onset nephrotic syndrome associated with WT1 missense mutations. Kidney Int. 53(6): 1594–1600.

Sharma SK, Goloubinoff P, Christen P (2008) Heavy metal ions are potent inhibitors of protein folding. Biochem Biophys Res Commun. 372(2): 341-5.

Shaw BP, Sahu SK, Mishra RK (2004) Heavy metal induced oxidative damage in terrestrial plants. In: MNV Prasad (ed.), Heavy meal stress in plants. From Biomolecules to ecosystems. pp. 84–126. Springer-Verlag Berlin-Heidelberg.

Shi LB, Verkman AS (1996) Selected cysteine point mutations confer mercurial sensitivity to the mercurial-insensitive water channel MIWC/AQP4. Biochemistry. 35(2): 538–544.

Siddiqui KS, Poljak A, Guilhaus M, Feller G, D'Amico S, Gerday C, Cavicchioli R (2005) Role of disulfide bridges in the activity and stability of a cold-active α-Amylase. J. Bacteriol. 187(17): 6206-12.

Singleton C, Banci L, Ciofi-Baffoni S, Tenori L, Kihlken MA, Boetzel R, Le Brun NE (2008) Structure and Cu(I)-binding properties of the N-terminal soluble domains of *Bacillus subtilis* CopA. Biochem J. 411(3): 571-579.

Slavik J (1982) Intracellular pH of yeast cells measured with fluorescent probes. FEBS Lett. 140(1): 22-26.

Smolin N, Li B, Beck DAC, Daggett V (2008) Side-chain dynamics are critical for water permeation through aquaporin-1. Biophys J. 95(3): 1089–98.

Sohlenkamp C, Wood CC, Roeb GW, Udvardi M (2002) Characterization of Arabidopsis AtAMT2, a high-affinity ammonium transporter of the plasma membrane. Plant Physiol. 130(4): 1788-96.

Søgaard R, Alsterfjord M, MacAulay N, Zeuthen T (2009) Ammonium ion transport by the AMT/Rh homolog TaAMT1;1 is stimulated by acidic pH. Pflügers Arch - Eur J Physiol. 458(4): 733-743.

Suga S, Maeshima M (2004) Water channel activity of radish plasma membrane aquaporins heterologously expressed in yeast and their modification by site-directed mutagenesis. Plant Cell Physiol. 45(7): 823–830.

Sui H, Han BG, Lee JK, Walian P, Jap BK (2001) Structural basis of water-specific transport through the AQP1 water channel. Nature. 414 (6866): 872-8.

Sutka M, Li G, Boudet J, Boursiac Y, Doumas P, Maurel C (2011) Natural variation of root hydraulics in Arabidopsis grown in normal and salt-stressed conditions. Plant Physiol. 155(3): 1264-76.

Tajkhorshid E, Nollert P, Jensen MØ, Miercke LJ, O'Connell J, Stroud RM, Schulten K (2002) Control of the selectivity of the aquaporin water channel family by global orientational tuning. Science. 296(5567): 525-30.

Tani K, Mitsuma T, Hiroaki Y, Kamegawa A, Nishikawa K, Tanimura Y, Fujiyoshi Y (2009) Mechanism of aquaporin-4's fast and highly selective water conduction and proton exclusion. J Mol Biol. 389(4): 694-706.

Tournaire-Roux C, Sutka M, Javot H, Gout E, Gerbeau P, Luu DT, Bligny R, Maurel C (2003) Cytosolic pH regulates root water transport during anoxic stress through gating of aquaporins. Nature. 425(6956): 393-397.

Törnroth-Horsefield S, Wang Y, Hedfalk K, Johanson U, Karlsson M, Tajkhorshid E, Neutze R, Kjellbom P (2006) Structural mechanism of plant aquaporin gating. Nature. 439(7077): 688-94.

Törnroth-Horsefield S, Hedfalk K, Fischer G, Lindkvist-Petersson K, Neutze R (2010) Structural insights into eukaryotic aquaporin regulation. FEBS Lett. 584(12): 2580-8.

Tsai HC, Doong RA (2005) Simultaneous determination of pH, urea, acetylcholine and heavy metals using array-based enzymatic optical biosensor. Biosens Bioelectron. 20(9): 1796-804.

Tsukaguchi H, Shayakul C, Berger UV, Mackenzie B, Devidas S, Guggino WB, van Hoek AN, Hediger MA (1998) Molecular characterization of a broad selectivity neutral solute channel. J Biol Chem. 273(38): 24737–43.

Uehlein N, Lovisolo C, Siefritz F, Kaldenhoff R (2003) The tobacco aquaporin NtAQP1 is a membrane CO_2 pore with physiological functions. Nature. 425(6959): 734-7.

Ullmann GM (2001) Charge transfer properties of photosynthetic and respiratory proteins. In: HS Nalwa (ed.), Supramolecular photosensitive and electroactive materials. pp. 525-584. Academic Press, USA.

van Heeswijk MP, van Os CH (1986) Osmotic water permeabilities of brush border and basolateral membrane vesicles from rat renal cortex and small intestine. J Membr Biol. 92(2): 183-193.

Vemana S, Pandey S, Larsson HP (2008) Intracellular Mg^{2+} is a voltage-dependent pore blocker of HCN channels. Am J Physiol Cell Physiol. 295(2): C557-65.

Verdoucq L, Grondin A, Maurel C (2008) Structure-function analysis of plant aquaporin AtPIP2;1 gating by divalent cations and protons. Biochem J 415:409–416

Verkman AS, Shi LB, Frigeri A, Hasegawa H, Farinas J, Mitra A, Skach W, Brown D, Van Hoek AN, Ma T (1995) Structure and function of kidney water channels. Kidney Int. 48(4): 1069-81.

Wallace IS, Roberts DM (2004) Homology modeling of representative subfamilies of Arabidopsis major intrinsic proteins. Classification based on the aromatic/arginine selectivity filter. Plant Physiol. 135(2): 1059-68.

Walz T, Fujiyoshi Y, Engel A (2009) The AQP structure and funtional implications. In: E Beitz (ed.), Aquaporins: Handb Exp Pharmac. (190): 31-56. Springer-Verlag Berlin-Heidelberg.

Wang J, Wang T, Mallhi H, Liu Y, Ban H, Ladwig K (2007) The role of ammonia on mercury leaching from coal fly ash. Chemosphere. 69(10): 1586-92.

Wang Y, Cohen J, Boron WF, Schulten K, Tajkhorshid E (2007) Exploring gas permeability of cellular membranes and membrane channels with molecular dynamics. J Str Biol. 157(3): 534–544.

Wang Y, Tajkhorshid E (2010) Nitric oxide conduction by the brain aquaporin AQP4. Proteins. 78(3): 661–670.

Wang Y, Schulten K, Tajkhorshid E (2005) What makes an aquaporin a glycerol channel? A comparative study of AqpZ and GlpF. Structure. 13(8): 1107-18.

Watanabe S, Kaneko T, Aida K (2005) Aquaporin-3 expressed in the basolateral membrane of gill chloride cells in Mozambique tilapia *Oreochromis mossambicus* adapted to freshwater and seawater. J Exp Biol. 208 (Pt 14): 2673-82.

Winkler FK (2006) Amt/MEP/Rh proteins conduct ammonia. Pflügers Arch – Eur J Physiol. 451(6): 701–707.

Woeber KA, Reid EL, Kein I, Hills AG (1963) Diffusion of gases out of the distal nephron-segment in man. I. NH_3. J Clinical Investig. 42(11): 1689-704.

Wright PA (1995) Nitrogen excretion: three end products, many physiological roles. J Exp Biol. 198(Pt 2): 273-281.

Wu B, Steinbronn C, Alsterfjord M, Zeuthen T, Beitz, E (2009) Concerted action of two cation filters in the aquaporin water channel. EMBO J. 28(15): 2188-94.

Wudick MM, Luu DT, Maurel C (2009) A look inside: localization patterns and functions of intracellular plant aquaporins. New Phytologist. 184(2): 289–302.

Wülfing C, Lombardero J, Plückthun A (1994) An Escherichia coli protein consisting of a domain homologous to FK506-binding proteins (FKBP) and a new metal binding motif. J Biol Chem. 269: 2895-2901.

Yakata K, Tani K, Fujiyoshi Y (2011) Water permeability and characterization of aquaporin-11. J Struc Biol. 174(2): 315-20.

Yakata K, Hiroaki Y, Ishibashi K, Sohara E, Sasaki S, Mitsuoka K, Fujiyoshi Y (2007) Aquaporin-11 containing a divergent NPA motif has normal water channel activity. Biochim Biophys Acta. 1768(3): 688-93.

Yang B, Fukuda N, van Hoek A, Matthay MA, Ma T, Verkman AS (2000) Carbon dioxide permeability of aquaporin-1 measured in erythrocytes and lung of aquaporin-1 null mice and in reconstituted proteoliposomes. J Biol Chem. 275(4): 2686-92.

Yang B, Kim JK, Verkman AS (2006) Comparative efficacy of $HgCl_2$ with candidate aquaporin-1 inhibitors DMSO, gold, TEA^+ and acetazolamide. FEBS Lett. 580(28-29): 6679–84.

Yang H, Xu Y, Zhu W, Chen K, Jiang H (2007) Detailed mechanism for AmtB conducting NH_4^+/NH_3: molecular dynamics simulations. Biophys J. 92(3): 877-85.

Yasui M, Hazama A, Kwon TH, Nielsen S, Guggino WB, Agre P (1999) Rapid gating and anion permeability of an intracellular aquaporin. Nature. 402(6758): 184–187

Yool AJ, Weinstein AM (2002) New roles for old holes: ion channel function in aquaporin-1. News in Physiol Sci. 17(2): 68-72.

Yruela I (2005) Copper in plants. Braz J Plant Physiol. 17(1): 145-156.

Yu J, Yool A.J, Schulten K, Tajkhorshid E (2006) Mechanism of gating and ion conductivity of a possible tetrameric pore in aquaporin-1. Structure. 14(9): 1411–23.

Yukutake Y, Hirano Y, Suematsu M, Yasui M (2009) Rapid and reversible inhibition of aquaporin-4 by zinc. Biochemistry. 48(51): 12059-61.

Yukutake Y, Tsuji S, Hirano Y, Adachi T, Takahashi T, Fujihara K, Agre P, Yasui M, Suematsu M (2008) Mercury chloride decreases the water permeability of aquaporin-4-reconstituted proteoliposomes. Biol Cell. 100(6): 355–363.

Zaborska W, Krajewska B, Olech Z (2004) Heavy metal ions inhibition of jack bean urease: potential for rapid contaminant probing. J Enzyme Inhib Med Chem. 19(1): 65-69.

Zelenina M, Zelenin S, Bondar AA, Brismar H, Aperia A (2002) Water permeability of aquaporin-4 is decreased by protein kinase C and dopamine. Am J Physiol Renal Physiol. 283(2): F309-18.

Zelenina M, Bondar AA, Zelenin S, Aperia A (2003) Nickel and extracellular acidification inhibit the water permeability of human aquaporin-3 in lung epithelial cells. J Biol Chem. 278(32): 30037-43.

Zelenina M, Tritto S, Bondar AA, Zelenin S, Aperia A (2004) Copper inhibits the water and glycerol permeability of aquaporin-3. J Biol Chem. 279(50): 51939-43.

Zeuthen T, Wu B, Pavlovic-Djuranovic S, Holm LM, Uzcategui NL, Duszenko M, Kun JF, Schultz JE, Beitz E (2006) Ammonia permeability of the aquaglyceroporins from *Plasmodium falciparum*, *Toxoplasma gondii* and *Trypansoma brucei*. Mol Microbiol. 61(6): 1598-608.

Zhang M, Lü S, Li G, Mao Z, Yu X, Sun W, Tang Z, Long M, Su W (2010) Identification of a residue in helix 2 of rice plasma membrane intrinsic proteins that influences water permeability. J Biol Chem. 285(53): 41982-92.

Zheng L, Kostrewa D, Bernéche S Winkler FK, Li XD (2004) The mechanism of ammonia transport based on the crystal structure of AmtB of *Escherichia coli*. Proc Nat Acad Sci USA. 101(49): 17090–5.

Zilli L, Schiavone R, Chauvigné F, Cerdà J, Storelli C, Vilella S (2009) Evidence for the involvement of aquaporins in sperm motility activation of the teleost gilthead sea bream (*Sparus aurata*). Biol Reprod. 81(5): 880-8.

6 APPENDICES

Appendix 1A

Table: The values of rate constant and the coefficient of water permeability calculated for each of the representative time courses in various Cys-to-Ala mutants.

	TaTIP2;2-WT				C63A			
	w/o Hg		with Hg		w/o Hg		with Hg	
	ki	P_f	***ki***	P_f	***ki***	P_f	***ki***	P_f
	30,17	0,116456	33,65	0,129889	20	0,0772	18,41	0,071063
	24,1	0,093026	31,58	0,121899	21,48	0,082913	17,33	0,066894
	26,34	0,101672	31,26	0,120664	22,61	0,087275	21,25	0,082025
	24,78	0,095651	31,2	0,120432	20,39	0,078705	18,47	0,071294
	28,44	0,109778	31,41	0,121243	19,1	0,073726	15,66	0,060448
	23,92	0,092331	31,53	0,121706	20,79	0,080249	22,92	0,088471
	30,4	0,117344	32,26	0,124524	19,85	0,076621	25,74	0,099356
	20,2	0,077972	34,83	0,134444	18,92	0,073031	22,41	0,086503
	27,43	0,10588	28,13	0,108582	25,66	0,099048	29,12	0,112403
	28,91	0,111593	30,74	0,118656	19,58	0,075579	35,55	0,137223
	33,78	0,130391	30,36	0,11719	25,12	0,096963	27,15	0,104799
	29,44	0,113638	30,7	0,118502	30,53	0,117846	33,29	0,128499
	31,95	0,123327	31,03	0,119776	25,37	0,097928	27,6	0,106536
	28,32	0,109315	26,94	0,103988	24,17	0,093296	20,98	0,080983
	31,34	0,120972	30,34	0,117112	23,46	0,090556	43,53	0,168026
	29,97	0,115684	30,3	0,116958	49,9	0,192614	43,01	0,166019
	36,32	0,140195	31,1	0,120046	48,08	0,185589	41,13	0,158762
	34,56	0,133402	35,34	0,136412	42,12	0,162583	41,03	0,158376
	34,08	0,131549	31,7	0,122362	47,13	0,181922	40,73	0,157218
	35,96	0,138806	33,15	0,127959	49,44	0,190838	38,11	0,147105
	38,36	0,14807	35,03	0,135216	48,11	0,185705	43,1	0,166366
	39,24	0,151466	33,14	0,12792	49,64	0,19161	35,43	0,13676
	34,96	0,134946	25,18	0,097195	46,38	0,179027		
	31,83	0,122864	24,32	0,093875				
	37,51	0,144789	31,63	0,122092				
	34,66	0,133788	26,36	0,10175				
	33,9	0,130854	30,54	0,117884				
	33,33	0,128654	31,69	0,122323				
	34,32	0,132475	24,74	0,095496				
	32,68	0,126145	23,77	0,091752				
	35,14	0,13564						
	35,55	0,137223						
Mean	31,62	0,122	30,47	0,118	31,21	0,121	30,09	0,116
SE of Mean		0,0031		0,00219		0,01013		0,00794

Appendix 1A continued from the previous page …….

	C123A				A117C/C123A	
	w/o Hg		with Hg		w/o Hg	
	ki	P_f	***ki***	P_f	***ki***	P_f
	51,6	0,199176	45,47	0,175514	49,29	0,190259
	49,89	0,192575	42,09	0,162467	45,26	0,174704
	49,96	0,192846	45,29	0,174819	46,11	0,177985
	51,78	0,199871	44	0,16984	47,43	0,18308
	47,56	0,183582	44,14	0,17038	46,13	0,178062
	49,32	0,190375	44	0,16984	48,54	0,187364
	49,96	0,192846	42,9	0,165594	48,08	0,185589
	51,99	0,200681	43,29	0,167099	49,64	0,19161
	51,22	0,197709	33,82	0,130545	36,04	0,139114
	36,44	0,140658	34,9	0,134714	37	0,14282
	34,56	0,133402	36,48	0,140813	36,22	0,139809
	35,33	0,136374	35,63	0,137532	37,61	0,145175
	33,53	0,129426	34,5	0,13317	36,59	0,141237
	36,76	0,141894	38,31	0,147877	35,06	0,135332
	37,63	0,145252	36,91	0,142473	44,39	0,171345
	35,94	0,138728	36,58	0,141199	40,85	0,157681
	37,38	0,144287	35,51	0,137069	41,98	0,162043
	38,02	0,146757	35,66	0,137648	46,44	0,179258
	36,76	0,141894	26,35	0,101711	39,18	0,151235
	30,12	0,116263	29,97	0,115684	43,26	0,166984
	38,66	0,149228	28,27	0,109122	44,21	0,170651
	37,23	0,143708	33,27	0,128422	38,45	0,148417
	31,09	0,120007	29,97	0,115684		
	31,51	0,121629	29,42	0,113561		
	31,82	0,122825	30,16	0,116418		
	37,84	0,146062	29,78	0,114951		
	44,83	0,173044	32,69	0,126183		
			31,7	0,122362		
Mean	40,69	0,157	36,11	0,14	42,63	0,164
SE of Mean		0,00561		0,00422		0,00402

Appendix 1A continued from the previous page …….

	C63A/C123A					
	with Hg		**w/o Hg**		**with Hg**	
	ki	P_f	***ki***	P_f	***ki***	P_f
	29,53	0,113986	46,55	0,179683	63,33	0,244454
	27,55	0,106343	58,51	0,225849	51,46	0,198636
	32,19	0,124253	48,18	0,185975	34,8	0,134328
	31,87	0,123018	58,67	0,226466	30,15	0,116379
	30,68	0,118425	43,7	0,168682	48,9	0,188754
	33,11	0,127805	48,7	0,187982	53,06	0,204812
	35,68	0,137725	41,37	0,159688	43,24	0,166906
	30,74	0,118656	59,1	0,228126	43,39	0,167485
	21,32	0,082295	53,42	0,206201	36,28	0,140041
	21,06	0,081292	44,98	0,173623	57,61	0,222375
	23,05	0,088973	47,67	0,184006	61,06	0,235692
	22,54	0,087004	48,8	0,188368	51,93	0,20045
	20,81	0,080327	54,22	0,209289	40,9	0,157874
	22,46	0,086696	63,89	0,246615	40,42	0,156021
	22,05	0,085113	53,12	0,205043	38,61	0,149035
	22,26	0,085924	39,85	0,153821	38,56	0,148842
	29,14	0,11248	36,8	0,142048	38,95	0,150347
	29,88	0,115337	35,4	0,136644	39,3	0,151698
	26,39	0,101865	41,1	0,158646	36,6	0,141276
	28,25	0,109045	35,44	0,136798	38,4	0,148224
	27,98	0,108003	38,28	0,147761	36,74	0,141816
	30,17	0,116456	36	0,13896	37,15	0,143399
	28,16	0,108698	39,86	0,15386	48,26	0,186284
	28,81	0,111207	45,02	0,173777	49,77	0,192112
			45,34	0,175012	46,26	0,178564
			54,03	0,208556	47,05	0,181613
			47,84	0,184662	45,76	0,176634
			45,17	0,174356	45,81	0,176827
			44,07	0,17011	47,13	0,181922
			51,68	0,199485	45,04	0,173854
			46,63	0,179992	49,28	0,190221
			48,18	0,185975	47,21	0,182231
			47,7	0,184122		
			47,73	0,184238		
Mean	27,32	0,106	46,97	0,181	44,76	0,173
SE of Mean		0,00342		0,00473		0,00524

Appendix1B

Table: The values of rate constant and the coefficient of ammonia permeability calculated for each of the representative time courses in various Cys-to-Ala mutants.

	TaTIP2;2-WT				**C63A**			
	w/o Hg		**with Hg**		**w/o Hg**		**with Hg**	
	ki	P_{NH_3}	***ki***	P_{NH_3}	***ki***	P_{NH_3}	***ki***	P_{NH_3}
	3,99	0,026424	1,45	0,009603	3,65	0,024172	1,03	0,006821
	3,46	0,022914	0,90	0,00596	3,45	0,022848	1,30	0,008609
	4,14	0,027417	0,89	0,005894	2,83	0,018742	1,14	0,00755
	4,16	0,02755	1,02	0,006755	2,77	0,018344	0,99	0,006556
	3,86	0,025563	1,02	0,006755	2,56	0,016954	0,84	0,005563
	3,44	0,022781	0,98	0,00649	2,96	0,019603	0,77	0,005099
	3,30	0,021854	0,74	0,004901	2,67	0,017682	0,67	0,004437
	3,15	0,020861	0,60	0,003974	2,45	0,016225	0,63	0,004172
	3,13	0,020728	1,16	0,007682	4,43	0,029338	0,58	0,003841
	4,70	0,031126	0,84	0,005563	2,99	0,019801	1,12	0,007417
	4,03	0,026689	0,78	0,005166	2,82	0,018675	0,87	0,005762
	3,45	0,022848	0,72	0,004768	3,01	0,019934	0,81	0,005364
	3,30	0,021854	0,73	0,004834	3,18	0,02106	0,81	0,005364
	3,53	0,023377	0,7	0,004636	3,02	0,02	0,50	0,003311
	3,07	0,020331	0,56	0,003709	2,89	0,019139	0,58	0,003841
	2,77	0,018344	0,5	0,003311	2,73	0,018079	0,42	0,002781
	2,50	0,016556	0,63	0,004172	2,63	0,017417	0,36	0,002384
	4,30	0,028477	0,58	0,003841	2,98	0,019735	0,39	0,002583
	3,95	0,026159	0,61	0,00404	2,67	0,017682	0,34	0,002252
	3,17	0,020993			2,70	0,017881	0,35	0,002318
	3,25	0,021523			2,66	0,017616		
	3,77	0,024967			2,61	0,017285		
	3,43	0,022715			2,59	0,017152		
	2,97	0,019669			2,54	0,088145		
	2,83	0,018742						
Mean		0,023		0,0054		0,019		0,0048
SE of Mean		0,00071		0,00036		0,00292		0,00043

Appendix 1B continued from the previous page…….

	C123A				C63/123A	
	w/o Hg		with Hg		w/o Hg	
	ki	P_{NH_3}	***ki***	P_{NH_3}	***ki***	P_{NH_3}
	5,17	0,034238	1,68	0,011126	6,42	0,042517
	4,71	0,031192	1,25	0,008278	6,58	0,043576
	4,84	0,032053	1,21	0,008013	4,89	0,032384
	4,52	0,029934	1,23	0,008146	4,49	0,029735
	4,27	0,028278	0,89	0,005894	4,98	0,03298
	4,18	0,027682	0,84	0,005563	5,17	0,034238
	4,09	0,027086	0,87	0,005762	4,78	0,031656
	3,75	0,024834	0,82	0,00543	4,19	0,027748
	3,65	0,024172	0,76	0,005033	4,15	0,027483
	4,29	0,028411	0,91	0,006026	6,01	0,039801
	6,43	0,042583	0,91	0,006026	5,58	0,036954
	5,05	0,033444	0,86	0,005695	4,11	0,027219
	5,58	0,036954	0,74	0,004901	3,95	0,026159
	5,58	0,036954	0,74	0,004901	4,06	0,026887
	4,51	0,029868	0,66	0,004371	4,54	0,030066
	3,89	0,025762	0,67	0,004437	4,65	0,030795
	3,70	0,024503	0,62	0,004106	4,19	0,027748
	3,87	0,025629	0,5	0,003311	3,98	0,026358
	5,36	0,035497	0,52	0,003444	4,35	0,028808
	5,18	0,034305	0,68	0,004503	3,44	0,022781
	4,53	0,03	0,57	0,003775	3,59	0,023775
	3,88	0,025695	0,58	0,003841	3,8	0,025166
	3,96	0,026225			3,69	0,024437
	4,53	0,03			3,5	0,023179
	4,44	0,029404			3,13	0,020728
	4,14	0,027417			2,98	0,019735
	4,04	0,026755			2,74	0,018146
Mean		0,03		0,00557		0,029
SE of Mean		0,00087		0,0004		0,00124

Appendix 1B continued from the previous page…….

A117C/C123A					
with Hg		**w/o Hg**		**with Hg**	
ki	P_{NH_3}	***ki***	P_{NH_3}	***ki***	P_{NH_3}
1,68	0,011126	5,96	0,03947	0,87	0,005762
1,25	0,008278	5,92	0,039205	0,66	0,004371
1,21	0,008013	5,98	0,039603	0,65	0,004305
1,23	0,008146	6,02	0,039868	0,57	0,003775
0,89	0,005894	4,81	0,031854	0,55	0,003642
0,84	0,005563	4,62	0,030596	0,46	0,003046
0,87	0,005762	4,47	0,029603	0,59	0,003907
0,82	0,00543	4,06	0,026887	0,57	0,003775
0,76	0,005033	3,79	0,025099	0,48	0,003179
0,91	0,006026	4,18	0,027682	0,45	0,00298
0,91	0,006026	4,64	0,030728	0,5	0,003311
0,86	0,005695	4,7	0,031126	0,36	0,002384
0,74	0,004901	4,87	0,032252	0,44	0,002914
0,74	0,004901	3,81	0,025232	0,41	0,002715
0,66	0,004371	3,21	0,021258	0,38	0,002517
0,67	0,004437	3,32	0,021987	0,32	0,002119
0,62	0,004106	2,87	0,019007	0,28	0,001854
0,5	0,003311	2,56	0,016954	0,29	0,001921
0,52	0,003444	5,27	0,034901	0,28	0,001854
0,68	0,004503	5,79	0,038344	0,24	0,001589
0,57	0,003775	6,2	0,04106	0,22	0,001457
0,58	0,003841	4,02	0,026623		
		4,77	0,031589		
		4,24	0,028079		
		4,02	0,026623		
		3,97	0,026291		
		3,57	0,023642		
Mean	0,00557		0,03		0,003
SE of Mean	0,0004		0,00129		0,00024

Appendix 1C

Table: The values of rate constant and the coefficient of water permeability calculated for each of the representative time courses in various NtPIP2;1 mutants.

NtPIP2;1-WT		**V117I**		**V197L**	
ki	P_f	***ki***	P_f	***ki***	P_f
84,15	0,324819	148,8	0,574368	53,41	0,2061626
74,43	0,2872998	142,35	0,549471	58,9	0,227354
82,56	0,3186816	140,57	0,5426002	56,63	0,2185918
67,45	0,260357	171,02	0,6601372	52,25	0,201685
73,3	0,282938	175,48	0,6773528	56,45	0,217897
85,84	0,3313424	175,11	0,6759246	58,51	0,2258486
75,56	0,2916616	193,71	0,7477206	57,23	0,2209078
79,77	0,3079122	157,68	0,6086448	55,77	0,2152722
75,74	0,2923564	147,03	0,5675358	55,97	0,2160442
81,25	0,313625	167,24	0,6455464	52,9	0,204194
77,94	0,3008484	184,61	0,7125946	54,84	0,2116824
93,96	0,3626856	184,22	0,7110892	52,54	0,2028044
94,97	0,3665842	175,87	0,6788582	50,66	0,1955476
89,75	0,346435	125,22	0,4833492	56,09	0,2165074
103,75	0,400475	155,97	0,6020442	46,76	0,1804936
104,43	0,4030998	202,3	0,780878	49,31	0,1903366
96,07	0,3708302	135,5	0,52303	50,8	0,196088
104,44	0,4031384	115,18	0,4445948	48,51	0,1872486
92,32	0,3563552	170,18	0,6568948	49,19	0,1898734
67,69	0,2612834	164,66	0,6355876	48,16	0,1858976
72,7	0,280622	128,22	0,4949292	50,55	0,195123
80,29	0,3099194	142,33	0,5493938	61,64	0,2379304
71,72	0,2768392	159,91	0,6172526	48,79	0,1883294
76,72	0,2961392	159,73	0,6165578	48,09	0,1856274
85,36	0,3294896	133,96	0,5170856	46,5	0,17949
73,78	0,2847908	152	0,58672	49,44	0,1908384
79,26	0,3059436	137,65	0,531329	45,8	0,176788
68,13	0,2629818	117,33	0,4528938	50,18	0,1936948
		122,66	0,4734676	47,6	0,183736
		147,18	0,5681148	46,77	0,1805322
		174,15	0,672219	46,75	0,180455
		117	0,45162	47,57	0,1836202
		143,98	0,5557628	46,93	0,1811498
		114,55	0,442163	45,76	0,1766336
		164	0,63304	46	0,17756
		138,63	0,5351118	46,75	0,180455
		179,62	0,6933332		
		145,74	0,5625564		
		141,64	0,5467304		

			125,55	0,484623		
			164,43	0,6346998		
			140,23	0,5412878		
			124,63	0,4810718		
Mean	82,56	0,319	151,35	0,584	51,11	0,197
SE of Mean	2,095	0,008	3,434	0,013	0,736	0,0028

Appendix 1C continued from the previous page…….

A256G		**V117I/V197L**		**V117I/V197L/A256G**	
ki	P_f	***ki***	P_f	***ki***	P_f
44,81	0,172967	54,49	0,210331	23,31	0,089977
35,98	0,138883	43,17	0,166636	26,53	0,102406
40,15	0,154979	54,4	0,209984	29,74	0,114796
41,05	0,158453	53,94	0,208208	28,89	0,111515
38,93	0,15027	37,77	0,145792	23,78	0,091791
41,33	0,159534	56,64	0,21863	26,96	0,104066
38	0,14668	56,12	0,216623	24,33	0,093914
34,4	0,132784	68,53	0,264526	23,98	0,092563
38,38	0,148147	105,72	0,408079	24,59	0,094917
40,75	0,157295	81,85	0,315941	28,28	0,109161
37,7	0,145522	92,12	0,355583	28,13	0,108582
35,11	0,135525	79,19	0,305673	23,74	0,091636
39,47	0,152354	56,08	0,216469	26,81	0,103487
42,26	0,163124	84,51	0,326209	16,16	0,062378
40,58	0,156639	76,55	0,295483	24,4	0,094184
57,07	0,22029	61,24	0,236386	26,04	0,100514
46,74	0,180416	70,8	0,273288	20,96	0,080906
44,46	0,171616	43,53	0,168026	16,18	0,062455
47,58	0,183659	64,1	0,247426	18,5	0,07141
45,17	0,174356	85,38	0,329567	28,81	0,111207
48,14	0,18582	82,39	0,318025	17,36	0,06701
45,03	0,173816	96,13	0,371062	18,61	0,071835
47,67	0,184006	82,81	0,319647	20,98	0,080983
45,71	0,176441	71,85	0,277341	21,13	0,081562
47,7	0,184122	64,32	0,248275	16,23	0,062648
48,63	0,187712	85,34	0,329412	26,07	0,10063
46,66	0,180108	59,03	0,227856	29,43	0,1136
40	0,1544	66,17	0,255416	32,2	0,124292
40,82	0,157565	62,48	0,241173	26,73	0,103178
39,13	0,151042	67,61	0,260975	29,87	0,115298
44,28	0,170921	77,61	0,299575	25,48	0,098353
43,72	0,168759	63,41	0,244763	25,68	0,099125
43,74	0,168836			26,19	0,101093

	45,2	0,174472			24,51	0,094609
	38,83	0,149884			25,42	0,098121
	41,57	0,16046			21,34	0,082372
	37,12	0,143283			25,07	0,09677
	46,57	0,17976			26,33	0,101634
	42,6	0,164436			25,75	0,099395
	42,41	0,163703			24,69	0,095303
					20,02	0,077277
					23,94	0,092408
					24,64	0,09511
					24,51	0,094609
					25,23	0,097388
					24,96	0,096346
					20,46	0,078976
					26,35	0,101711
Mean	42,64	0,165	68,92	0,266	24,36	0,094
SE of Mean	0,709	0,0027	2,821	0,011	0,541	0,0021

Appendix 1D

Table: The values of rate constant and the coefficient of water permeability calculated for each of the representative time courses in various TaTIP2;2 mutants.

TaTIP2;2 - WT		**I97L**		**L168V**	
ki	P_f	***ki***	P_f	***ki***	P_f
40,47	0,156214	47,6	0,183736	44	0,16984
40,24	0,155326	50,84	0,196242	44,5	0,17177
40,96	0,158106	50,51	0,194969	46,67	0,180146
42,96	0,165826	48,6	0,187596	48,48	0,187133
40,79	0,157449	48,72	0,188059	45,57	0,1759
44,18	0,170535	47,46	0,183196	45,27	0,174742
40,98	0,158183	48,62	0,187673	44,74	0,172696
44,77	0,172812	47,23	0,182308	44,79	0,172889
45,16	0,174318	44,95	0,173507	45,34	0,175012
43,88	0,169377	50,89	0,196435	42,82	0,165285
42,93	0,16571	46,57	0,17976	42,65	0,164629
43,13	0,166482	37,92	0,146371	45,98	0,177483
42,92	0,165671	37,98	0,146603	41,2	0,159032
42,36	0,16351	44,4	0,171384	41,72	0,161039
42,7	0,164822	39,7	0,153242	40,05	0,154593
42,46	0,163896	44,7	0,172542	39,29	0,151659
43,26	0,166984	44,74	0,172696	40,61	0,156755

	46,77	0,180532	38,88	0,150077	36,43	0,14062
	44,3	0,170998	40,39	0,155905	37,76	0,145754
	38,37	0,148108	42,84	0,165362	42,65	0,164629
	41,72	0,161039	40,8	0,157488	36,73	0,141778
	39,51	0,152509	37,89	0,146255	39,77	0,153512
	41,83	0,161464	56,53	0,218206	39,2	0,151312
	41,91	0,161773	48,04	0,185434	39,16	0,151158
	39,6	0,152856	53,56	0,206742	49,93	0,19273
	41,26	0,159264	50,54	0,195084	45,51	0,175669
	39,8	0,153628	52,08	0,201029	46,4	0,179104
	41,25	0,159225	53,44	0,206278	48,9	0,188754
	40,06	0,154632	53,98	0,208363	46,21	0,178371
	42,31	0,163317	49,63	0,191572	45,53	0,175746
	41,56	0,160422	49,18	0,189835	45,38	0,175167
	45	0,1737	50,93	0,19659	49,61	0,191495
	43,6	0,168296	48,42	0,186901	46,16	0,178178
	41,78	0,161271	54,4	0,209984	49,85	0,192421
	43,98	0,169763	48,32	0,186515	49,71	0,191881
	41,86	0,16158	50,8	0,196088	51,91	0,200373
	40,58	0,156639			45,21	0,174511
	40,57	0,1566			48,08	0,185589
	41,46	0,160036				
	40,38	0,155867				
	44,93	0,17343				
	40,98	0,158183				
	45,22	0,174549				
	44,19	0,170573				
Mean	42,25	0,1631	47,28	0,1825	44,31	0,1711
SE of Mean		0,0011		0,0033		0,0025

Appendix 1D continued from the previous page …….

G224A		I97L/L168V		I97L/L168V/G224A	
ki	P_f	***ki***	P_f	***ki***	P_f
56,48	0,218013	32,54	0,125604	34,78	0,134251
54,52	0,210447	31,26	0,120664	34,28	0,132321
57,42	0,221641	31,58	0,121899	33,83	0,130584
48,9	0,188754	30,14	0,11634	32,35	0,124871
49,2	0,189912	31,75	0,122555	33,92	0,130931
50,5	0,19493	28,67	0,110666	32,65	0,126029
56,46	0,217936	31,93	0,12325	33,53	0,129426
54,93	0,21203	32,08	0,123829	33,31	0,128577
56,81	0,219287	30,84	0,119042	33,14	0,12792
53,9	0,208054	30,51	0,117769	33,03	0,127496
59,08	0,228049	31,33	0,120934	33,06	0,127612
54,68	0,211065	30,64	0,11827	36,66	0,141508
57,3	0,221178	30,88	0,119197	34,4	0,132784
54,01	0,208479	33,54	0,129464	35,12	0,135563
53,78	0,207591	31	0,11966	36,51	0,140929
52,76	0,203654	33,06	0,127612	35,22	0,135949
53,14	0,20512	31,63	0,122092	36,29	0,140079
49,58	0,191379	30,92	0,119351	37,12	0,143283
55,4	0,213844	28,77	0,111052	36,06	0,139192
51,6	0,199176	31,54	0,121744	36,44	0,140658
51,19	0,197593	28,77	0,111052	37,05	0,143013
40,36	0,15579	34,17	0,131896	36,36	0,14035
44,78	0,172851	34,04	0,131394	32,67	0,126106
46,02	0,177637	31,66	0,122208	35,97	0,138844
46,13	0,178062	33,4	0,128924	33,37	0,128808
43,21	0,166791	31,03	0,119776	34,71	0,133981
43,49	0,167871	33,57	0,12958	33,34	0,128692
42,56	0,164282	34,53	0,133286	34,17	0,131896
43,72	0,168759	33,66	0,129928	33,14	0,12792
41,75	0,161155	34,47	0,133054	33,75	0,130275
44,73	0,172658	33,67	0,129966	33,86	0,1307
42,18	0,162815	34,65	0,133749	33,56	0,129542
44,16	0,170458	31,84	0,122902		
43,49	0,167871	33,05	0,127573		
43,56	0,168142	33,55	0,129503		
44,13	0,170342				
42,19	0,162853				
44,7	0,172542				
42,23	0,163008				
43,82	0,169145				
52,05	0,200913				
49,8	0,192228				

	51,31	0,198057				
	45,13	0,174202				
	49,6	0,191456				
	50,69	0,195663				
	47,1	0,181806				
	50,24	0,193926				
	47,6	0,183736				
	51,74	0,199716				
Mean	49,08	0,1895	32,02	0,1236	34,49	0,1331
SE of Mean		0,0028		0,0011		0,001

Appendix 1E

Table: The values of rate constant and the coefficient of ammonia permeability calculated for each of the representative time courses in various TaTIP2;2 mutants.

TaTIP2;2 - WT		**I97L**		**L168V**	
ki	P_{NH_3}	***ki***	P_{NH_3}	***ki***	P_{NH_3}
1,49	0,009868	1,39	0,009205298	1,64	0,010861
1,5	0,009934	1,53	0,01013245	1,6	0,010596
1,44	0,009536	1,51	0,01	1,67	0,01106
1,51	0,01	1,57	0,010397351	1,69	0,011192
1,46	0,009669	1,53	0,01013245	1,64	0,010861
1,44	0,009536	1,5	0,009933775	1,52	0,010066
1,4	0,009272	1,45	0,009602649	1,54	0,010199
1,4	0,009272	1,45	0,009602649	1,49	0,009868
1,37	0,009073	1,44	0,009536424	1,48	0,009801
1,96	0,01298	1,4	0,009271523	1,43	0,00947
1,8	0,011921	1,43	0,009470199	1,46	0,009669
1,75	0,011589	1,48	0,009801325	1,49	0,009868
1,75	0,011589	1,55	0,010264901	1,61	0,010662
1,66	0,010993	1,65	0,010927152	1,64	0,010861
1,65	0,010927	1,67	0,011059603	1,62	0,010728
1,66	0,010993	1,57	0,010397351	1,5	0,009934
1,62	0,010728	1,45	0,009602649	1,5	0,009934
1,59	0,01053	1,45	0,009602649	1,43	0,00947
1,52	0,010066	1,36	0,009006623	1,37	0,009073
1,48	0,009801	1,39	0,009205298	1,34	0,008874
1,45	0,009603	1,39	0,009205298	1,36	0,009007
1,21	0,008013	1,37	0,009072848	1,78	0,011788
1,32	0,008742	1,32	0,008741722	1,57	0,010397
1,32	0,008742	1,58	0,010463576	1,85	0,012252

	1,39	0,009205	1,55	0,010264901	1,79	0,011854
	1,49	0,009868	1,58	0,010463576	1,78	0,011788
	1,58	0,010464	1,63	0,010794702	1,74	0,011523
	1,56	0,010331	1,56	0,010331126	1,64	0,010861
	1,41	0,009338	1,51	0,01	1,72	0,011391
	1,51	0,01	1,46	0,009668874	1,6	0,010596
	1,5	0,009934	1,46	0,009668874	1,56	0,010331
	1,52	0,010066	1,45	0,009602649	1,55	0,010265
	1,4	0,009272	1,44	0,009536424	1,56	0,010331
Mean	1,52	0,01	1,49	0,0099	1,58	0,0105
SE of Mean	0,0267	0,00018	0,015	0,0001	0,0225	0,00015

Appendix 1E continued from the previous page …….

G224A		**I97L/L168V**		**I97L/L168V/G224A**	
ki	P_{NH_3}	***ki***	P_{NH_3}	***ki***	P_{NH_3}
1,46	0,009669	1,83	0,012119	1,22	0,008079
1,51	0,01	1,65	0,010927	1,34	0,008874
1,57	0,010397	1,65	0,010927	1,4	0,009272
1,62	0,010728	1,57	0,010397	1,38	0,009139
1,66	0,010993	1,54	0,010199	1,3	0,008609
1,56	0,010331	1,46	0,009669	1,2	0,007947
1,51	0,01	1,43	0,00947	1,14	0,00755
1,45	0,009603	1,39	0,009205	1,16	0,007682
1,45	0,009603	1,34	0,008874	1,13	0,007483
1,4	0,009272	1,37	0,009073	1,15	0,007616
1,62	0,010728	1,76	0,011656	1,32	0,008742
1,46	0,009669	1,76	0,011656	1,42	0,009404
1,37	0,009073	1,82	0,012053	1,44	0,009536
1,39	0,009205	1,83	0,012119	1,38	0,009139
1,3	0,008609	1,76	0,011656	1,33	0,008808
1,29	0,008543	1,71	0,011325	1,27	0,008411
1,26	0,008344	1,68	0,011126	1,25	0,008278
1,24	0,008212	1,64	0,010861	1,24	0,008212
1,74	0,011523	1,53	0,010132	1,24	0,008212
1,71	0,011325	1,55	0,010265	1,21	0,008013
1,76	0,011656	1,56	0,010331	1,2	0,007947
1,8	0,011921	1,47	0,009735	1,15	0,007616
1,72	0,011391	1,33	0,008808		
1,71	0,011325	1,45	0,009603		
1,64	0,010861	1,45	0,009603		
1,68	0,011126	1,5	0,009934		
1,66	0,010993	1,43	0,00947		
1,59	0,01053	1,41	0,009338		

	1,57	0,010397	1,36	0,009007		
	1,52	0,010066	1,34	0,008874		
	1,46	0,009669	1,3	0,008609		
			1,28	0,008477		
			1,27	0,008411		
			1,28	0,008477		
Mean	1,54	0,0102	1,52	0,0101	1,27	0,0084
SE of Mean	0,0278	0,00018	0,03	0,0002	0,0208	0,00014

Appendix 2

Logoplots of the amino acid residues around the ar/R constriction in AQPs.

Figure: Logoplots of the amino acid residues around the aromatic/Arg restriction regions. The water permeable AQP1 has been aligned against the ammonia-permeable aquaporins AQP3, 7, 8, 9, and 10. The numbers belong to the constituents of the SF tetrad and represent corresponding positions in AQP1. The left panel includes the H2 position of the SF region. The right panel also includes the so-called "consensus region of metal sensitivity" which is located N-terminus to the second NPA motif and has been often referred to in the present study. The position H5 has His residue in ammonia- and glycerol-permeable AQPs. This position is usually replaced by a Gly in the case of the ammonia- and water permeable AQP8, an Ile. The variations in molecular signatures apart from the SF region have been highlighted by arrows. In case of aqua-ammoniaporins, the position 184 would always contain a Gly and the position 190 either an Ala or a Cys residue. (Adopted from Litman *et al*., 2009).

Appendix 3

Yeast expression Vectors used in the present study

pYES/CT:
Adopted from www.invitrogen.com

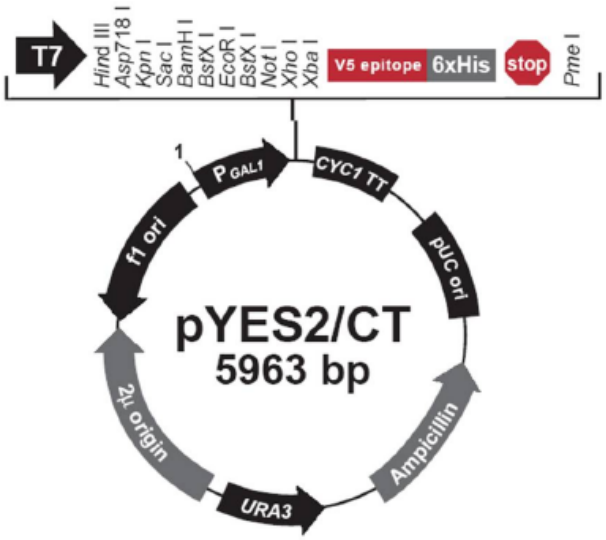

pYES/CT:
Adopted from www.invitrogen.com

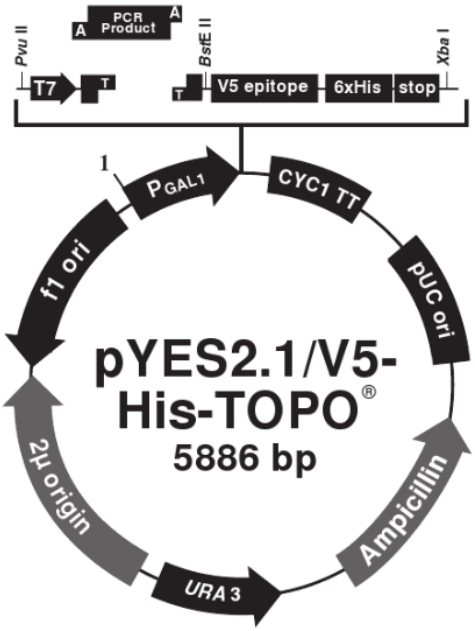

Appendix 4

List of Abbreviations

xg	x gravity
AQP	Aquaporin
dNTP	deoxy-Nukleosidtidtriphosphat
EDTA	Ethylendiamintetraacetat
hAQP1	human Aquaporin 1
NtPIP2;1	*Nicotiana tabacum* plasma membrane intrinsic protein 2;1
PAGE	Polyacylamide gel electrophoresis
PCMBS	*p*-chloromercuribenzene sulfonate
PCR	Polymerase chain reaction
P_f	Osmotic permeability coefficient
P_{NH_3}	Ammonia permeability coefficient
rpm	revolutions per minute
SDS	Sodium Dodecylsulfate
TaTIP2;2	*Triticum aestivum* tonoplast intrinsic protein 2;1
Taq	*Thermophilus aquaticus*
TEMED	(N, N, N', N'-tetramethylethylenediamine)
U	Unit

Appendix 5

Single and triple genetic codes of amino acids

A	Ala	Alanin
C	Cys	Cystein
D	Asp	Asparaginsäure
E	Glu	Glutaminsäure
F	Phe	Phenylalanin
G	Gly	Glycin
H	His	Histidin
I	Ile	Isoleucin
K	Lys	Lysin
L	Leu	Leucin
M	Met	Methionin
N	Asn	Asparagin
P	Pro	Prolin
Q	Gln	Glutamin
R	Arg	Arginin
S	Ser	Serin
T	Thr	Threonin
V	Val	Valin
W	Trp	Tryptophan
Y	Tyr	Tyrosin

Appendix 6

Amino Acid Sequences

Amino acids sequence of TaTIP2;2

MPGSIAFGRFDDSFSLASFKAYIAEFISTLIFVFAGVGSAIAYTKVSGGAPLDPSGLIAVAIC
HGFGLFVAVAIGANISGGHVNPAVTFGLALGGQITILTGIFYWVAQLLGAIVGAFLVQFC
TGVATPTHGLSGVGAFEGVVMEIIVTFGLVYTVYATAADPKKGSLGTIAPIAIGFIVGANI
LVAGPFSGGSMNPARSFGPAVASGDFTNIWIYWAGPLIGGGLAGVVYRYVYMCDDHSS
VAGNDY

Amino acids sequence of NtPIP2;1

MSKDVIEEGQ VHQQHGKDYV DPPPAPLLDF AELKLWSFHR ALIAEFIATL
LFLYVTVATV IGHKKLNGAD KCDGVGILGI SWAFGGMIFV LVYCTAGISG
GHINPAVTFG LFLARKVSLL RAVGYIIAQS LGAICGVGLV KGFMKHYYNT
LGGGANFVQP GYNKGTALGA EIIGTFVLVY TVFSATDPKR SARDSHVPVL
APLPIGFAVF MVHLATIPIT GTGINPARTF GAAVIYNTEK IWDDQWIFWV
GPFVGALVAA VYHQYILRGS AIKALGSFRS NPTN*

Curriculum Vitae

Name:	Muhammad Ayaz
Date of Birth:	January 1, 1973
Place of Birth:	Multan (Pakistan)
Marital status:	Single
Nationality:	Pakistani

Academic Achievements:

1982	Primary-level certificate	(Pakistan)
1987	Secondary-level certificate	(Pakistan)
1990	Higher-Sec-level certificate	(Pakistan)
1996	BSc (Hons) in Agriculture	Univ of Arid Agriculture Rawalpindi, (Pakistan)
1999	MPhil in Botany	Department of Biological Sciences, Quaid-e-Azam Univ; Islamabad (Pak) (Advisor: Dr M. Fayyaz Chaudhary)
1999- 2002	Research assistant (volunteer)	Plant Tissue Culture/Transformation Lab, National Agri Res Center, Islamabad/ Quaid-e-Azam Univ; Islamabad (Pak)
2003-2006	No academic achievements	
2006-2011	PhD candidate	Tech. Univ. Darmstadt, Germany (Advisor: Prof Dr Ralf Kaldenhoff)
	2006-2008 (Full-time)	
	2008-2011 (Part-time)	

Ehrenwörtliche Erklärung:

Ich erkläre hiermit ehrenwörtlich, dass ich die vorliegende Arbeit selbständig angefertigt habe. Sämtliche aus fremden Quellen direkt oder indirekt übernommene Gedanken sind als solche kenntlich gemacht. Die Arbeit wurde bisher keiner anderen Prüfungsbehörde vorgelegt und noch nicht veröffentlicht.

Muhammad Ayaz

..... Darmstadt, den ……
(Unterschrift)